Topics in Nano-Biophotonics: Fabrication of Plasmonic Metasurfaces that Attract and Spectroscopically Interrogate Cancer Cells

2018 CNF REU Intern: Vivek Anil

2018 CNF REU Intern Affiliation: Engineering Science, Physics, The Pennsylvania State University

CNF Project: 2018 Cornell NanoScale Science and Technology Facility Research Experience for Undergraduates Program

CNF REU Principal Investigator: Professor Gennady Shvets, School of Applied and Engineering Physics, Cornell University

CNF REU Mentors: Dr. Steven He Huang, School of Applied and Engineering Physics, Cornell University; Dr. Maxim Shcherbakov, School of Applied and Engineering Physics, Cornell University

Primary Source of CNF REU Funding: National Science Foundation via the National Nanotechnology Coordinated Infrastructure (NNCI) Grant No. ECCS-1542081

Contact: vivek3anil@gmail.com, gs656@cornell.edu, hh623@cornell.edu, mrs356@cornell.edu

Website: http://www.cnf.cornell.edu/cnf_2018reu.html

Primary CNF Tools Used: E-beam resist spinners, JEOL 9500, Anatech resist strip, AJA ion mill, Zeiss Ultra SEM, Zeiss Supra SEM, Even-Hour evaporator, P10 profilometer

Abstract:

Current methods for detecting cancer rely heavily on imaging or tumor markers that are often inaccurate and inefficient. Meanwhile, Fourier transform infrared spectroscopy (FTIR) has been widely studied as a method for label-free biosensing because the characteristic vibrational modes of most biomolecules oscillate at mid-IR frequencies [1]. More recently, plasmonic metasurfaces have drawn interest because they can be engineered to have a resonant electromagnetic response over a broad range of frequencies. Their unique properties enable them to confine light to nanoscale regions (high local field concentration) and have a wavelength-specific response, which is ideal for molecular sensing by spectroscopy [2]. Infrared (IR) plasmonic metamaterials are particularly useful for biosensing: the resonant response of these materials can be tuned to match that of the vibrational modes in biomolecules so that biomolecules can be sensed via surface-enhanced IR spectroscopy. We investigated the use of plasmonic metasurfaces for detection of selected vibrational modes by fabricating gold metasurfaces on an infrared-transparent calcium fluoride (CaF_2) substrate; the metasurfaces were patterned using electron-beam lithography. We successfully fabricated three different types of structures: Fano resonant asymmetric metamaterials (FRAMMs), nanoantennae, and nanoslits, and validated the presence of resonance peaks by performing FTIR on the metasurfaces to obtain reflectance spectra. By adjusting the structures' dimensions, the resonances (quality factor Q~10) seen in each structure's reflectance spectra were tuned to match the amide I (~ 1650 cm^{-1}) and carbohydrate (~ 2900 cm^{-1}) molecular resonances, which are present in cells. Our results demonstrate the potential to develop an improved method of cancer detection via surface-enhanced IR spectroscopy with engineered plasmonic metasurfaces.

Summary of Research:

Introduction. Biomolecular components in cells possess characteristic vibrational modes in the IR, which can be spectroscopically probed to obtain information from cells [1]. The signals from these vibrational modes are often weak, and so we propose using a plasmonic metasurface to enhance these signals. The dimensions and spatial arrangements of the structures were chosen such that the metasurface resonated at frequencies similar to cellular vibrations. Each set of structures with the same dimensions were fabricated together, with consistent spacing between structures, in squares, called pixels. This was done for the sake of testing simplicity: each pixel could be probed as an individual metasurface, and so we could assess how well each set of dimensions enabled us to tune to a particular resonance.

Fabrication. For the FRAMMs and nanoantennae, the fabrication process was as follows: CaF_2 wafers were washed and dried thoroughly, and then ~ 240 nm PMMA was spin-coated onto the wafers. The wafer was then baked at 170°C. We patterned the metasurface using the JEOL 9500 electron-beam lithography system. We developed the PMMA from the patterned areas using a methyl isobutyl ketone-isopropanol developer (MIBK:IPA 1:3). We evaporated 10 nm Cr and 70 nm Au onto the substrate at 1 A/s each. Remaining PMMA was lifted-off in an overnight acetone bath. The process for fabricating nanoslits was similar, except that we evaporated Au between cleaning and spin-coating, and added an extra ion mill etching step after development and before lift-off.

FTIR Experiment. The metasurface was integrated into a polydimethylsiloxane microfluidic chamber; a solution — phosphate buffer saline (PBS), ethanol, or DI water — was injected into the chamber, and an IR spectroscopy was done on the metasurface (probing pixel by pixel) in the chamber using a Bruker-Hyperion FTIR-microscope system.

Results and Conclusions:

We were able to successfully tune our FRAMM (pi structure) and nanoantenna resonances to the desired frequencies, as seen in Figure 1 — where the "Pi_5" (d = *225.1 nm* and L = *1.727 μm* as in Figure 2a) and "Nanoantenna_2" (w = *234.8 nm* and L = *1.693 μm* as in Figure 2b) pixels resonate at the amide I frequency (~1650 cm^{-1}) and the "Pi_3" (d = *66.19 nm* and L = *0.9555 μm* as in Figure 2a) and "Nanoantenna_1" (w = *238.3 nm* and L = *0.9624 μm* as in Figure 2b) pixels resonate at the carbohydrate frequency (~2900 cm^{-1}). In general, we saw that as we increase the size of FRAMM structures, we decrease the position of the resonant frequency (Figure 3); this relationship proved useful for tuning resonances.

We also successfully fabricated nanoslits and adjusted structure dimensions (w ~ *50 nm* and L ~ *700 nm* for "slit_1" and w ~ *50 nm* and L ~ *1500 nm* for "slit_2") such that we observed the interference between the nanoslit peaks and the deionized (DI) water (~1660 cm^{-1} and 3400 cm^{-1}) and ethanol (~3000 cm^{-1} and 3400 cm^{-1}) resonances (Figure 4). Figure 4 suggests the potential for biosensing by tuning resonances to observe similar interference between biomolecular vibrations in cells and our metasurfaces' resonances. Furthermore, integrating our metasurface into the microfluidic chamber shows even more promise for developing a device for biosensing by surface-enhanced spectroscopy.

Future Work:

Future work will include refining nanoslit fabrication and resonance tuning, attaching cancer cells to the metasurface and performing FTIR to obtain biomolecular information from cells, comparing nanoantennae and nanoslits to determine which shows greater near field enhancement, and analyzing spectra to understand how we can use them to distinguish between healthy and cancerous cells.

Acknowledgements:

I would like to thank my PI, Prof. Gennady Shvets, my mentors, Dr. Steven Huang and Dr. Maxim Shcherbakov, CNF staff, and the National Science Foundation (NNCI Grant No. ECCS-1542081) for giving me the opportunity to participate in this Research Experience for Undergraduates Program.

References:

[1] Baker, M. J., et al. (2014). Using Fourier transform IR spectroscopy to analyze biological materials. Nature Protocols,9, 1771-1791.

[2] Wu, C., et al. Fano-resonant asymmetric metamaterials for ultrasensitive spectroscopy and identification of molecular monolayers. Nature Materials,11(1), 69-75.

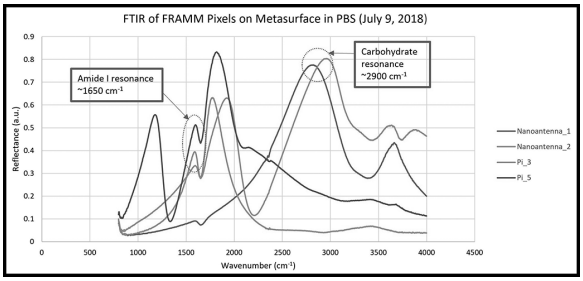

Figure 1: Reflectance spectra of FRAMM and nanoantenna pixels in PBS, tuned to match amide I and carbohydrate resonances.

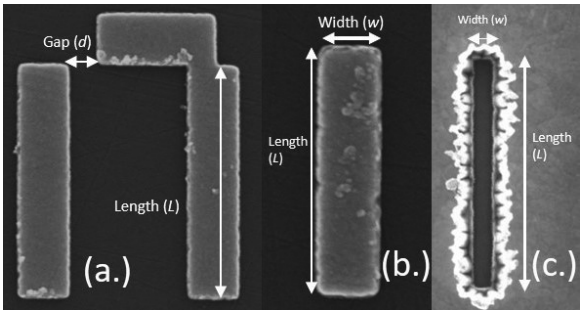

Figure 2: Scanning electron microscopy images (taken at 20.00 kV) of (a) FRAMM (pi), (b) nanoantenna, and (c) nanoslit structures.

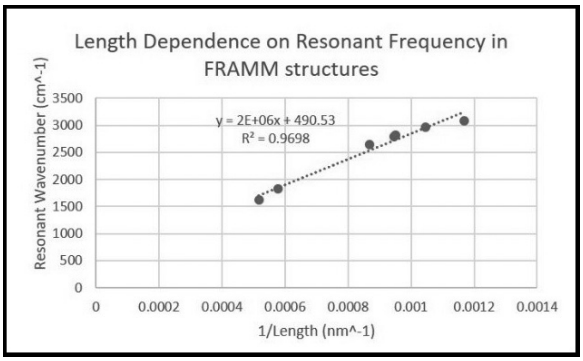

Figure 3: Relationship between length and position of the resonance seen in reflectance spectra for FRAMMs in PBS.

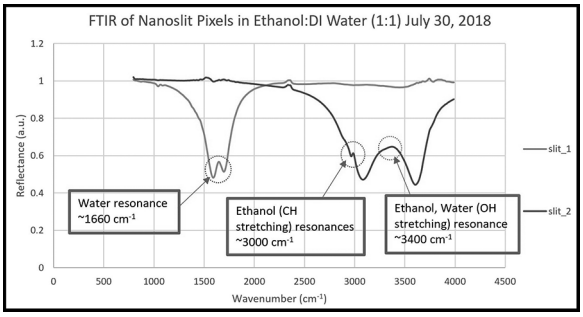

Figure 4: Reflectance spectra for 50 nm wide nanoslits in ethanol-DI water mixture showing water and ethanol resonances.

Microfluidic Mixer for Time-Resolved Single-Molecule Fluorescence Experiments using Flip-Chip Bonded SU-8 Structures

CNF Project Number: 692-98

Principal Investigator: Lois Pollack

User: Alexander Plumridge

Affiliation: Applied and Engineering Physics, Cornell University

Primary Source of Research Funding: National Institute of Health

Contact: LP26@cornell.edu, ap866@cornell.edu

Website: https://pollack.research.engineering.cornell.edu/

Primary CNF Tools Used: ABM contact aligner, class 2 resist room, VersaLaser engraver/cutter

Abstract:

We report the fabrication procedure for a microfluidic mixer capable of detecting single, fluorescently labeled biological molecules as they progress through a reaction. Precise flow control and device longevity is achieved using hard materials (SU-8) for fabrication, in place of traditional replica molding.

Summary of Research:

Single-molecule fluorescence experiments are powerful tools for elucidating structural characteristics of biological molecules [1]. Techniques such as fluorescence correlation spectroscopy (FCS) report global molecular size, while Förster resonance energy transfer (FRET) experiments yield distances between labelled residues with Angstrom precision. Critically, these techniques can probe single-molecules, granting detailed information about the underlying population that is smeared out in a bulk measurement. Long measurement times are required to gather statistics from a small (1 μm^3) focal volume, often requiring tens of minutes of data acquisition per condition.

While single-molecule experiments are routinely performed at equilibrium, the dynamic nature of biology demands an approach that embraces the time evolution of these systems. A typical strategy to provide time-resolution in fluorescence experiments exploits microfluidic mixing (e.g., ref 2). Molecules are rapidly introduced to initiate a reaction, then spatially separated to provide time-resolution. These technologies are limited to bulk measurements due to the flow speed and exposure times associated with these devices. Furthermore, the length of time required to obtain a single-molecule data set (typically several hours), paired with the pressures required to precisely control the flow (~ 1000-5000 mbar) presents challenges for conventional soft material approaches, though some have been developed and applied [3]. To meet these criteria, we designed and fabricated microfluidic devices from SU-8 to rapidly mix reagents, then subsequently slow the flow speed to a range compatible with single-molecule detection (~ μm/ms).

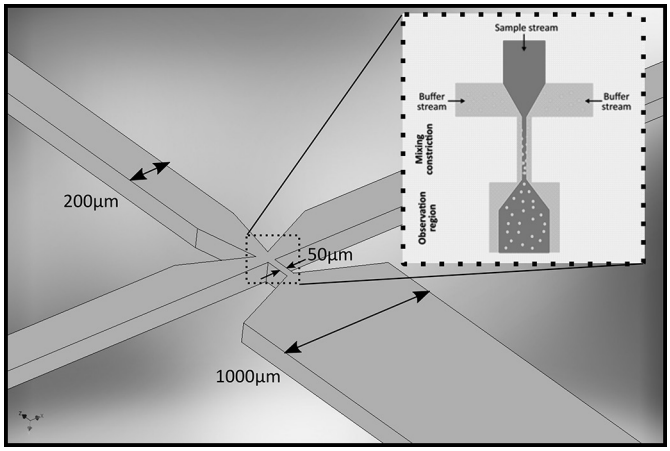

Figure 1: The device design (main panel) is based on the principle of hydrodynamic focusing (inset).

The device design is based on the hydrodynamic focusing principle (Figure 1 inset), where a sample stream is squeezed by flanking buffer streams and forced through a narrow constriction [4]. This yields a micron-sized sample stream in the constriction. Diffusion occurs rapidly across this stream, introducing a reactant from the buffer that initiates a given reaction. This narrow stream is then expanded out into a wide probing channel, which

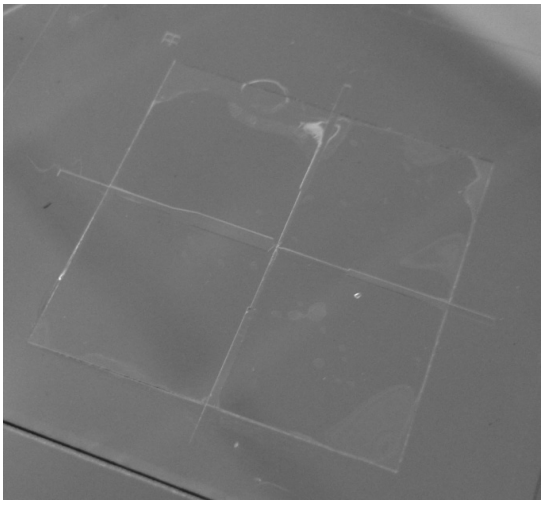

Figure 2: Stereoscopic image of a completed device.

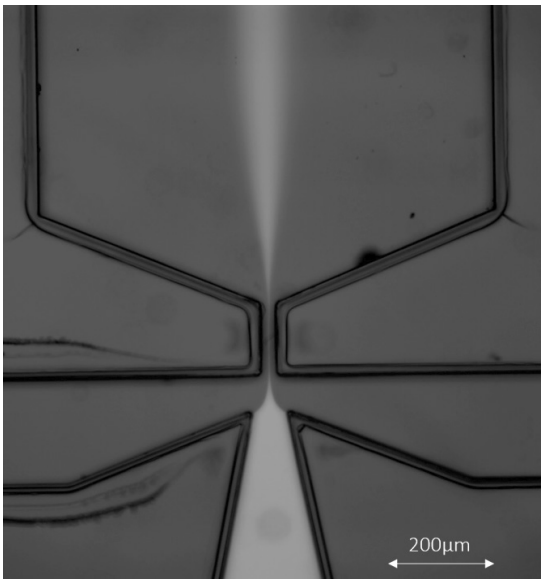

Figure 3: False colored fluorescent image showing a test sample (fluorescent dye Rhodamine 6G, bright) flowing in the device.

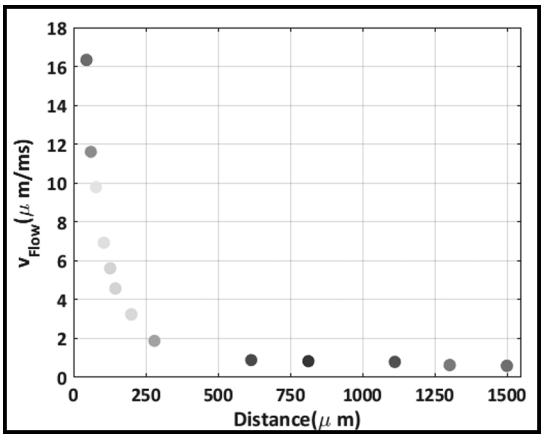

Figure 4: Flow speeds (in microns per millisecond) as a function of distance from the end of the constriction as measured by FCS.

acts to slow the flow speed down to detectable levels. Probing at different spatial locations along the observation channel provides different time delays after the reaction is initiated.

The design in Figure 1 was first replicated in a chrome mask using the Heidelberg 6600 mask writer. The device is then fabricated from four layers: two glass layers that act as windows on the top and bottom, one layer of SU-8 that defines the channel geometry, and one sealing SU-8 layer. In the first process, a 100 μm thick layer of SU-82050 is spun on borofloat, and subsequently exposed, baked and developed to yield the channel geometry. A thin sealing layer of SU-82005 is next deposited over the existing geometry, and a glass cover slide installed on top of this layer. The stack is then baked and exposed through the glass cover slide with the same mask used to pattern the channel geometry. This step acts to polymerize the sealing SU-8 2005 layer in all regions except the underlying channels. Excess SU-8 from the sealing layer that may have entered the channels is then removed by development, yielding fluidic channels which are sealed, clear and flanked solely by glass. A stereoscopic image of a completed device is shown in Figure 2.

To demonstrate the device and flow stream, we used a fluorescent dye (Rhodamine 6G), to act as a control sample, and water on the flanking buffer channels. Figure 3 shows a false colored image of this experiment, where fluorescence intensity is denoted by brightness. The sample stream clearly shrinks in the mixing constriction, before slowing and expanding in the observation region. Measurements of the sample jet widths in the constriction place it between 5-9 μm depending on the flow rates. This results in tunable mixing times between 4-10 ms for added salts and small molecules.

Finally, the flow speed in the observation region can be probed by FCS (Figure 4). For the test system of Rhodamine 6G, the flow can be reduced to less than 1 μm/ms, easily compatible with the dwell time required for confocal microscopy. For this system, the flow in the observation region slowed to single-molecule detectable levels at a time point corresponding to 30 ms after mixing is complete. Thus, in this case the device can access time points ranging from 30-3000 ms in the single-molecule regime.

The mixer lends itself well to our future applications in studying the non-equilibrium collapse of regulatory RNA elements. These motifs sense metabolites and ion levels in the cell, and drastically alter their conformation depending on the ligand concentration [5]. Molecular re-arrangements occur on time-scales ranging from 10 ms to many seconds, but detailed characterization of the sub second structural response is lacking due to the absence of appropriate experimental technology.

References:

[1] Joo, C., et al., Annu. Rev. Biochem. 2008, 77 (1), 51-76.

[2] Park, H. Y.; Qiu, X.; Rhoades, E.; Korlach, J.; Kwok, L. W.; Zipfel, W. R.; Webb, W. W.; Pollack, L. Anal. Chem. 2006, 78 (13), 4465-4473.

[3] Gambin, Y.; Vandelinder, V.; Ferreon, A. C. M.; Lemke, E. A.; Groisman, A.; Deniz, A. A. Nat. Methods 2011, 8 (3).

[4] Knight, J, et al., Phys. Rev. Lett. 1998, 80 (17), 3863-3866.

[5] Montange, R. K.; Batey, R. T. Annu. Rev. Biophys. 2008, 37, 117-133.

Body-on-a-Chip Systems for Drug Development

CNF Project Number: 731-98

Principal Investigators: Michael L. Shuler, Harold G. Craighead

Users: Ying Wang, Paula Miller, Danielle LaValley

Affiliations: Nancy E. and Peter C. Meinig School of Biomedical Engineering, Robert Frederick Smith School of Chemical and Biomolecular Engineering; Cornell University

Primary Sources of Research Funding: National Center for Advancing Translational Sciences, National Science Foundation, National Institutes of Health

Contact: MLS50@cornell.edu, hgc1@cornell.edu, ying.wang@cornell.edu, pgm6@cornell.edu, DJL339@cornell.edu

Primary CNF Tools Used: VersaLaser Engraver/Cutter tool, ABM contact aligner, SU-8 hot plates, SUEX/ADEX laminator, PDMS casting station, hot press

Abstract:

Organ-on-a-chips are tissue-engineered microsystems that mimic human organs, modeling both structure and function [1]. Human cell-based multi-organ-on-a-chip systems, or body-on-a-chips (BOC), could be a paradigm-shifting technology for drug development [2]. Such microscale biomimetics of human organs with organ-organ interactions hold the promise to simulate human physiology and disease progression, and thus offer more accurate predictions of human responses to therapeutics and provide mechanistic insights into human diseases, while significantly reduce drug development cost and animal usage. Currently, we are developing several BOC systems, which are fabricated with tools at CNF and will be used to study chemotherapeutic toxicity, model cancer cell metastasis, and simulate immune responses.

Summary of Research:

Tumor-Liver-Bone Marrow Chip. A three-organ microphysiological system has been created to study chemotherapeutic toxicity with relevant drug metabolism and hematological side effects. The device contains three chambers for seeding HCT-116 colon tumor spheroids, $HepG_2$/C3A hepatocytes, and HL-60 promyeloblasts encapsulated within 3D hydrogels. Microfluidic channels were etched into a layer of poly (methyl methacrylate) (PMMA) and designed to mimic human blood flow rates [3-5]. The silicone cell culture layer and PMMA channel layer were sandwiched between silicone gaskets and outer PMMA housing pieces. All layers were fabricated using the VersaLaser CO_2 laser cutter at CNF. Utilizing gravity-driven flow on a customized programmable rocker, a common medium is recirculated between the two reservoirs.

Colon-Liver Chip. We have developed a colon-liver dual-organ-on-a-chip system to model colorectal cancer (CRC) liver metastasis. The microphysiological system is based on a pumpless platform [6,7]. Two organ chambers representing colon and liver are interconnected and perfused with gravity-driven flow at physiological perfusion rates. The device is fabricated mainly in PMMA with silicone (gaskets) for sealing. PMMA and silicone sheets are patterned with laser ablation using the VersaLaser CO_2 laser cutter at CNF. The flow dynamics are characterized computationally and experimentally. Flow rates were measured to be within 15% of the designed values. The prototype devices tested with colon and liver cells maintained greater than 85% cell viability.

Using this colon-liver platform, we will incorporate organotypic CRC model and 3D liver constructs and investigate the metabolic stress due to CRC liver metastasis. We will investigate the cellular interaction, differentiation, migration and invasion of primary tumor and metastatic fibroblast tumor microenvironment to evaluate contributing factors in CRC metastasis.

A 5-Compartment Microphysiological System for Drug Screening. We developed a 5-organ BOC system to emulate *in vivo* drug absorption, distribution, metabolism and toxicity, as well as immune responses. The five organ chambers represent bone marrow, inflamed spleen, GI tract, liver and kidney (Figure 1). The 5-Organ Chip consists of five layers: a top cover layer and a bottom

channel layer made of PMMA, a cell chamber layer and a flow dispersion layer made of silicone, and a porous polycarbonate membrane (Figure 1).

The top cover layer and the two silicone layers were patterned using the VersaLaser CO_2 laser cutter at CNF. The bottom PMMA channel layer was fabricated using photolithography and hot embossing. The channel layer pattern was first transferred from a photomask to SUEX epoxy thick dry film using a laminator and standard photolithography technique. A polydimethylsiloxane (PDMS) replica was then created from the SUEX master and was silanized under vacuum overnight. A heat resistant epoxy mold for hot embossing was then created from the silanized PDMS mold using a high-temperature epoxy casting system. The PMMA channel layer was fabricated using a hot press at CNF as shown in Figure 2. The molded PMMA plate was then cut with the VersaLaser to form the channel layer. The assembled device is transparent and allows for real time optical interrogation.

This five-chamber device is being used to study preclinical anti-leishmaniesis drug toxicity and response.

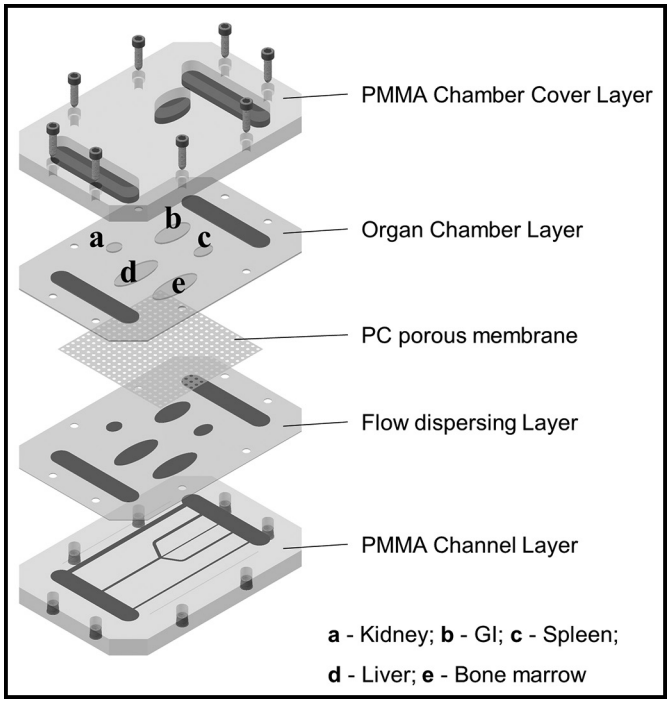

Figure 1: Design of the 5-compartment microphysiological system. Schematic exploded view of the microfluidic platform.

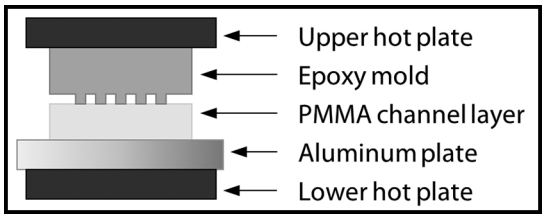

Figure 2: PMMA sheet and epoxy mold assembly for PMMA channel layer fabrication using hot embossing.

References:

[1] NIH/NCATS. What are tissue chips, and why are they important? https://ncats.nih.gov/tissuechip/about/faq#chips.

[2] Wang YI, Carmona C, Hickman JJ, Shuler ML. Multiorgan Microphysiological Systems for Drug Development: Strategies, Advances, and Challenges. Adv Healthc Mater. 2018;7(2):1701000. doi:10.1002/adhm.201701000.

[3] Price PS, Conolly RB, Chaisson CF, Gross EA, Young JS, Mathis ET, Tedder DR. Modeling interindividual variation in physiological factors used in PBPK models of humans. Crit Rev Toxicol. 2003;33(5):469-503. doi:10.1080/713608360.

[4] Brown RP, Delp MD, Lindstedt SL, Rhomberg LR, Beliles RP. Physiological Parameter Values for Physiologically Based Pharmacokinetic Models. Toxicol Ind Health. 1997;13(4):407-484. doi:10.1177/074823379701300401.

[5] Forrester DW, Spence VA, Walker WF. The measurement of colonic mucosal.submucosal blood flow in man. J Physiol. 1980;299(1):1-11. doi:10.1113/jphysiol.1980.sp013106.

[6] Wang YI, Oleaga C, Long CJ, Esch MB, McAleer CW, Miller PG, Hickman JJ, Shuler ML. Self-contained, low-cost Body-on-a-Chip systems for drug development. Exp Biol Med. 2017;(November):153537021769410. doi:10.1177/1535370217694101.

[7] Sung JH, Kam C, Shuler ML. A microfluidic device for a pharmacokinetic–pharmacodynamic (PK-PD) model on a chip. Lab Chip. 2010;10(4):446. doi:10.1039/b917763a.

Micropillar-Based Microfluidic Device for Cell Capture and DNA Analysis

CNF Project Number: 762-99

Principal Investigator: Harold G. Craighead

User: Harvey C. Tian

Affiliation: Applied and Engineering Physics, Cornell University, Ithaca

Primary Source of Research Funding: Cornell University

Contact: hgc1@cornell.edu, hct33@cornell.edu

Primary CNF Tools Used: Unaxis, ABM contact aligner, photoresist spinning and baking stations

Abstract:

We present a valveless dual-channel microfluidic device for targeted cell capture, imaging, and on-chip DNA analysis. The two channels are positioned with a perpendicular intersection filled by an array of micropillars. These micropillars are functionalized with DNA aptamers, analogous to antibodies, which are used to bind targeted cells such as cancer cells. These bound cells can then be imaged in place or lysed to extract their DNA for further analysis. Our past work has demonstrated high efficiency DNA extraction using micropillar arrays from varying cell counts (hundreds) down to a single cell [1] as well as an improvement to DNA amplification uniformity as compared to conventional methods. Here, we sought to integrate the various capabilities published in our previous work into a single device. We report the device's ability to perform cancer-cell specific capture with the DOV4 aptamer as well target-specific isothermal amplification [2]. Furthermore, we expanded upon our previous year's DNA amplification work to show an improved amplification uniformity in single cell whole genome amplification as measured by exome sequencing. We report a 33.5% improvement in genome mapping and up to 81.08% genome coverage at 10x read depth [3].

Summary of Research:

The dual-channel device shown in Figure 1 is composed of two perpendicularly intersecting microfluidic channels. One channel is designed for cell loading and surface functionalization of micropillars while the other channel is designed for DNA lysis. The intersection of the two channels, shown in Figure 1 (left panel), contain an array of 50 μm diameter pillars rotated 4° to increase cell-pillar collision rates during cell capture. These capture cells are then lysed towards the direction of a second pillar array region consisting of densely spaced 1.5 μm diameter pillars, shown in Figure 1 (right panel).

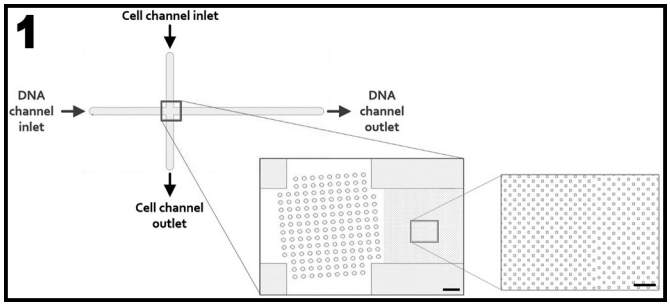

Figure 1: Dual-channel device.

Through functionalizing the 50 μm diameter pillars with DNA aptamer DOV4 which has been reported as a cancer-cell specific aptamer [4], we were able to capture two cancer cell lines tested, HeLa human cervical cancer cell line and CAOV-3 human ovarian cancer cell line. Our positive controls, performed with human non-cancer ovarian cell lines Ect1/E6E7 and End1/E6E7 did not bind to the DOV4 micropillars indicating successful aptamer driven cell capture. Figure 2 then shows our ability to lyse the captured cells, in this case CAOV-3 cells, and stain and image the DNA in-channel.

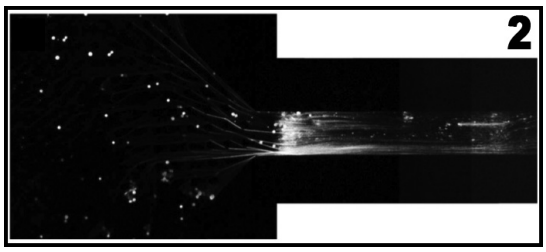

Figure 2: Shows our ability to lyse the captured cells, in this case CAOV-3 cells, and stain and image the DNA in-channel.

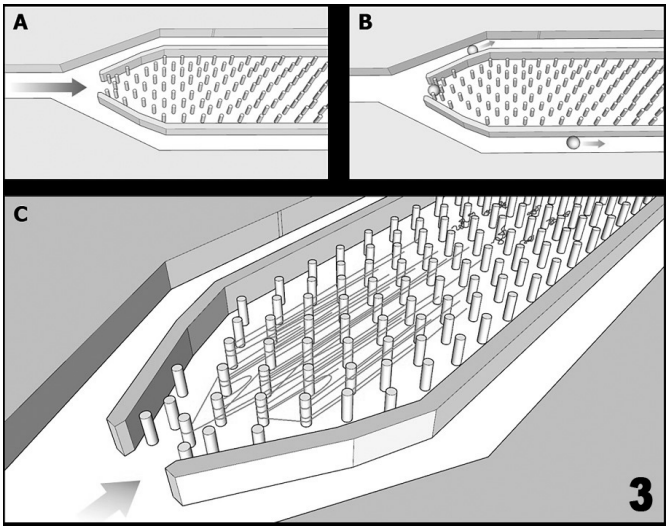

Figure 3: Cartoon of DNA amplification device.

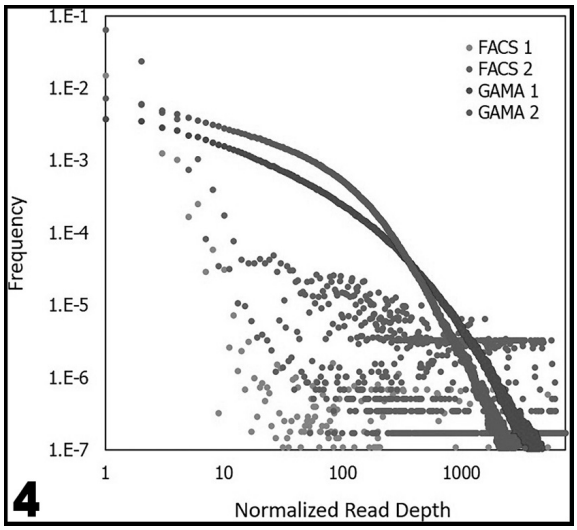

Figure 4: Two on-chip single cell samples.

Our DNA amplification device, as depicted by the cartoon representation in Figure 3(A), contains a micropillar array region enclosed by a barrier. At the front of the barrier is an opening wide enough to fit a single cell. In Figure 3(B), a suspension of human cervical cancer cells (HeLa cells) are loaded into the input single cells were captured at the apex of the micropillar array while excess uncaptured cells flow through to the output ports where they were removed. Upon introducing a cell lysis agent into the channel Figure 3(C), the genonic DNA of entrapped cell become physically entangled on the micropillars immediately downstream from the original position of the cell and this gDNA can be used for in-channel chemistries such as DNA amplification or be directly imaged on-chip after fluorescence DNA staining.

The extracted gDNA can then be isothermally whole genome amplified on-chip using commercially available multiple displacement amplification (MDA) reagents. Because the amplified DNA fragments are below the size threshold necessary to become entangled upon the 2 μm diameter micropillars, they flow through the pillars and can be collected at the output port at the end of the amplification.

To assess amplification bias, we compared our amplified DNA pools to DNA amplified within a 96-well plate from single cell isolated through fluorescence activated cell sorting (FACS). From analyzing the exome sequencing data on more than 20,000 loci across the genome, we determined that we were able to map 98.5% of the reads from our on-chip samples whereas control samples with FACS only reached 65.0% reads mapped.

Shown in Figure 4, the two on-chip single cell samples show a slower decaying distribution of read count as depth increases indicating much more uniform amplification of the genome. Furthermore, we were able to cover 70.35% of the loci with a 1x read depth and 80.8% of the loci with a 1x read depth, comparable to other leading single cell DNA amplification technologies.

References:

[1] "Microfluidic extraction, stretching and analysis of human chromosomal DNA from single cells", JJ Benitez, J Topolancik, HC Tian, CB Wallin, DR Latulippe, K Szeto, PJ Murphy, BR Cipriany, SL Levy, PD Soloway, HG Craighead, Lab Chip, (2012).

[2] "Microfluidic Device for Aptamer-Based Cancer Cell Capture and Genetic Mutation Detection", S. J. Reinholt, H. G. Craighead, Analytical Chemistry, (2018).

[3] "Single cell on-chip whole genome amplification via micropillar arrays for reduced amplification bias", H. C. Tian, J. J. Benitez, H. G. Craighead, PLOS One, (2018).

[4] "Study of the Molecular Recognition of Aptamers Selected through Ovarian Cancer Cell-SELEX", D. V. Simaeys, D. Lopez-Colon, K. Sefah, R. Sutphen, E. Jimenez, W. Tan, PLOS One, (2010).

The Number of SNARE Complexes Changing Conformation in Vesicle Fusion Events

CNF Project Number: 848-00

Principal Investigator: Manfred Lindau

Users: Ying Zhao, Qinghua Fang

Affiliations: 1. Applied and Engineering Physics, Cornell University; 2. Laboratory for Nanoscale Cell Biology, Max Planck Institute for Biophysical Chemistry, D-37077 Göttingen, Germany

Primary Research Funding: NIH Grant GM085808 (to M.L.) and, MH060600 (to W.A.), European Research Council Advanced Grant No. 322699 (to M.L.), NSF Grant ECS-0335765

Contact: ML95@cornell.edu, yz86@cornell.edu, qf24@cornell.edu

Primary CNF Tools Used: Heidelberg Mask Writer DWL2000, ABM Contact Aligner, Oxford 81 Etcher, Oxford PECVD, Dicing Saw - DISCO

Abstract:

The SNARE complex is a core component of the fusion nanomachine, and the zipping of SNARE complexes is thought to provide the force and energy to overcome the energy barrier for membrane fusion. Here, the SNARE Complex REporter2 (SCORE2), a FRET probe of SNAP25, was overexpressed to detect the SNARE complex conformation change during the membrane fusion. Time and location of individual fusion events were detected using microfabricated ElectroChemical Detector (ECD) arrays. Our studies show, under endogenous condition, there are approximately seven (26% of 26.4) endogenous SNAP25 molecules change the conformational during the membrane fusion.

Summary of Research:

In previous studies, we have detected a SNARE conformational change preceding the fusion pore opening [1] in SCORE2 overexpressing SNAP25 KO mouse chromaffin cells. *In vitro* studies [2] have shown that SCORE2 molecules can exhibit the highest FRET efficiency in the presence of excess syntaxin and synaptobrevin 2 by forming the SNARE core complex. In our *in vivo* experiments, the low FRET efficiency of SCORE2 was determined in SCORE2-alone overexpressing. To estimate the *in vivo* high SCORE2 FRET efficiency, SCORE2 were co-expressed with high level of syntaxin by introducing IRES in the transfection construct. By photobleaching the FRET acceptor Venus in both, the low and the high FRET states, the $FRET_{high}$ and $FRET_{low}$ efficiencies were determined as 0.38 (E_{high}) and 0.21(E_{low}), respectively.

The FRET ratio R can be expressed as a simplified function of FRET efficiency E [2].

$$R = A + B \times \frac{E}{1-E} \quad (1)$$

The measured FRET ratios in the low and high FRET states are R_{low} = 1.01 and R_{high} = 1.85, respectively. Based on the values of $E_{low,high}$ and $R_{low,high}$, the coefficients A and B are calculated as 0.37 and 2.42, respectively.

The pre- and post-fusion FRET ratios at the fusion sites R = 1.066 and R = 1.184 [1] correspond to pre- and post-fusion FRET efficiencies of 0.223 and 0.252, respectively, indicating a FRET efficiency increase preceding vesicle fusion within a in a 0.1 μm^2 area surrounding the fusion site. Assuming that the different apparent FRET efficiencies reflect different fractions of SCORE2 molecules in the two distinct FRET states, the fluorescence intensity ratio becomes

$$R = A + B \times \frac{E_{low}+\alpha\times(E_{high}-E_{low})}{1-[E_{low}+\alpha\times(E_{high}-E_{low})]} \quad (2)$$

where α is the fraction of molecules in the high FRET state. The fraction α can be calculated from the apparent FRET efficiency

$$E_{app} = E_{low} + \alpha \times (E_{high} - E_{low}),$$

$$a = \frac{E_{app}-E_{low}}{E_{high}-E_{low}} \quad (3)$$

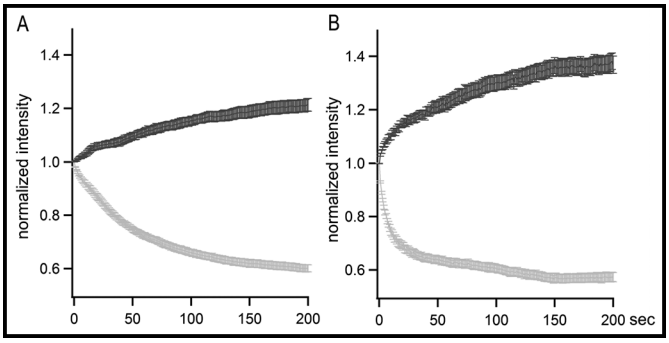

Figure 1: Determination of FRET efficiency by acceptor photobleaching. SCORE2 molecules alone (A) or with 10-fold higher Syntaxin (B) were overexpressed in SNAP25$^{-/-}$ mouse embryonal chromaffin cells and alternately excited for 100 ms at 442 nm in laser TIRF mode while images were acquired and for 1s with epifluorescence lamp excitation at 510/20 nm to bleach the acceptor. Intensities of Venus and mCerulean3 recorded from individual cells were normalized to the respective values before bleaching and the averaged increase in the mCeruleans3 channel indicates an average basal and high FRET efficiency of 21% and 38%, respectively.

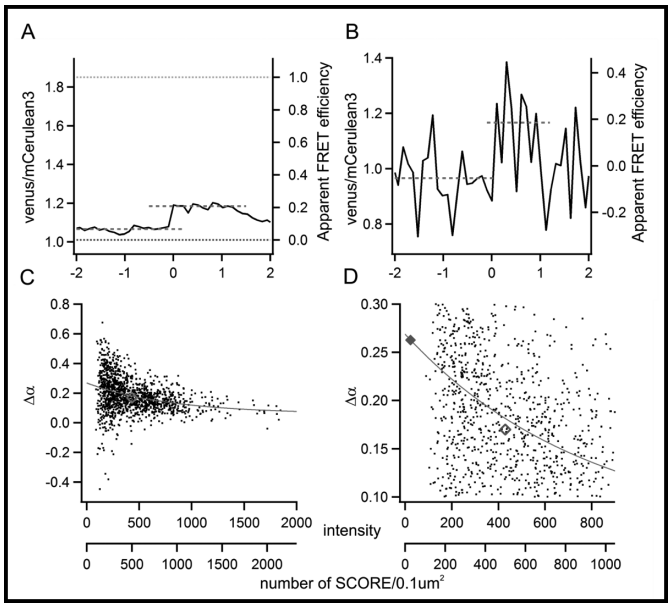

Figure 2: The fraction of SNAP25 molecules undergoing a conformational change as a function of expression level. FRET efficiency changes of all averaged fusion events (A) and of a single event (B), FRET ratio and corresponding apparent FRET efficiency before and after the fusion indicated by red dotted lines. (C-D) plots of Δα of individual events versus corresponding mCerulean3 intensities fitted by a single exponential (continuous red line). The open and filled red diamonds indicate the averaged Δα at average overexpression level and endogenous SNAP25 level, respectively.

According to equation (3), pre and post-function FRET efficiencies of 0.227 and 0.259 correspond to a value of α 0.076 and 0.247 (Figure 2A), suggesting that ~ 17% ($\Delta\alpha = E_{app,post} - E_{app,pre}$) of the SCORE2 molecules undergo a conformational transition from the low FRET state to the high FRET state just before fusion. With 500 SCORE2 molecules present in the fusion area at typical overexpression levels (data not shown), this corresponds to 85 molecules.

Immunostaining shows, however, that the overexpression level of SCORE2 molecules was ~ 19 fold higher than the amount of wild type SNAP25 molecules in untransfected wt cells, suggesting that only ~ 26 endogenous SNAP25 molecules are present at the vesicle fusion site.

To estimate the number of endogenous SNAP25 molecules undergoing conformational change during fusion, the change of α (Δα) was calculated for individual events (Figure 2B) and was plotted versus corresponding FRET donor (mCerulean3) intensities at releasing sites, indicating the expression level (Figure 2C).

Due to the low signal-to-noise ratio of individual events the points scatter widely (Figures 2C and 2D), but can be fitted well with a single exponential. In wild type cells we estimate ~26 SNAP25 molecules. Extrapolating the fit to this value, the Δα value of 0.26 is obtained, suggesting that on average, approximately seven endogenous SNAP25 molecules (26% of 26) undergo a conformational change before a fusion event.

References:

[1] Zhao Y., et al., SNARE conformational change precedes the fusion pore opening. CNF report 2017.

[2] An, S. J., and Almers, W. (2004) Tracking SNARE complex formation in live endocrine cells. Science 306, 1042-1046.

[3] Zhao, Y., Fang, Q., Herbst, A. D., Berberian, K. N., Almers, W., and Lindau, M. (2013) Rapid structural change in synaptosomal-associated protein 25 (SNAP25) precedes the fusion of single vesicles with the plasma membrane in live chromaffin cells. Proceedings of the National Academy of Sciences of the United States of America 110, 14249-14254.

Nanoneedles for Intracellular Measurements

CNF Project Number: 900-00

Principal Investigator: Paul L. McEuen

Users: Samantha Norris, Yanxin Ji, Alejandro Cortese

Affiliations: Department of Physics, Department of Electrical and Computer Engineering; Cornell University

Primary Source of Research Funding: Multi-University Research Initiative Grant FA2386-13-1-4118

Contact: plm23@cornell.edu, sn588@cornell.edu, yj323@cornell.edu, ajc383@cornell.edu

Website: http://www.mceuengroup.lassp.cornell.edu/

Primary CNF Tools used: Odd/even evaporators, Oxford 81 and 100 reaction ion etchers, ABM contact aligner, AJA sputter tool

Abstract:

The ability to measure a cell's membrane potential is crucial to understanding many cellular characteristics such as excitability, intracellular kinetics, and networking behavior. We report on the fabrication of releasable nanoneedle devices for insertion into a cell.

Summary of Research:

Sharp electrode intracellular recording is a standard technique involving piercing the cellular membrane with a micropipette filled with conductive fluid; this micropipette typically has a sub-micron diameter [1].

To more readily investigate the size-scale at which needle insertion can damage or kill cells, we have produced nanoneedle devices that can be released from a substrate, picked up with a micromanipulator, and inserted into cells. Each fabrication layer in the process uses standard photolithographic techniques and all layers are exposed with the ABM contact aligner. The final device before release is depicted in Figure 1.

Devices were fabricated on silicon-on-insulator wafers (SOI) allowing for release of the completed unit after fabrication. The nanoneedles protruding out of the end of the device were made by e-beam evaporation of platinum with a titanium adhesion layer (Ti-Pt) at a 70° angle, to allow for a nanoneedle width smaller than the minimum pattern width achievable with the contact aligner. A scanning electron microscope (SEM) image of a nanoneedle is shown in Figure 2.

After patterning of aluminum release tabs, the Xactix xenon difluoride etcher was then used to etch the silicon handle, resulting in suspended devices. The aluminum was then selectively etched to release the nanoneedle devices into solution. Free-floating devices could then be pipetted up using a standard hand pipette, and dispersed into fluid.

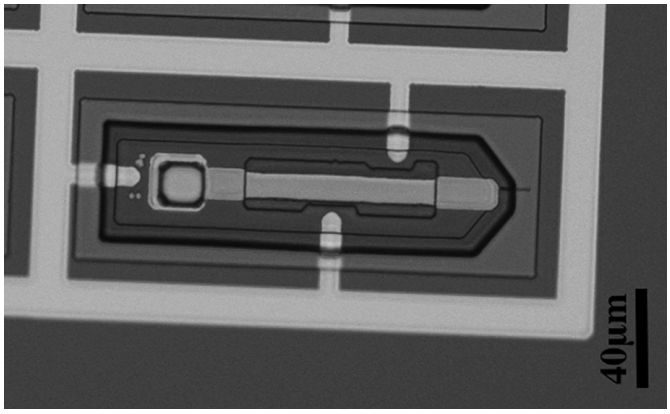

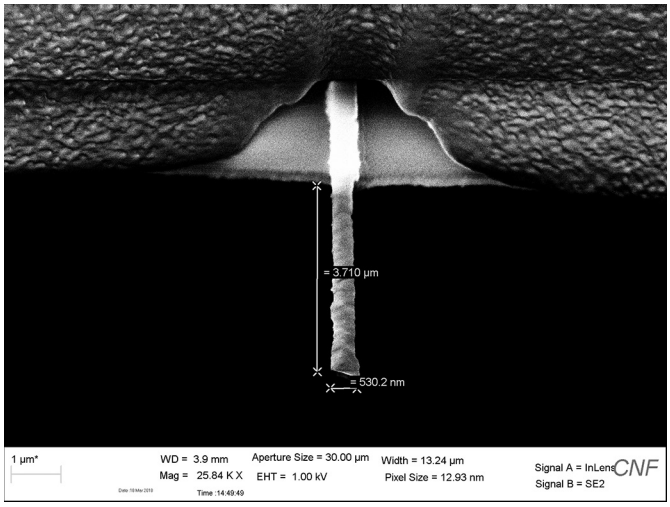

Figure 1, top: *An optical microscope image of a completed nanoneedle device.* ***Figure 2, bottom:*** *An SEM image of a typical nanoneedle after evaporation.*

Although devices survive the full process with remaining nanoneedles, the xenon difluoride etching the oxide under the needles and the pipetting force used cause many needles to break off.

To test the ability of our devices to penetrate the cellular membrane without causing cell death, we cultured HL-1 cardiomyocytes in Petri® dishes. When the cells were approaching confluence, we used a pipette to disperse the nanoneedle devices into the cell media. To monitor cell health while performing experiments, a green fluorescent protein (GFP, Cal-520 AM) was used for concurrent calcium imaging. If the cell membrane is punctured irreparably, the GFP will cause the cell to fluoresce as the calcium present in the surrounding fluid enters the cell.

The nanoneedles devices were then manipulated either by poking into the SU-8 encapsulation layer with a microprobe or using a small micropipette under vacuum to create enough suction to lift the device. Using a micromanipulator, the devices' protruding nanoneedle could then be controllably forced into a cell. In Figure 3, we show a nanoneedle device being manipulated by micropipette suction. The white regions of the cell indicate fluorescence of the GFP. The cell continues to spontaneously blink indicating that the cell has not died; however, the white region near the nanoneedle indicates that membrane penetration may have taken place. The fabrication of an exposed platinum pad at the end of the device opposite the nanoneedle in theory allows for electrical contact to determine whether the nanoneedle is inside, but the large ratio between the surface area of the pad and the surface area of the nanoneedle means that the nanoneedle must have an excellent seal with the membrane to detect the penetration electrically. Further experiments and improvements to the nanoneedle fabrication are being investigated.

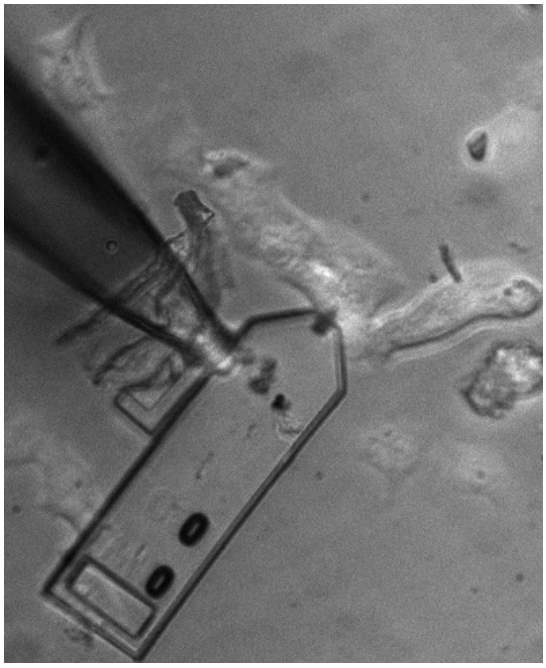

Figure 3: A nanoneedle device being manipulated to puncture a cardiomyocyte.

References:

[1] Yang, R., et al. Investigation of penetration using atomic force microscope: potential biomarkers of cell membrane. IET Micro and Nano Letters 10 (2015).

MoS_2 Pixel Sensors for Optical Detection of Redox Molecules

CNF Project Number: 900-00

Principal Investigators: Paul L. McEuen[1,2], Jiwoong Park[3], Daniel C. Ralph[4]

Users: Michael F. Reynolds[1], Marcos H.D. Guimarães[1,2], Hui Gao[3,5], Kibum Kang[3,5], Alejandro J. Cortese[1]

Affiliations: 1. Laboratory of Atomic and Solid State Physics, 2. Kavli Institute at Cornell for Nanoscale Science, 3. Department of Chemistry and Chemical Biology, 4. Department of Physics; Cornell University, Ithaca NY: 5. Department of Chemistry, Institute for Molecular Engineering, and James Franck Institute, University of Chicago, Chicago IL

Primary Sources of Research Funding: Cornell Center for Materials Research with funding from the NSF MRSEC program (DMR-1719875), Air Force Office of Scientific Research (AFSOR) multidisciplinary research program of the university research initiative Grant FA2386-13-1-4118

Contact: plm23@cornell.edu, mfr74@cornell.edu

Primary CNF Tools Used: Autostep i-line, ABM contact aligner, SC4500 evaporator, Oxford 81 etcher, VersaLine etcher

Abstract:

Spatially-resolved detection of redox molecules in solution is important for understanding chemical and biological systems. Optical detection is advantageously wire-free and easily multiplexed. We demonstrate that monolayer molybdenum disulfide (MoS_2) is a fast, sensitive, optical sensor for redox molecules.

Summary of Research:

Redox molecule detection has applications from detection of neurotransmitters in the brain to trace chemical detection in water samples. Traditional techniques, such as cyclic voltammetry, provide sensitive detection at a single electrode, but do not spatially resolve the variation in redox concentration. More advanced approaches including multiplexed electrode arrays [1,2] and numerous optical detection techniques [3-6] allow researchers to image redox molecules.

We demonstrate a wireless, optical approach for fast, sensitive redox imaging using a flexible, transferrable monolayer of MoS_2. MoS_2 photoluminesces at about 650 nm [7], with an intensity that increases as the concentration of electrons on the MoS_2 decreases, as shown by back-gating [8] and chemical doping [9].

We use the doping dependence of MoS_2 photoluminescence (PL) to detect ferrocene/ferrocenium as a test redox couple. Metal-organic chemical vapor deposition MoS_2 samples [10], grown by Prof. Park's group, are patterned with a two-step fabrication process. First, we pattern contact pads on the MoS_2 with electron-beam evaporation. Second, we etch away the MoS_2 to define our device and pixel geometries, which are shown in Figure 1.

We performed two experiments to demonstrate that our MoS_2 pixel sensors measure the chemical potential of the solution. First, with a fixed total concentration of ferrocene/ferrocenium, we varied the ratio of the concentration of ferrocenium (Fc+) to ferrocene (Fc) in our solution while monitoring the PL of the MoS_2 (Figure 2A). The MoS_2 shows a marked increase in PL as Fc+/Fc increases. Second, in a solution without any ferrocene or ferrocenium, we apply a potential to the solution (denoted V_{LG} for liquid gate voltage) while grounding a contacted MoS_2 device. The PL is high at negative values for V_{LG}, but decreases as V_{LG} is swept to positive values (Figure 2B, red curve). We compare the PL *versus* liquid gate voltage to PL *versus* change in chemical potential, where the change in chemical potential of the solution is given by

$$\Delta\mu = \frac{k_B T}{e} \ln \frac{[Fc]}{[Fc+]},$$

according to the Nernst equation (Figure 2B, blue dots). The good agreement between the two curves indicates that the PL of electrically floating pixels is set by the chemical potential of the solution.

Having characterized the MoS_2 sensors, we measure diffusion to demonstrate their speed and spatial resolution. We apply a voltage pulse to a microelectrode positioned above our MoS_2 pixel array in a solution of 1 mM ferrocene. The pulse oxidizes ferrocene to ferrocenium, which diffuses away from the probe tip, creating a spreading ferrocenium concentration that is imaged by the MoS_2 pixels (Figure 3). From these data, we extract a ferrocenium diffusion constant of about 1.8×10^{-9} m^2/s, matching previous measurements [11].

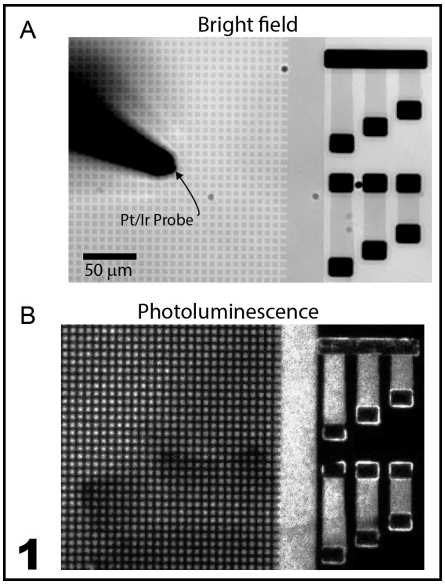

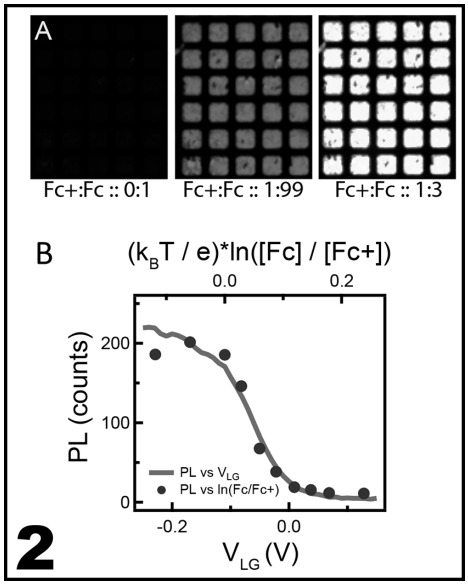

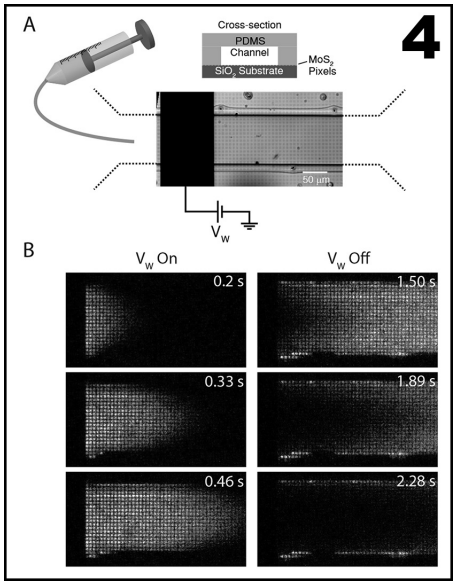

Figure 1, left: *A, Bright-field and B, PL (549 nm excitation, 650 emission) images of MoS_2 pixels and devices.* ***Figure 2, middle:*** *A, PL images of MoS_2 with varied ferrocenium/ferrocene ratios, showing increased PL with increased ferrocene concentration. B, PL versus liquid gate voltage for grounded device (red line) and versus solution chemical potential (blue dots), showing that MoS_2 sensors are Nernstian.* **Figure 4, right:** *A, Schematic and bright-field image showing PDMS microfluidic channel placed over MoS_2 pixel array. A pulse on the surface electrode oxidizes ferrocene to ferrocenium while a syringe pump flows the solution through the channel. B, MoS_2 PL imaging flow of ferrocene in the channel.*

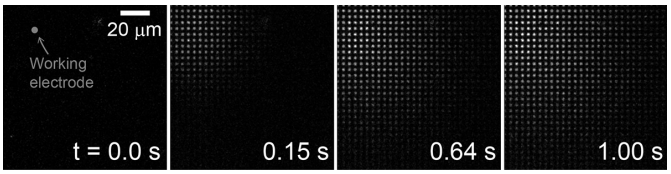

Figure 3: Frames from PL video imaging diffusion of ferrocenium away from a microelectrode after its potential is pulsed to 0.8 V versus the solution potential.

Finally, we use these sensors to image the flow of redox molecules in microfluidic channels. We mold polydimethylsiloxane (PDMS) microfluidic channels using silicon wafer masters patterned with the Plasma-Therm deep silicon etcher and place them over MoS_2 pixel arrays with platinum surface electrodes (Figure 4A). While flowing a ferrocene solution through the channel, we applied voltage pulses to the surface electrodes to oxidize ferrocene to ferrocenium and image laminar flow of the solution in MoS_2 PL (Figure 4B). These experiments show that MoS_2 can be used for real-time, spatially resolved imaging of redox molecules. The sensor could be improved by increasing the quantum efficiency of the MoS_2 PL in solution. In the future, these sensors could find applications in biological sensing experiments, e.g. spatially resolved detection of dopamine efflux from neurons.

References:

[1] J. Wang, R. Trouillon, Y. Lin, M. I. Svensson, A. G. Ewing, Individually Addressable Thin-Film Ultramicroelectrode Array for Spatial Measurements of Single Vesicle Release. Anal. Chem. 85, 5600–5608 (2013).

[2] D. L. Bellin, et al., Electrochemical camera chip for simultaneous imaging of multiple metabolites in biofilms. Nat. Commun. 7, 10535 (2016).

[3] X. Shan, U. Patel, S. Wang, R. Iglesias, N. Tao, Imaging local electrochemical current via surface plasmon resonance. Science. 327, 1363-6 (2010).

[4] A. Jane, R. Dronov, A. Hodges, N. H. Voelcker, Porous silicon biosensors on the advance. Trends Biotechnol. 27, 230-239 (2009).

[5] S. Kruss, et al., High-resolution imaging of cellular dopamine efflux using a fluorescent nanosensor array. Proc. Natl. Acad. Sci. U. S. A. 114, 1789-1794 (2017).

[6] D. G. Hafeman, J. W. Parce, H. M. McConnell, Light-Addressable Potentiometric Sensor for Biochemical Systems (available at http://science.sciencemag.org/content/sci/240/4856/1182.full.pdf).

[7] K. F. Mak, C. Lee, J. Hone, J. Shan, T. F. Heinz, Atomically Thin MoS_2: A New Direct-Gap Semiconductor. Phys. Rev. Lett. 105, 136805 (2010).

[8] K. F. Mak, et al., Tightly bound trions in monolayer MoS_2. Nat. Mater. 12, 207-211 (2013).

[9] S. Mouri, Y. Miyauchi, K. Matsuda, Tunable Photoluminescence of Monolayer MoS_2 via Chemical Doping. Nano Lett. 13, 5944-5948 (2013).

[10] K. Kang, et al., High-mobility three-atom-thick semiconducting films with wafer-scale homogeneity. Nature. 520, 656-660 (2015).

[11] Y. Wang, E. I. Rogers, R. G. Compton, The measurement of the diffusion coefficients of ferrocene and ferrocenium and their temperature dependence in acetonitrile using double potential step microdisk electrode chronoamperometry. J. Electroanal. Chem. 648, 15-19 (2010).

Silicon Nitride Cantilevers for Muscle Myofibril Force Measurements

CNF Project Number: 1255-04

Principal Investigator: Walter Herzog

Users: Timothy Leonard, Andrew Sawatsky

Affiliation: Faculty of Kinesiology, University of Calgary, Calgary, Canada

Primary Source of Research Funding: Natural Sciences and Engineering Research Council of Canada, Canadian Institutes of Health Research and the Canada Research Chair for Cellular and Molecular Biomechanics

Contact: wherzog@ucalgary.ca, leonard@ucalgary.ca, ajsawats@ucalgary.ca

Website: www.ucalgary.ca/knes

Primary CNF Tools Used: GCA 5X stepper, photolith spinners, Oxford 81 ion etcher

Abstract:

To measure muscle forces in the nano-Newton range, silicon nitride cantilever pairs were manufactured using the GCA 5x-stepper photolithography system and the Oxford 81 ion etching system at the CNF, and then used in our lab in Canada. We investigated titin mechanical properties using a skeletal muscle myofibril model. Our experiments demonstrate sarcomeres in skeletal muscle are not unstable when suddenly made weaker relative to the sarcomeres adjacent to them.

Summary of Research:

Muscle (the smallest functional unit being the sarcomere) generates active force through cyclic interactions between myosin and actin and the amount of active isometric force generated is proportional to the length of the sarcomere [1]. Passive forces in the sarcomere are also length dependent and are supported by the molecular spring-like protein titin [2]. Instability of sarcomeres has been proposed as a mechanism for injury in muscle since sarcomeres arranged in-series must sustain the same force along a myofibril and sarcomeres that are weaker than adjacent ones are expected to over-lengthen since there is a disparity in active force producing potential. This instability results in a sarcomere that is rapidly lengthened (termed "popping") until only passive structures (titin) sustain the in-series force, with damage occurring to that sarcomere [3]. The purpose of this study was to measure the length of each sarcomere in a single myofibril during activation and then follow these sarcomeres with time as portions of the sample are deactivated to see whether weaker sarcomeres behave as predicted, and do in fact, over-lengthen.

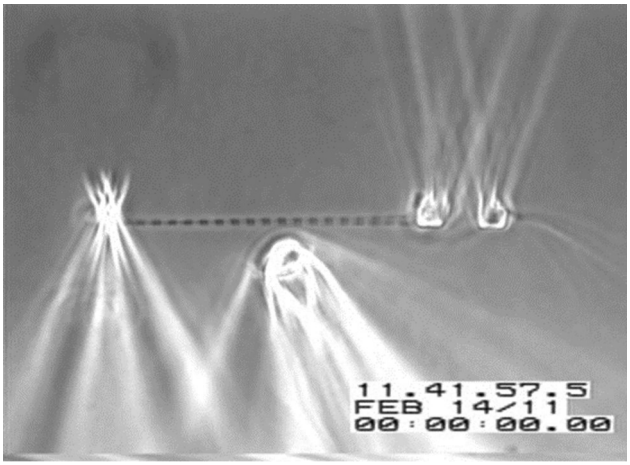

Figure 1: Myofibril attached to a glass needle for stretch-shortening and cantilevers for force measurement. An example of a single myofibril with 19 sarcomeres in-series. The glass tube (center) is used to deliver a focused stream of deactivating solution.

Methods:

Skeletal muscle myofibrils were generated using rabbit psoas muscle as previously described in reference [4] and were placed in an experimental chamber atop an inverted microscope. Single myofibrils (n=6) were attached at one end to a glass needle/motor assembly for specimen length control and at the other end to a micro-fabricated silicon nitride cantilever pair (68 nN/μm stiffness) for measuring force. High-resolution (88 nm per pixel) video data (30 fps) were collected continuously during the experiment and analyzed using custom MATLAB

analysis code. The myofibril was initially in a relaxed state and the myofibril length adjusted to an average sarcomere length (SL) of approximately 2.4 μm. Then the Ca+2 rich activating solution was delivered and once the myofibril was fully activated, a second stream of relaxing solution was targeted to the left side of the myofibril (Figure 1). This resulted in a wave of deactivation that started at the left and propagated rightward until it encompassed the entire myofibril, and the myofibril returned to the relaxed state.

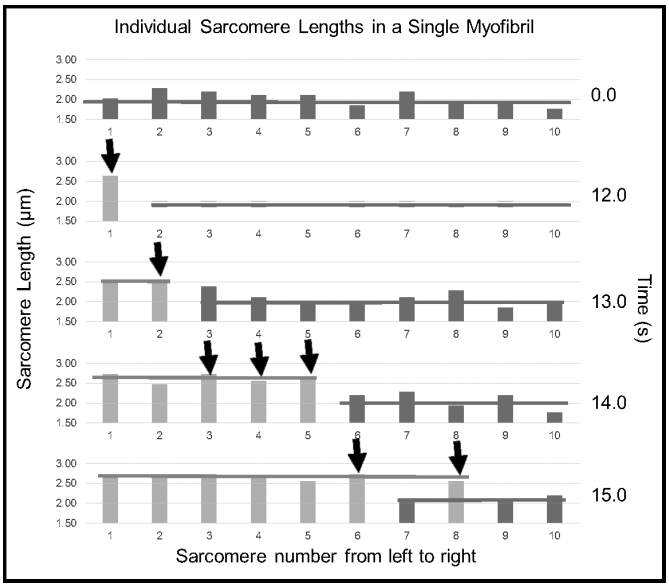

Figure 2: Sarcomere length in an activated myofibril as a wave of deactivation solution moves from left to right. Black arrows highlight activated sarcomeres (dark grey) that transition rapidly to passive (light grey). Dark grey and light grey horizontal bars indicate the mean SL for sarcomeres belonging to groups classified as active or passive.

Results and Discussion:

In Figure 2, for one typical experiment, the mean SL upon activation was 2.1 μm and the stress measured (not shown) was 209 nN/μm^2. The infusion of the localized stream of relaxing solution at time-point 12s resulted in the first sarcomere (sarcomere #1) rapidly lengthening from a SL of 2.47 μm to 2.65 μm. At 13s, the next sarcomere (#2) lengthened from 2.21 μm to 2.47 μm and at 14s, #3 lengthens from 2.29 μm to 2.74 μm. At time point 15s, more than half of the sarcomeres have relaxed, the total stress is 110 nN/μm^2 and the mean relaxed SL (light grey horizontal line; Figure 1) is 2.65 μm and the remaining active sarcomeres have a mean SL of 2.15 μm (dark grey horizontal line). At time 15s, seven sarcomeres out of ten have lengthened from their initial active length and are positioned on the descending limb of the force-length relationship. Instability theory would predict these sarcomeres to over-lengthen. In fact, these deactivated sarcomeres would need to lengthen considerably if they were to passively support the 110 nN/μm^2 of stress still detected; A SL of near 4.0 μm would be required and passive force does not appear in this preparation until SL of about 2.8 μm. These passive sarcomeres are presumably sustaining this tension by titin alone, and in this example, with the titin stiffness being modulated so that a relaxed sarcomere at 2.6 μm can sustain the load.

Conclusions:

Weak (deactivated) sarcomeres do not "pop". We speculate that popping is prevented by a "stiffening" of the molecular spring titin. The mechanisms underlying this stiffening of titin need further elucidation.

References:

[1] Gordon, A.M., Huxley, A.F., Julian, F.J., 1966. The variation in isometric tension with sarcomere length in vertebrate muscle fibres. J. Physiol. 184, 170-192.

[2] Trombitas, K., Greaser, M., Labeit, S., Jin, J.-P., Kellermayer, M.S.Z., Helmes, M., Granzier, H.L.M., 1998. Titin extensibility in situ: entropic elasticity of permanently folded and permanently unfolded molecular segments. J. Cell Biol. 140, 853-859.

[3] Morgan, D.L., 1990. New insights into the behavior of muscle during active lengthening. Biophys. J. 57, 209-221.

[4] Joumaa, V., Rassier, D.E., Leonard, T.R., Herzog, W., 2008. The origin of passive force enhancement in skeletal muscle. Am. J. Physiol. Cell Physiol. 294, C74-78. https://doi.org/10.1152/ajpcell.00218.2007.

DNA Unzipping by Resonator-Based nSWATs

CNF Project Number: 1738-08

Principal Investigator: Michelle D. Wang

User: Fan Ye

Affiliations: a) Department of Physics, Cornell University; b) Howard Hughes Medical Institute, Chevy Chase, Maryland

Primary Source of Research Funding: Howard Hughes Medical Institute

Contact: mdw17@cornell.edu, fy72@cornell.edu

Website: http://wanglab.lassp.cornell.edu/

Primary CNF Tools Used: ASML deep uUV stepper, Oxford 100 plasma etcher, Unaxis 770 deep Si etcher, Heidelberg mask writer DWL2000, SÜSS MA6-BA6 contact aligner, Gamma automatic coat-develop tool, LPCVD nitride - B4 furnace, wet/dry oxide - B2 furnace, AJA sputter deposition, CVC sputter deposition, GSI and Oxford PECVD, SC4500 odd-hour evaporator, Zeiss Supra and Ultra SEM

Abstract:

A nanophotonic trapping platform based on chip-based tunable optical interference allows parallel processing of biomolecules and holds promise to make single molecule manipulations and precision measurements more easily and broadly available. The Wang lab has developed and implemented such an on-chip device based on Si or Si_3N_4 waveguides, coined a nanophotonic standing-wave array trap (nSWAT), that allows for controlled and precise manipulation of trapped nano/micro particle arrays [1-4]. We present here the latest generation of nSWAT devices that contains the following features: (1) local force enhancement are achieved by a resonator-based design; (2) response time of the phase modulation heaters are drastically shortened by a balanced and differential micro heater design; and (3) the thermal drifts of the whole device due to local heating of micro heaters are diminished by a novel sample holder design and cleaver micro heater re-arrangement. With all these crucial improvements, we have for the first time successfully unzipped DNA molecules on an nSWAT device. This is a benchmark achievement, making the nSWAT devices much more relevant in the single molecule field.

Summary of Research:

Optical trapping is a powerful manipulation and measurement technique widely employed in the biological and materials sciences. Miniaturizing bulky and expensive optical trapping instruments onto optofluidic platforms holds promise for high throughput lab-on-chip applications that can be readily integrated with other novel lab-on-chip innovations such as fluorescent detectors or on-chip lasers.

Recently, we have demonstrated a high-throughput, near-field nanophotonic trapping platform that achieved stable trapping with precision controllable repositioning [1-4]. The core concept of the platform is nanophotonic standing-wave interferometry, where laser light travels through a nanophotonic waveguide, is split into two equal intensity laser beams, the two beams are guided by the waveguides and meet each other, which ultimately leads to interference of two counter-propagating laser beams and results in the formation of standing waves. The evanescent field of the antinodes of the standing wave forms an array of stable three-dimensional optical traps. We call this type of trap a nanophotonic standing-wave array trap (nSWAT). By tuning the phase difference between the two counter-propagating laser beams, the antinode locations can be precisely repositioned, and consequently, the optical trap positions can be precisely manipulated. The nSWAT device holds the capability for high throughput precision measurements on-chip.

In the past year, we have advanced the nSWAT concept in several aspects. (1) We have implemented a resonator-based design for ultimate local intensity enhancement into the nSWAT devcies. Among all designs, this resonator design gives the highest force enhancement factor, limited only by the total scattering loss of the trapped beads onto the waveguide. We have measured around three times force enhancement, larger than our previous force-double design [4]. (2) We have implemented a balanced layout and differential operation mode for the micro heaters. This greatly reduced the response time of the micro heaters (from ~30 μs to ~1 μs). This is shown to be crucial for maintaining high trapping forces for a

trapped bead under strong biased forces under single molecule manipulations. (3) We have also designed a special sample holder for the nSWAT chip that can greatly reduce (by two orders of magnitude) the thermal drift of the sample caused by the micro heaters. This greatly enhanced the thermal stability of the nSWAT devices.

Thanks to the above described improvements, we have achieved DNA unzipping on the nSWAT devices for the first time. We are currently preparing a manuscript on these latest advancements on the resonator based nSWAT devices.

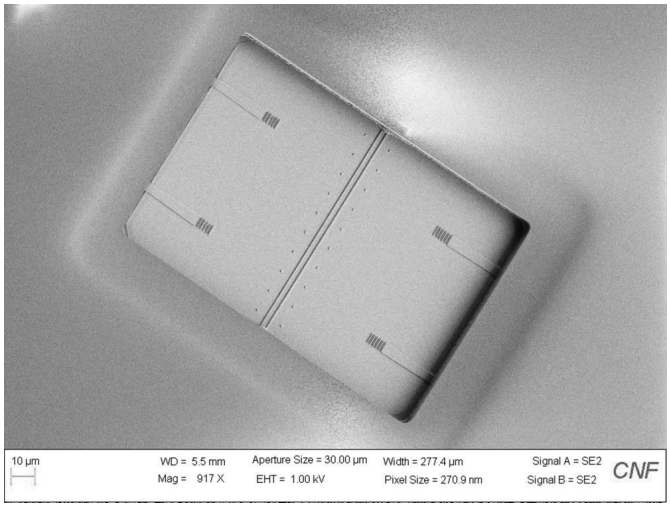

Figure 1: A tilted SEM image of the active trapping waveguides in the fluid pool region (big rectangle) of the latest resonator based nSWAT devices. The two parallel Si_3N_4 waveguides cut through the fluid pool in the middle, with two adjacent arrays of circular dots serving as local fiducial for real time motion tracking for trapped beads. Under operation, two arrays of polystyrene nanospheres (with 380 nm diameter) are trapped onto the two parallel waveguides. DNA molecules attached between two beads on both waveguides can be manipulated and studied by controlling the beads on each waveguide independently. The four wider Si_3N_4 waveguides terminating with free-space coupling gratings are carefully designed local laser intensity indicators for the two trapping waveguides.

References:

[1] M. Soltani, J. Lin, R. A. Forties, J. T. Inman, S. N. Saraf, R. M. Fulbright, M. Lipson, and M. D. Wang, "Nanophotonic trapping for precise manipulation of biomolecular arrays," Nature Nanotechnology 9(6), 448-452 (2014).

[2] F. Ye, R. P. Badman, J. T. Inman, M. Soltani, J. L. Killian, and M. D. Wang, "Biocompatible and high stiffness nanophotonic trap array for precise and versatile manipulation," Nano Letters 16(10), 6661-6667 (2016).

[3] J. E. Baker, R. P. Badman, and M. D. Wang, "Nanophotonic trapping: precise manipulation and measurement of biomolecular arrays," WIREs Nanomed Nanobiotechnol. e1477 (2017).

[4] F. Ye, M. Soltani, J. T. Inman, and M. D. Wang, "Tunable nanophotonic array traps with enhanced force and stability," Optics Express 25 (7) 7907-7918 (2017).

Generalized Platform for Antibody Detection Immunosensor

CNF Project Number: 1757-09

Principal Investigator: Christopher K. Ober[1]

Users: Roselynn Cordero[1], Wei-Liang Chen[2]

Affiliations: 1. Department of Materials Science and Engineering,
2. Department of Chemistry and Chemical Biology; Cornell University

Primary Source of Research Funding: National Science Foundation

Contact: cko3@cornell.edu, rc634@cornell.edu, wc497@cornell.edu

Primary CNF Tools Used: ABM contact aligner, MVD 100

Abstract:

Immunosensors are diagnostic devices that convert specific antigen-antibody interactions, by means of a transducer, into an electrical signal. Immunosensors are very efficient, simple, affordable, and cost-effective point-of-care systems for medical diagnosis. Our study focuses on the use of polymer chemistry and photolithography to create a unique antibody detection platform. This immunosensor takes advantage of the antibody catalyzed water oxidation pathway (ACWOP) process, in which all antibodies catalyze the production of hydrogen peroxide that can be detected using a colorimetric assay. This report focuses on the fabrication of the platform that make up our immunosensor device.

Summary of Research:

Pandemic infectious diseases have affected many people throughout history, sometimes killing millions of people such as the Plague in 14th century Europe, and the flu. One of the most common methods of detecting such diseases is through antibody detection using a serological assay. In our group, Welch, et al., in 2014 developed an immunobiosensor based on patterned polymer brushes on gold, which demonstrated extremely high sensitivity (2pM) for the specific antibody [1]. This design took advantage of the excellent properties of poly(oligo(ethylene glycol) methacrylate) (POEGMA) polymer brushes by preventing non-specific adsorption and allowing the anchoring of the functional haptens [2].

With that in mind, we would like to improve this sensor by using colorimetric detection as the electrochemical signal in the original design was not as intuitive and required additional parameters complicating our immunosensor. This sensor consists of patterned poly (oligoethylene glycol methacrylate) (POEGMA) polymer brushes on a glass substrate that were polymerized using atom transfer radical polymerization (ATRP), surrounded by a photosensitizer that was functionalized onto the surface of the silica platform.

Photosensitizer is responsible for the production of singlet oxygen reacting with water to produce hydrogen peroxide. In the past, our group used a ruthenium-based photosensitizer that was electropolymerized on a gold surface. To enable an economic colorimetric design, we selected to utilize Rose Bengal rather than Ru(4-vinyl-4′-methyl-2,2′-bipyridine)3]$^{+2}$ as photosensitizer due to its high quantum yield (0.75)[3], low price and ease of anchoring.

The detection mechanism is based on antibody catalyzed water oxidation pathway (ACWOP)[4], which is the same as previous work in our group as shown in Figure 1.

The dimension requirement for the sensor is well above the micron level (150 μm line pattern), which could be easily achieved with 365 nm UV photolithography using the ABM contact aligner. The bottom-up patterning process suits this application better for the resulting structural integrity. Since we already know that the monolayer made of silane compounds is unable to completely block all the reactive sites on the silicon substrates, deposition of the second chemical species must be conducted while the photoresist is still present on the surface, otherwise, the mixed chemical species will show up in the pre-defined area.

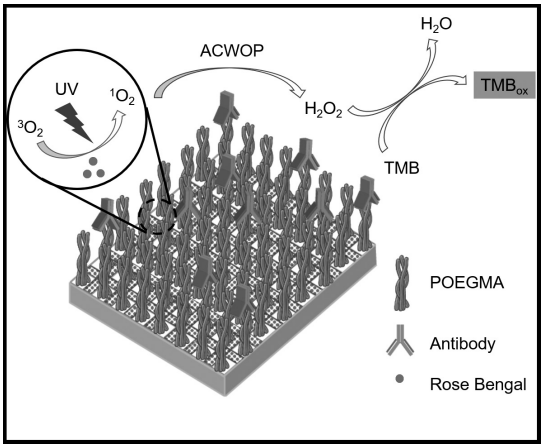

Figure 1: Detection mechanism for the proposed immunosensor. Under UV light exposure, singlet oxygen is formed by exciting Rose Bengal. Hydrogen peroxide is then produced through ACWOP. Hydrogen peroxide subsequently oxides TMB resulting in a change from clear to blue color for colorimetric readout. TMB: 3,3′,5,5′ tetramethylbenzidine.

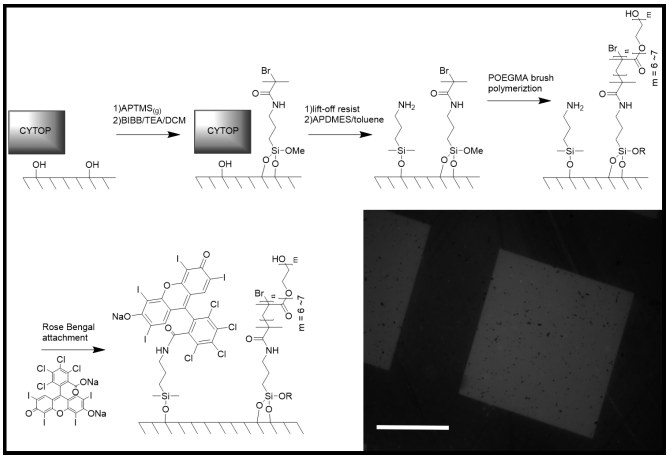

Figure 2: Process flow for the fabrication of the biosensor platform and the picture of the platform taken with a fluorescent microscope.

The CYTOP bottom-up patterning process was then applied to fabricate the functional surface. The fabrication process and results are shown in Figure 2. The 3-aminopropyltrimethoxysilane (APTMS) must be deposited before polymerization since it could also react with the hydroxy group on the POEGMA polymer brushes. This surface functionalization was done using the molecular vapor deposition tool (MVD100). However, it turned out that the Rose Bengal could still adsorb on the surface with POEGMA polymer brushes even though the amount is limited. This happened because an esterification reaction used for anchoring Rose Bengal on an amine could also anchor it on a hydroxy group.

To create more defined patterns, in the future other orthogonal reactions should be selected to anchor the compounds onto the surface. For example, 3-mercaptopropyltrimethoxysilane could be used instead of the APTMS to be the anchoring group, which could be reacted by a thiol-ene click reaction. Another issue that was encountered was that the Rose Bengal monolayer on the surface is not enough to trigger significant signal. Such problems may be further solved by using polymer brushes on the surface to provide more surface area for the anchoring of the Rose Bengal. If the thickness of the polymer brushes is high enough, the amount of the Rose Bengal could be increased to more than 100 times the amount grafted on the surface and this should be enough to create detectable signal. With the orthogonal anchoring chemistry for the functional groups and polymer brushes for Rose Bengal anchoring, this platform could be more applicable for fabrication and provide easy detection by colorimetric methods.

In conclusion, a CYTOP patterning process could be easily extended to other fields and enable better complex platform fabrication.

References:

[1] Welch, M. E., et al. Generalized Platform for Antibody Detection using the Antibody Catalyzed Water Oxidation Pathway. J. Am. Chem. Soc. 136, 1879-1883 (2014).

[2] Harder, P., Grunze, M., Dahint, R., Whitesides, G. M. and Laibinis, P. E. Molecular Conformation in Oligo(ethylene glycol)-Terminated Self-Assembled Monolayers on Gold and Silver Surfaces Determines Their Ability To Resist Protein Adsorption. J. Phys. Chem. B 102, 426-436 (1998).

[3] DeRosa, M. Photosensitized singlet oxygen and its applications. Coord. Chem. Rev. 233-234, 351-371 (2002).

[4] Wentworth Jr., P. Antibody Catalysis of the Oxidation of Water. Science 293, 1806-1811 (2001).

Development of a Salivary Microfluidic Diagnostic Device Using Hot Embossing

CNF Project Number: 1872-10

Principal Investigator: David Erickson

User: Elizabeth Rey

Affiliation: Sibley School of Mechanical and Aerospace Engineering, Cornell University

Primary Source of Research Funding: National Science Foundation

Contact: de54@cornell.edu, egr42@cornell.edu

Primary CNF Tools Used: Hot press, photolithography room, ABM contact aligner, Unaxis 770 deep Si etcher, Microdrill, Objet30 3D printer

Abstract:

Point of care diagnostic devices allow people to get fast, accurate information about their health and well-being without the need to go to a clinic or hospital. The device that we are designing will determine the concentration of cortisol from a sample of the user's saliva. Cortisol is a steroid hormone associated with stress levels and expressed in human saliva [1,2]. This microfluidic device contains a microbead-based immunoassay, which we are optimizing to determine the cortisol content from a saliva sample. The device is manufactured using a hot embossing process, which uses a silicon master made with traditional lithographic processes. The device is made from a thermoplastic called Zeonor 1020R, which is a transparent, semi-rigid plastic which can be used in large-scale manufacturing processes such as injection molding and hot embossing. Nearly all the fabrication of the device is being done in the Cornell NanoScale Facility.

Summary of Research:

The microfluidic device is made using a hot embossing process, which involves the high-temperature pressing of a mold into a piece of thermoplastic. The mold that we use in our process is made of silicon and is fabricated using photolithographic processes. The design for the mold is made using L-Edit and transferred to a photomask using the Heidelberg mask writer (DWL2000). This mask is then used to transfer a pattern to a photoresist on a silicon wafer. The photoresist (SPR-220-7.0) is spun onto a bare silicon wafer, which has been previously primed in the YES Vapor Prime Oven, to a thickness of approximately 7 μm. After spinning, the photoresist is soft baked on a 115°C hot plate for 2 minutes and 30 seconds. The wafer is allowed to sit for an hour and then exposed using the mask and the ABM contact aligner. The wafer is again allowed to sit for an hour and then is developed using the Hamatech Steag wafer processor. The pattern is now developed and can be used to etch the silicon wafer.

We etched the wafer using the Unaxis 770 deep Si etcher to a depth of 50 μm. We monitored the etch depth and etch rate using the P10 profilometer. Upon reaching the desired depth, we removed the photoresist in the chemical strip bath. We then used the Unaxis 770 again to deposit a thin layer of fluoropolymer onto the wafer in order to prevent sticking in the hot emboss process. Our masters are then ready to be used in the hot emboss process.

The hot emboss process uses the CRC Prepreg Mini Test Press, which applies heat and even pressure. The silicon master is adhered to a glass backing, for strength, and then the plastic piece is placed on top of the master, with another glass piece on top of that. This whole stack is placed in the hot press once the hot press reaches the desired temperature and pressed for several minutes. The setup is allowed to cool below the glass transition temperature of the plastic and then the pressure is released and the plastic is de-embossed. The pattern is transferred from the master to the plastic. We then drill through-holes in a blank piece of plastic using the custom-made micro drill.

In our own lab, we perform a photografting procedure to increase hydrophilicity of the Zeonor surfaces and improve bonding. This blank piece is then thermally bonded to the patterned piece to create the microfluidic device in the hot press. Our microfluidic device is now

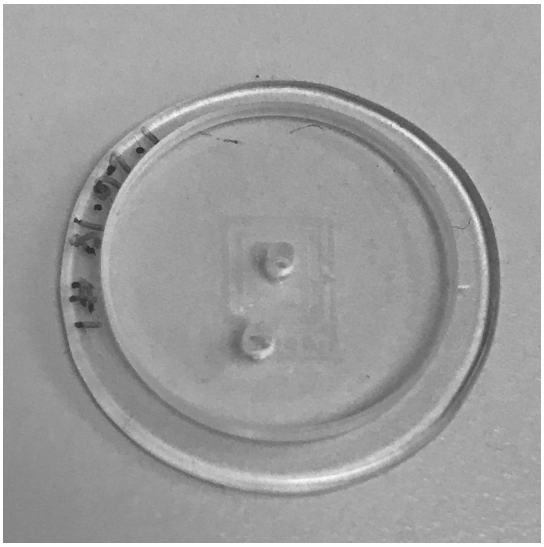

Figure 1: Image of completed microfluidic chip.

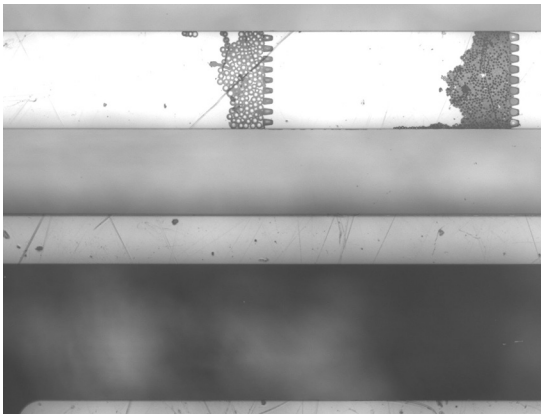

Figure 2: Microscope image of channels, pillars, and different sized bead zones.

Figure 3: Microscope image of fluorescence on beads after flowing of FITC through chip.

complete and ready to be turned into an immunoassay. An example can be seen in Figure 1.

We can now flow differently sized beads into the device to create areas for antibody-antigen-fluorophore interaction. The channels after the beads are successfully added can be seen in Figure 2. The differently-spaced pillars allow two zones with beads with different antibodies to be separated by size. We then flow fluid with cortisol and FITC-labeled antibodies through the device and measure the brightness of the fluorescence at the bead zones with a microscope or with our portable imaging device. A microscope image of the two bead zones with attached fluorophores can be seen in Figure 3.

The portable imaging device is a Raspberry Pi Zero W with a camera attached, fluorescent optics, a lithium-ion battery, LEDs, all assembled in a 3D-printed light-tight case. This case is printed using the Objet30 Pro 3D Printer, and can be seen with all parts assembled in Figure 4.

References:

[1] Kirschbaum C, Hellhammer DH. Salivary cortisol in psychoneuroendocrine research: recent developments and applications, Psychoneuroendocrinology, Volume 19, Issue 4, 1994, Pages 313-333.

[2] Umeda T, Hiramatsu R, Iwaoka T, et al. (1981). Use of saliva for monitoring unbound free cortisol levels in serum. Clin Chim Acta 110:245–253. doi: 10.1016/0009-8981(81)90353-3.

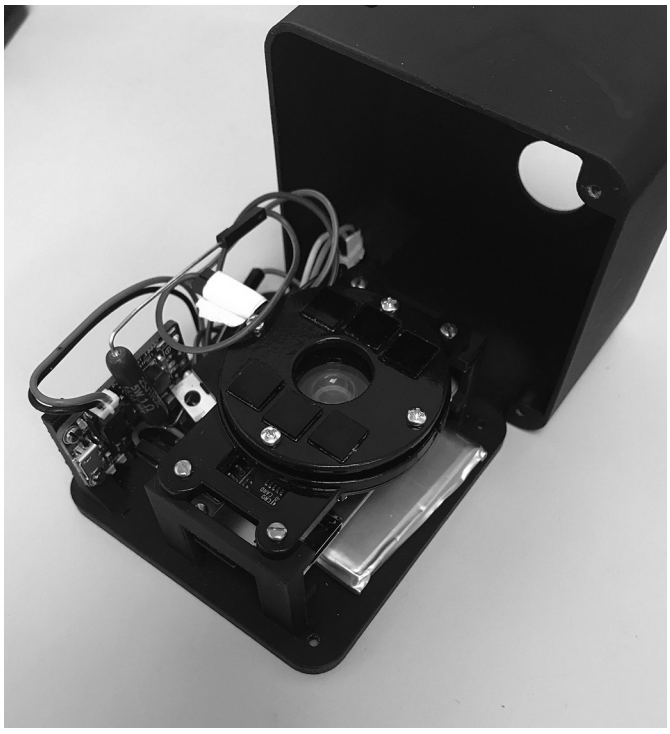

Figure 4: 3D-printed imaging device.

Rapid Detection of Antimicrobial Susceptibility at the Point-of-Care

CNF Project Number: 1872-10
Principal Investigator: David Erickson
User: Sasank Vemulapati

Affiliation: Sibley School of Mechanical and Aerospace Engineering, Cornell University
Primary Source of Research Funding: Atkinson Center Academic Venture Fund
Contact: de54@cornell.edu, sv379@cornell.edu
Primary CNF Tools Used: Objet 3D printer

Abstract:

The rise of antibiotic resistant bacteria poses a serious threat to the United States. In 2014 President Obama issued an Executive Order and the White House published the National Strategy for Combating Antibiotic Resistance [1,2]. This document describes: how as antibiotic resistance continues to increase "we will no longer be able to reliably and rapidly treat bacterial infections", how "drug choices have become increasingly limited and more expensive and, in some cases, nonexistent", and imagines a world in which "modern medical advances such as surgery, transplants, and chemotherapy may no longer be viable due to the threat of infection." Already the Centers for Disease Control and Prevention reports that each year in the US, at least two million people acquire bacterial infections resistant to one or more antibiotics and at least 23,000 people die each year as a result [3]. In this project we are working towards developing a point-of-care diagnostic test that can rapidly provide antibiotic susceptibility information bloodborne organisms causing bacteremia in about four hours following a short blood culture. The integrated sample-to-answer system is based upon two key technologies already demonstrated in our labs: rapid blood sample clean-up using magnetic nano-beads, and a capillary-based system that enhances our ability to monitor bacterial metabolic activity, significantly reduces the time required to determine the efficacy of a given antibiotic dose.

Summary of Research:

In our initial experiments, we have adopted a colorimetric phenotypic testing approach to assess the antibiotic susceptibility of an attenuated *E. coli* K12 strain. The pH indicator phenol red was used to provide a phenotypic indication of bacterial growth.

For our colorimetric phenotypic testing approach, we conducted bacterial growth tests with small sample volumes in a PDMS microchip. The *E. coli* strain with a kanamycin resistance gene as selection marker was first streaked and incubated overnight on LB agar plates containing kanamycin. Single colonies were subsequently picked and propagated in liquid bulk culture. Following overnight bulk culture to stationary phase, small volumes (~1uL) of culture were separately incubated on the PDMS chip in wells each containing a 19 μL mixture of fresh LB media, 0.05% phenol red, and the antibiotics kanamycin (control) and ampicillin (test). The metabolic activity of viable bacteria leads to an accumulation of organic acids in the growth media, which causes the phenol red to change in color from red to yellow, which we expect for the control group as the *E. coli* stain is kanamycin resistant. Images of the chip were taken every hour, and a significant color change was detected after four hours, as seen in Figure 1.

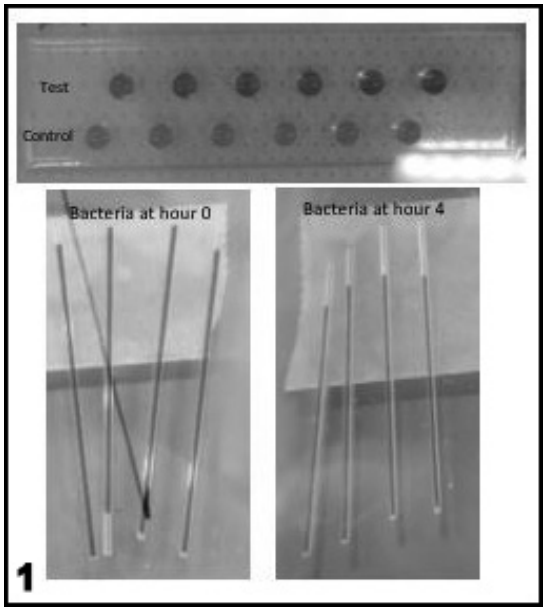

Figure 1: Color change over four hours.

Assessing Bacteria Growth in a Capillary:

A similar experiment was conducted by incubating the bacteria culture in capillary tubes designed to hold microliters of liquid. We hypothesized that the increased surface area to volume ratio of the tubes would induce an accelerated growth rate for the bacteria. First, an overnight experiment was conducted to verify that incubation inside capillary tubes supported bacteria growth. Following this verification experiment, a shorter timescale experiment was conducted with added antibiotics. Similar to the previous experiment, a significant color change was detected in the control group (kanamycin) at the 4-hour mark, as shown in Figure 1. No color change was observed in the ampicillin inhibited group.

To perform real time detection of bacterial growth, we manufactured a small portable adapter using the Objet 3D printer at Cornell NanoScale Science and Technology Facility (CNF) (Figure 2). White light is incident on one end of the capillary tube and the spectra is measured on the other end using a small portable spectrometer (OceanOptics). A difference is output spectra can give us insight into whether the organism is inhibited by antibiotic presence. As seen in Figure 3, we are able to verify bacterial viability within six hours with an apparent shift in wavelength easily distinguishable by eye.

Future Considerations:

Further testing will include real time tracking of bacteria growth. In particular, we plan on devising a portable imaging system that will allow for real time measurements of the absorbance of phenol red, which we will use as a proxy for tracking bacteria growth. We envision a system as depicted in Figure 4, wherein a simple laser and photodiode system is used to measure absorbance across and along the capillary, thus allowing us to infer the growth of bacteria.

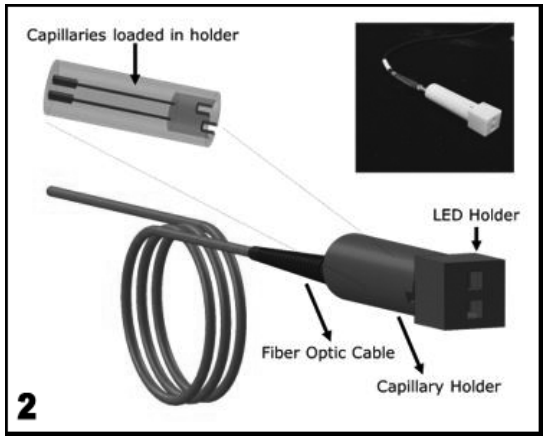

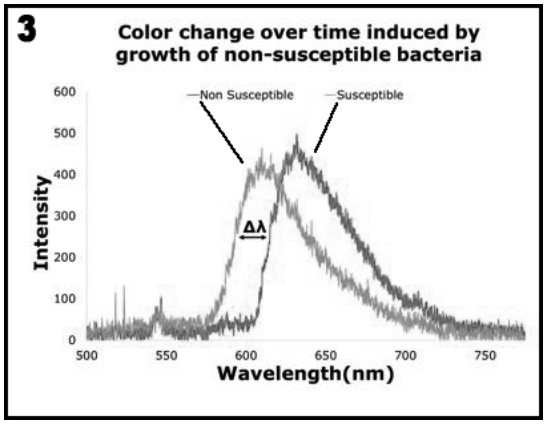

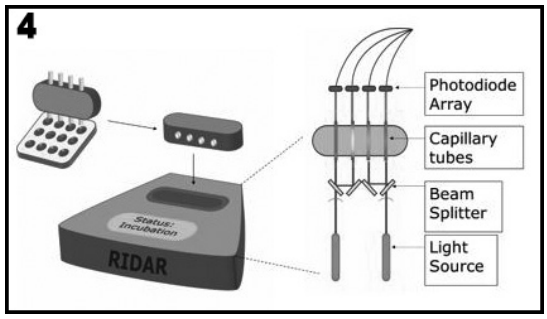

References:

[1] Report to the President on Combating Antibiotic Resistance - Executive Office of the President and President's Council of Advisors on Science and Technology. 2014; Available from:http://www.whitehouse.gov/sites/default/files/microsites/ostp/PCAST/pcast_carb_report_sept2014.pdf.

[2] National Strategy for Combatting Antibiotic Resistant Bacteria. 2014; Available from: http://www.whitehouse.gov/sites/default/files/docs/carb_national_strategy.pdf.

[3] Laxminarayan, R., A. Duse, C. Wattal, A.K.M. Zaidi, H.F.L. Wertheim, N. Sumpradit, E. Vlieghe, G.L. Hara, I.M. Gould, H. Goossens, C. Greko, A.D. So, M. Bigdeli, G. Tomson, W. Woodhouse, E. Ombaka, A.Q. Peralta, F.N. Qamar, F. Mir, S. Kariuki, Z.A. Bhutta, A. Coates, R. Bergstrom, G.D. Wright, E.D. Brown, and O. Cars, Antibiotic resistance—the need for global solutions. The Lancet Infectious Diseases. 13(12): p. 1057-1098 (December 2013).

An *in vacuo* Microfluidic Mixer for Biological X-Ray Solution Scattering

CNF Project Number: 1940-10

Principal Investigator: Richard E. Gillilan

User: Jesse Hopkins

Affiliations: Macromolecular Diffraction Facility of the Cornell High Energy Synchrotron Source (MacCHESS), Cornell High Energy Synchrotron Source (CHESS); Cornell University

Primary Source of Research Funding: National Institutes of Health GM-103485

Contact: reg8@cornell.edu, jbh246@cornell.edu

Website: www.macchess.cornell.edu/MacCHESS/bio_saxs.html

Primary CNF Tools Used: Heidelberg mask writer DWL2000, SUEX laminator, ABM contact aligner

Abstract:

Time-resolved small angle x-ray solution scattering (TR-SAXS) remains a challenging, but increasingly important experiment for structural biologists. Such experiments can tell researchers about multi-step conformational changes biological molecules undergo as part of their function. The continuous-flow mixing that utilizes the chaotic laminar flow regime of fluids provides a means of reaching single millisecond timescales with disposable plastic microchip construction and minimal sample consumption. Photolithographically fabricated mixing chips have been tested *in vacuo* to reduce parasitic x-ray scatter.

Summary of Research:

Small-angle x-ray solution scattering (SAXS) is a widely used technique in structural biology for gaining information about the behavior of molecules in solution. Time-dependent SAXS studies have been conducted for a number of years, with significant advances being made in design, sample consumption, and instrumentation [1]. But adoption of the method by non-specialists has been slow in coming, and the method remains a challenging experiment. To address the need for easier, more practical experiments, we introduced a system based on the principle of chaotic advection [2].

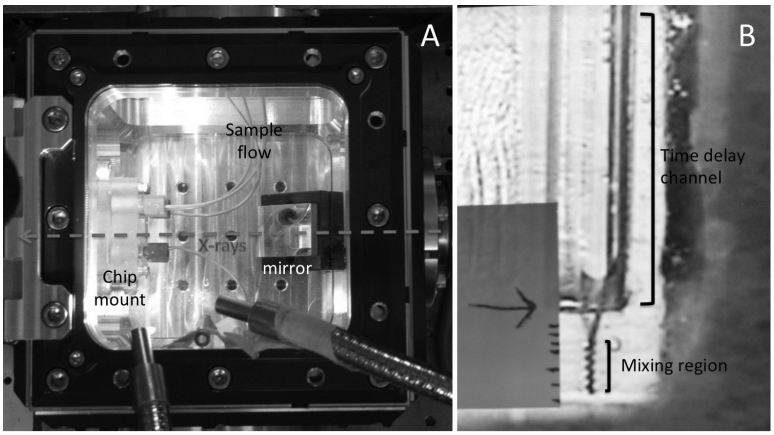

Figure 1: Microfluidic mixing chip for SAXS mounted in vacuo at CHESS beamline G1. A: X-rays (red) pass through cubic vacuum enclosure over viewing mirror and through microfluidic cell. B: Mixing region and time-delay channel of chip are visible in camera snapshot.

Our previously designed mixing chip, fabricated at CNF, is a composite of SUEX (DJ Microlaminates Sudbury, MA), polymethylmethacrylate (PMMA) and polyimide layers driven by a commercial piezo-controlled pressure system (ELVESYS, Paris, France).

Thin polyimide film (7 μm) serves as low-scatter windows for x-ray transmission. To eliminate x-ray scattering due to air and vacuum windows, we have designed an enclosed sample environment that allows mixing chips to operate in vacuum (Figure 1A). Polyether ether ketone (PEEK) sample feed tubing enters the vacuum through KF 50 blanks into the cubic sample enclosure (Ideal Vacuum, Albuquerque, NM) and connects to the microfluidic chip via flangeless fittings.

Positioning of the x-ray beam in the chip channel is accomplished by scanning the cube assembly in the x-ray beam and monitoring transmitted intensity. The chip can be viewed with a remote camera via a diagonal mirror just below the path of the x-ray beam (Figure 1A, right). The mixing and time-delay channels are visible in the camera image (Figure 1B). X-ray tests using a novel compound refractive optic for focusing down to 30 μm showed relatively low parasitic scatter though the time-delay channel.

References:

[1] Graceffa, R., et al., Sub-millisecond time-resolved SAXS using a continuous-flow mixer and x-ray microbeam. Journal of Synchrotron Radiation, 2013. 20: p. 820-825.

[2] Kane, et al. Microfluidic Mixers for the Investigation of Rapid Protein Folding Kinetics Using Synchrotron Radiation Circular Dichroism Spectroscopy. Anal. Chem. 2008, 80, 9534-9541.

Biomechanics of Bacteria

CNF Project Number: 1970-10

Principal Investigator: Christopher J. Hernandez

Users: Melanie F. Roberts, Christine E. Harper, Gabriel Guisado*

Affiliations: Sibley School of Mechanical and Aerospace Engineering, Meinig School of Biomedical Engineering; Cornell University (2017 CNF REU Program Intern)*

Primary Source of Research Funding: National Science Foundation 1463084, NSF NNCI Grant No. ECCS-1542081

Contact: cjh275@cornell.edu, mfr75@cornell.edu, ceh272@cornell.edu

Website: hernandezresearch.com

Primary CNF Tools Used: ASML, Oxford 100, AJA sputter deposition, VersaLaser engraver/cutter, MOS clean anneal

Abstract:

The mechanical properties of the bacterial cell envelope influence cell growth, cell division and subcellular localization of membrane proteins. Here we demonstrate the ability to apply mechanical loads to live bacteria, the first step toward determination of mechanical properties of bacterial components *in vivo*. Additionally, we show that devices based on the same concept have the ability to separate bacterial species/strains from one another based on the cell mechanical phenotype.

Summary of Research:

In bacteria, the ability to resist mechanical forces is necessary for survival and growth, allowing cells to withstand osmotic pressures while maintaining cell shape, cell growth and division. Hence, the mechanical properties of bacteria and bacterial structural components influence species competition and resistance to toxins and antibiotics. Our work involves the use of micro/nano fabricated devices as tools for mechanical testing of live bacteria. Within our devices, individual bacteria are flowed into tapered channels travel a distance related to whole cell stiffness: less stiff cells are able to travel further in to the channels (Figure 1).

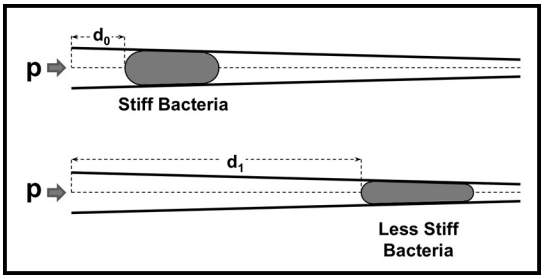

Figure 1: Bacteria under fluid pressure (p) are forced into tapered channels. The distance a cell travels into a tapered channel depends on cell stiffness with more compliant cells traveling further into the channels. The distance traveled by a cell into the tapered channel (d1) is therefore an indicator of cell stiffness. Viewing the deformation of a cell under two different applied pressures can be used to determine the mechanical properties of the cell envelope.

Key advantages of this microfluidic platform for profiling the biomechanical properties of bacteria include: minimal sample preparation, no chemical immobilization or labeling, and the ability to analyze hundreds of cells at once.

In our first series of experiments we manufactured devices on silica glass wafers using Deep UV photolithography to achieve nano-scale features (250 nm smallest dimension). These glass on glass devices were manufactured using the ASML, Oxford 100, AJA sputter deposition, VersaLaser and MOS clean anneal tools at the Cornell NanoScale Science and Technology Center.

In the first device, design bacteria in liquid culture were submitted to up to 12 different applied pressures to establish the biomechanical profile of two model organisms, *E. coli* and *B. subtilis*.

Our results demonstrated differences in stiffness between *E. coli* and *B. subtilis* (Figure 2) and suggested that a device with a shorter channel length would allow transport of *E. coli*, but not *B. subtilis*, potentially allowing for separation of bacteria based on the biomechanical properties [1]. When combined with theoretical mechanics models it allowed us to determine the stress distribution within individual bacteria and study their response to mechanical stimulation [2].

In our recent work we have explored the effects of mechanical loads on the assembly/disassembly of multicomponent efflux pumps. Multicomponent efflux pumps are three-part channels that cross the inner membrane, periplasm and outer membrane of bacteria and are used to remove toxins (excessive metal ions, antibiotics, etc.). Our data suggests that the assembly and function of multicomponent efflux pumps is sensitive to mechanical stress and strain [4].

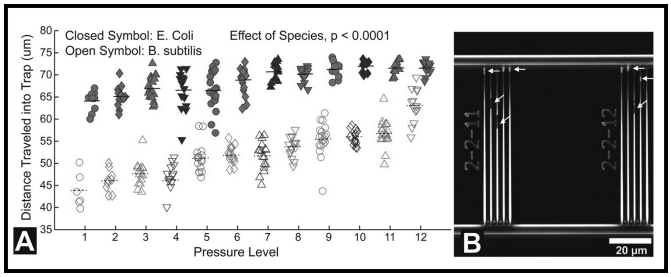

Figure 2: (A) The position of bacteria occupying trap channels at twelve different pressure levels (where level 1 is lowest and level 12 is greatest) in a single experiment are shown. Horizontal lines indicate averages at each pressure level. E. coli *travel further into the traps than* B. subtilis *overall ($p < 0.0001$, ANCOVA) as well as at each individual pressure level ($p < 0.0001$, t tests). (B) Differences in bacteria stiffness between species can be detected in a mixed culture.* E. coli *expressing GFP (green, indicated by the upper horizontal arrows) traveled further into the trap channels than* B. subtilis *(indicated by tilted arrows), demonstrating the possibility of separating bacteria based on mechanical phenotype.*

References:

[1] Sun, X., Weinlandt, W.H., Patel, H., Wu, M., Hernandez, C.J. (2014) "A Microfluidic Platform for Profiling Biomechanical Properties of Bacteria." Lab Chip. 14 (14), 2491-2498. NIHMS600175.

[2] M. F. Roberts, A. Srivastava, X. Sun, L. Kreminski, L. Ling, L. Wang, P. Chen, C-Y. Hui, C. J. Hernandez. "A Microfluidic Platform for Generating Non-Uniform Mechanical Stress in Cell Envelopes of Live Bacteria," American Society of Microbiology Annual Meeting. Boston, MA, USA. 2016.

[3] M.F. Roberts, A. Srivastava, L.M. Wang, C-Y Hui, L.A. Genova, P. Chen, C.J. Hernandez, "A microfluidic system for mechanical characterization and stimulus of individual bacteria," European Society of Biomechanics 2017.

[4] M.F. Roberts, L.A. Genova, L.M. Wang, P. Chen, C.J. Hernandez, "Non-Uniform Mechanical Stress Promotes Metal Efflux Pump Disassembly," 62nd Annual Meeting, Biophysical Society. San Francisco, CA, USA. 2018.

Design and Application of Microfluidic Devices to Study Cell Migration in Confined Environments

CNF Project Numbers: 2065-11, 2642-18

Principal Investigator: Jan Lammerding

Users: Aaron Windsor, Richard Armbruster, Vaishali Balachandran

Affiliations: Biomedical Engineering Department, Weill Institute, Cornell NanoScale Facility; Cornell University

Primary Source of Research Funding: National Institutes of Health award R01 HL082792; National Institutes of Health award 1U54 CA210184; Department of Defense Breast Cancer Research Program Breakthrough Award BC150580; National Science Foundation CAREER award CBET-1254846

Contact: jan.lammerding@cornell.edu, ajw49@cornell.edu, rwa79@cornell.edu, vb324@cornell.edu

Website: http://lammerding.wicmb.cornell.edu/

Primary CNF Tools Used: ABM contact aligner, SÜSS MA-6 contact aligner, MVD tool, Unaxis DRIE/RIE etcher, Anatech etcher, CVC sputtering tool, Tencor P-10 profilometer, Oxford 100 etcher, Trion etcher

Abstract:

It is becoming increasingly apparent that the physical properties of cells, including their size and deformability, play an important part in their function. One particular example is cell migration, which is crucial for physiological processes such as development and immune cell function, but also responsible for metastatic spreading in many cancers. To investigate how cells are able to squeeze through interstitial spaces smaller than the cross-section of the cell, we have developed microfluidic migration devices that provided 3D confinement and pore sizes mimicking physiological environments. Using these devices in combination with fluorescence time lapse-imaging, we have been able to confirm the role of nuclear deformability in confined migration, and also shown identified biological consequences of squeezing the nucleus through tight spaces, including transient nuclear envelope ruptures that result in DNA damage.

Summary of Research:

The ability of cells to migrate through tissues and interstitial spaces is an essential factor during development and tissue homeostasis, immune cell mobility, and in various human diseases. However, current methods to study the migration of cells in confining three-dimensional (3D) environments are limited by their imprecise control over the confinement, physiological relevance, and/or compatibility with high resolution imaging techniques.

We designed and built a polydimethylsiloxane (PDMS) microfluidic device composed of channels with precisely-defined constrictions mimicking physiological environments that enable high resolution imaging of live and fixed cells [1]. The device promotes easy cell loading and rapid, yet long-lasting (>24hrs) chemotactic gradient formation without the need for continuous perfusion, and is ideally suited for time-lapse imaging (Figure 1).

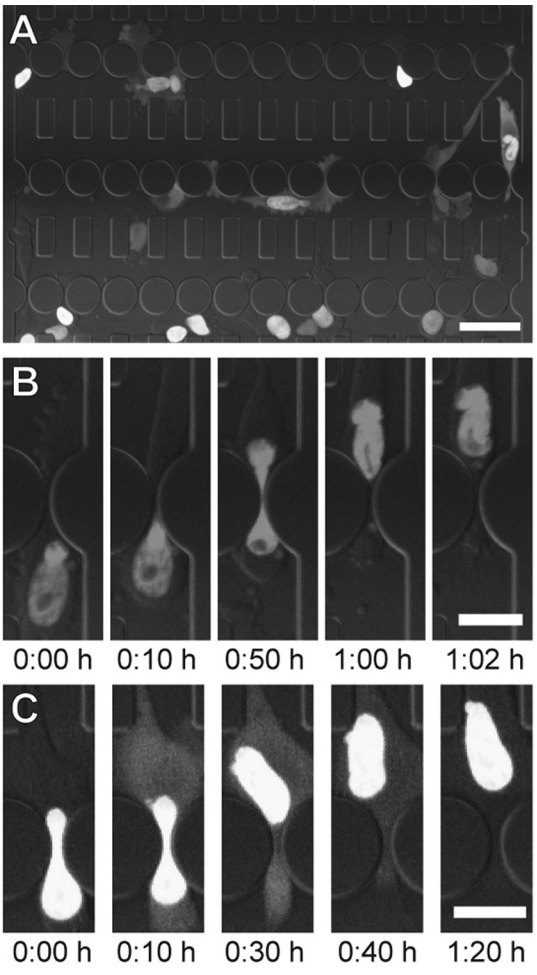

Figure 1: Cell migration through microfluidic constrictions. (A) Cells expressing NLS-GFP and H2B-tdTomato migrating through a microfluidic device. Scale bar: 50 µm. (B) Time series of a nucleus squeezing through a constriction. Scale: bar 20 µm. (C) Time series of a NE rupture event. NLS-GFP leaks into the cytoplasm upon NE rupture and is reimported into the nucleus as the NE is repaired. Scale bar: 20 µm. Figure reproduced from Elacqua, et al. PLoS one. 2018 [3]. See full color version on pages xxviii-xxix.

Using this device, we obtained detailed, quantitative measurements of dynamic nuclear deformation as cells migrate through tight spaces. We found that nuclear deformability, primarily governed by levels of lamin A/C, is a critical factor in determining the ability of cells to move through small constrictions. Furthermore, cells migrating through confined spaces incurred transient nuclear envelope rupture, nuclear fragmentation, and DNA damage, with ESCRT-III proteins playing an important role in restoring nuclear envelope integrity [2,3]. In addition, we showed that the exposure of genomic DNA to the cytoplasm during nuclear envelope rupture leads to activation of the cGAS/STING pathway, which promotes cancer metastasis [4].

The original device design was based on SU-8 soft photolithography [1]. While SU-8 was effective in creating these migration devices, this approach had several fabrication limitations. First, the reproducibility of the smallest SU-8 features (~1μm) was difficult to attain, which led to an over use of successful full wafer devices.

The repeated molding and removal of PDMS would overtime weaken the SU-8/silicon substrate bond, eventually resulting in the delaminating of features and device failure. In order to reliably reproduce and preserve our most critical features, we decided forgo SU-8 and instead etch the precise constrictions of our devices directly into the silicon substrate. We accomplished this "bottom-down" approach by using a negative photoresist mask and deep-reactive ion etching (DRIE). This approach enabled us to achieve the critical dimension features with consistent reproducibility (Figure 2), and it also cut the fabrication time in half.

Since our time-lapse studies identified nuclear deformability as a rate-limiting factor in confined migration, we set out to develop a microfluidic device to perform high throughput measurements of nuclear deformability, using the principle of micropipette aspiration.

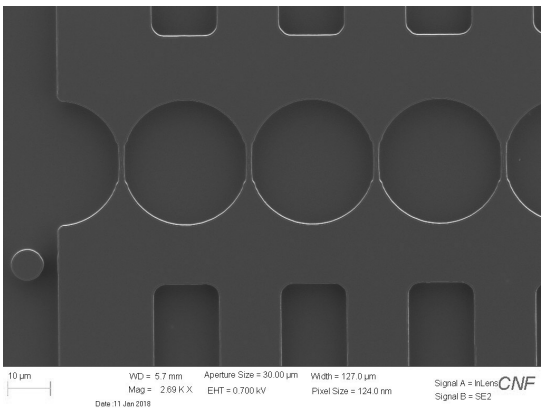

Figure 2: SEM image of a row of 1 µm constrictions created by etching 5 µm into silicon by deep-reactive ion etching.

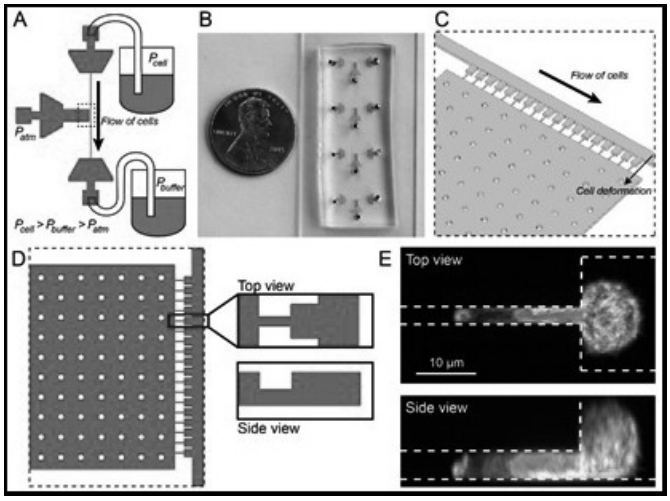

Figure 3: Overview of the microfluidic micropipette aspiration device. (A) Design overview, with applied external pressures indicated. (B) Image of four devices integrated onto a single glass slide. (C) Close-up of the design features containing the pockets and micropipette openings. (D) Top and side view of the same feature. (E) Confocal microscope images of a cell inside a pocket, with the nucleus (red) and cytoplasm (green) partially aspirated into the micropipette. See full color version on pages xxviii-xxix.

Cells in suspension are perfused into the device and segregated into single cells located in individual pockets, each equipped with a small micropipette-like opening (Figure 3). A large pressure gradient across the micropipette results in nuclear deformation (protrusion) into the micropipette, which can be quantified using automated image analysis and used to infer nuclear deformability.

In conclusion, the integration of our migration and micropipette aspiration devices with high resolution time-lapse imaging provides a powerful new approach to study intracellular mechanics and dynamics in a variety of physiologically relevant applications, ranging from cancer cell invasion to immune cell recruitment.

References:

[1] Davidson PM, Sliz J, Isermann P, Denais C, Lammerding J. Design of a microfluidic device to quantify dynamic intra-nuclear deformation during cell migration through confining environments. Integrative Biology. 7: 1534-1546, https://www.ncbi.nlm.nih.gov/pubmed/26549481 (2015).

[2] Denais CM, Gilbert RM, Isermann P, McGregor AL, te Lindert M, Weigelin B, Davidson PM, Friedl P, Wolf K, Lammerding J. Nuclear envelope rupture and repair during cancer cell migration. Science. 352(6283): 353-8, https://www.ncbi.nlm.nih.gov/pubmed/27013428 (2016).

[3] Elacqua JJ, McGregor AL, Lammerding J. Automated analysis of cell migration and nuclear envelope rupture in confined environments. PLoS One. 13(4): e0195664, https://www.ncbi.nlm.nih.gov/pubmed/29649271 (2018).

[4] Bakhoum S, Ngo B, et al. Chromosomal instability promotes metastasis through a cytosolic DNA response. Nature. 553(7689): 467-472, https://www.ncbi.nlm.nih.gov/pubmed/29342134 (2018).

Zero-Mode Waveguides on Thin Silicon Nitride Membranes for Efficient Single-Molecule Sequencing

CNF Project Number: 2214-13

Principal Investigator: Prof. Meni Wanunu

Users: Dr. Vivek Jadhav, Dr. Mohammad Amin Alibakhshi

Affiliation: School of Physics, Northeastern University

Primary Source of Research Funding: NIH award No. 1R01 HG009186

Contact: wanunu@neu.edu, v.jadhav@neu.edu, m.alibakhshi@northeastern.edu

Website: http://www.northeastern.edu/wanunu/

Primary CNF Tools Used: LPCVD CMOS Nitride – E4, JEOL 6300, SC4500 odd-hour evaporator, Zeiss Ultra SEM

Abstract:

Nanopores can generate localized electric fields to focus molecules to 3D positions with high precision. Previously, we have shown that the electrophoretic loading of nanopore zero-mode waveguides (NZMWs) is orders of magnitude more efficient than either diffusion or magnetic bead-based loading techniques. However, serial fabrication of uniform solid-state nanopores arrays is not currently feasible on a large scale. In this work, we demonstrate wafer-scale fabrication of porous membranes containing solid-state nanopore networks for large scale positioning of macromolecules using fabrication techniques derived from molecular layer deposition. These porous membranes will be used to fabricate porous zero-mode wave guides (PZMWs) as large-scale parallel replacements to NZMWs.

Summary of Research:

Zero-mode waveguides (ZMWs) are wavelength-scale apertures in aluminum films, used for single-molecule detection [1]. By immobilizing the DNA-polymerase template at the base of the ZMWs and imaging the incorporation of fluorescently-labeled nucleotide by polymerase a sequence of a single DNAs can be read [2]. Previously, it has been be demonstrated that by fabricating ZMWs on 50-nm-thick silicon nitride membranes, and drilling a 3-5 nm pore at the ZMW base, the efficiency of molecular loading is enhanced by orders of magnitude [3]. These ZMW structures were fabricated with e-beam lithography (JEOL 6300) at the CNF.

We continue to fabricate these ZMW devices for our DNA sequencing experiments. Figure 1 shows a darkfield microscope image of a device. The base of the ZMWs is modified by depositing molecule layer deposition to form a porous layer to facilitate more efficient capture of large DNA molecules. The ZMW surface is passivated using by SiO_2 deposited using atomic layer deposition (ALD) to protect it from electrochemistry with chloride buffer that may occur during voltage bias experiments.

These structures may be used for capturing DNA-polymerase complexes. In Figure 2, we show the SEM image (ZEISS Ultra) of Al pillars before lift-off process. In Figure 3, we show ZMW structure after the lift-off process.

References:

[1] Larkin, J., et al., Reversible Positioning of Single Molecules inside Zero-Mode Waveguides. Nano Letters, 2014. 14(10): p. 6023-6029.

[2] Eid, J., et al., Real-time DNA sequencing from single polymerase molecules. Science, 2009. 323(5910): p. 133-138.

[3] Larkin, J., Henley, R. Y., Jadhav, V., Korlach, J., and Wanunu, M. Length-independent DNA packing into nanopore zero-mode waveguides for low-input DNA sequencing. Nature Nanotechnol, 2017. 12, 1169-1175.

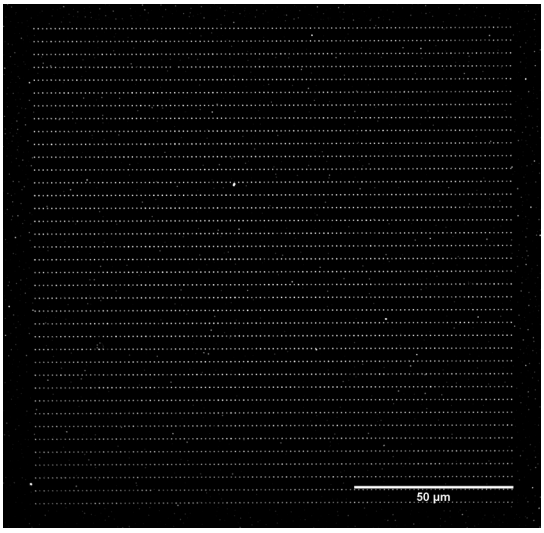

Figure 1: Conventional dark-field microscopy image of ZMWs on a thin SiN membrane after EBL.

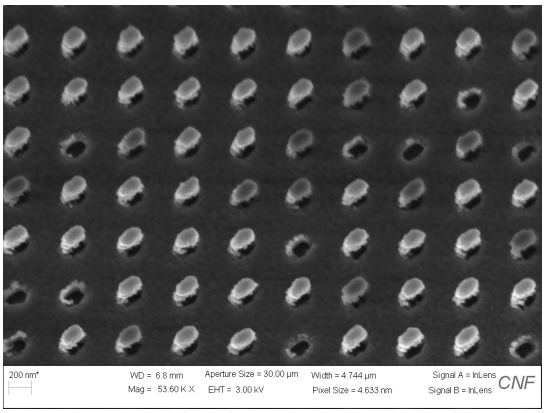

Figure 2: Scanning electron microscope image of Al pillars before lift-off process.

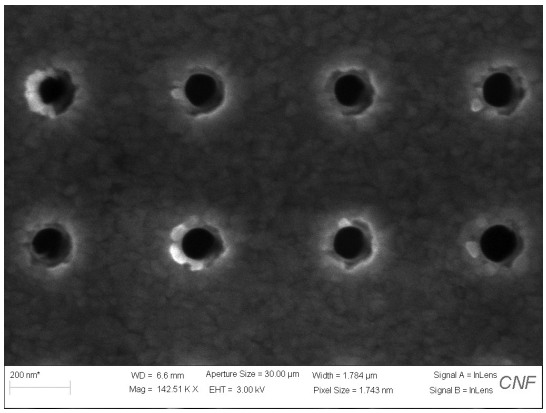

Figure 3: ZMW structure after the lift-off process.

Microfabricated Devices for Cell Organization

CNF Project Number: 2249-13
Principal Investigator: Minglin Ma
User: Wei Song

Affiliation: Department of Biological and Environmental Engineering, Cornell University
Primary Source of Research Funding: American Diabetes Association
Contact: mm826@cornell.edu, ws336@cornell.edu
Website: http://malab.bee.cornell.edu
Primary CNF Tools Used: DWL2000 mask writer, ABM contact aligner

Abstract:

Different types of cells dynamically self-assemble and organize themselves in a spatiotemporal and context-dependent manner [1]. In this study, we report the spatiotemporal dynamics of cell organization of a binary cellular mixture (MDA-MB-231 and MCF10A cells) seeded in microfabricated microwells. The initial seeding ratio of binary cells determined the degree of encapsulation of MCF0A cells by MDA-MB-231 cells. When cells were free to grow, the differential proliferation rate of MDA-MB-231 (low growth rate) and MCF10A cells (high growth rate) resulted in a reversed core (MDA-MB-231)-shell (MCF10A) organization at seeding ratio of 1:1 (MDA-MB-231:MCF10A) and a side-by-side aggregate structure at seeding ratio of 4:1 after long-term culture.

Summary of Research:

Fabrication of Polydimethylsiloxane (PDMS) Microwell. The photomask was prepared using DWL2000 mask writer (Heidelberg Instruments). The silicon wafer was spin-coated with SU-8 2150 photoresist (MicroChem) at 500 rpm for 40 sec and then 2500 rpm for 30 sec. The wafer was covered with the photomask and exposed by a UV photolithography machine (ABM contact aligner) for 32 sec. After being developed and post-baked, the SU-8 master wafer was fabricated. The SU-8 master wafer was then used to create PDMS (Sylgard 184, Dow Corning) mold. A mixture (10:1) of Sylgard 184 silicone elastomer components was casted onto the master wafer and cured at 60°C overnight to prepare a PDMS microwell. Figure 1 is a microscopic image of PDMS microwells.

Formation of Cell Aggregates in PDMS Microwells. PDMS microwells were autoclaved, placed in a 24-well plate, and coated with 1% (w/v) Pluronic® F127 (Sigma) solution before cell seeding to prevent cell attachment on PDMS surface and facilitate formation of cell aggregates. To form cell aggregates, cell suspensions of MDA-MB-231/MCF10A mixture (MDA-MB-231:MCF10A=1:1 and 4:1, total 1.0×10^6 cells) were added to each well of 24-well plate with PDMS microwells inside. After four hours of static culture, the cells that were adhered to the interspace between microwells were removed by medium change. The cells that fell into the microwells formed cell aggregates after overnight culture. The cell aggregates were cultured in microwells for nine days. The mixed medium (MDA-MB-231 medium:MCF10A medium=1:1 and 4:1) was changed every two days. Figure 2 is a fluorescent image of cell segregation of MDA-MB-231 (red colour) and MCF10A (green colour) cells at 1:1 cell seeding ratio over nine days of culture. Figure 3 is a fluorescent image of cell segregation of MDA-MB-231 (red colour) and MCF10A (green colour) cells at 4:1 cell seeding ratio over nine days of culture.

In summary, the initial seeding ratio and cell proliferation have significant effects on the evolution of cell organization of binary cellular mixture over long-term culture. Depending on the initial seeding ratios, the cell organization is either a core-shell (1:1) or side-by-side (4:1) aggregate by the differential proliferation rates of MDA-MB-231 and MCF10A cells.

References:

[1] Yoshiki Sasai. Cytosystems dynamics in self-organization of tissue architecture. Nature 2013, 493, 318-326.

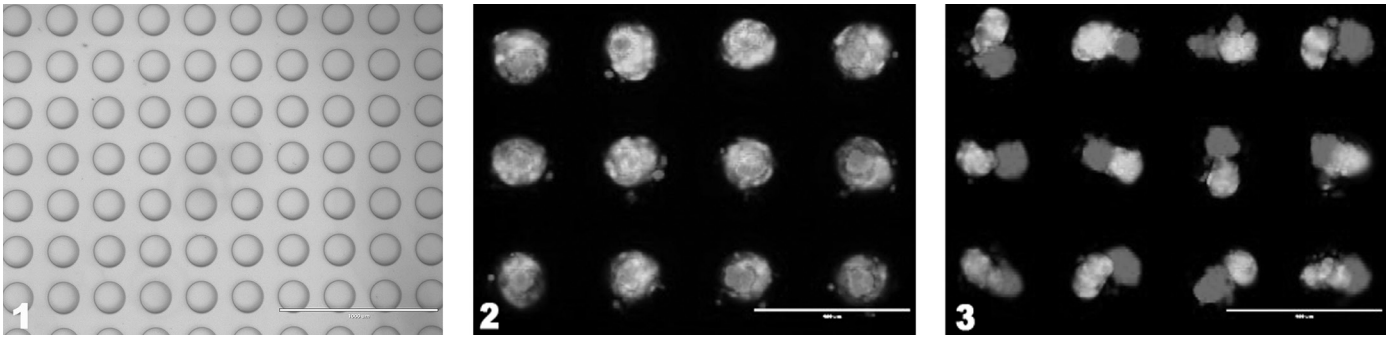

Figure 1, left: *A microscopic image of PDMS microwells. Scale bar: 1000 µm.* ***Figure 2, middle:*** *A fluorescent image of cell segregation of MDA-MB-231 (red colour) and MCF10A (green colour) cells at 1:1 cell seeding ratio over 9 days of culture. Scale bar: 400 µm.* *See full color version on pages xxviii-xxix.* ***Figure 3, right:*** *A fluorescent image of cell segregation of MDA-MB-231 (red colour) and MCF10A (green colour) cells at 4:1 cell seeding ratio over nine days of culture. Scale bar: 400 µm.* *See full color version on pages xxviii-xxix.*

Electrochemical Detection Array Combining Amperometry and Total Internal Reflection Fluorescence

CNF Project Number: 2260-13

Principal Investigator: Manfred Lindau

User: Meng Huang

Affiliation: School of Applied and Engineering Physics, Cornell University

Primary Source of Research Funding: National Institutes of Health

Contact: ML95@cornell.edu, mh2236@cornell.edu

Primary CNF Tools Used: ABM contact aligner, YES Asher, AJA sputtering system, Aura 1000 resist stripper, Image Reversal Oven, Oxford PECVD, Oxford 81 etcher

Abstract:

Neurotransmitters are released in a quantal event by fusion with membranes. The mechanism of this fusion event remains unknown but is crucial for molecular manipulation and various kinds of disease. We develop and fabricate an electrochemical detection array capable of combining amperometry measurement and total internal reflection fluorescence (TIRF). Amperometry provides the information for the releasing neurotransmitters from vesicles in the cell while TIRF enables direct visualization of vesicles with appropriate fluorescence labels. The combination of the two methods offers a new way for studying the exocytosis process.

Summary of Research:

Exocytosis is the process where neurotransmitters are released into the extracellular space [1]. The amperometry measurement provides precise details about the released transmitters in a single quantal event. While amperometry has the above-mentioned advantages, it measures the releasing contents reaching the electrodes and cannot directly characterize the releasing mechanisms. The total internal reflection fluorescence (TIRF) can detect the fluorescence signals at the substrate surface to visualize the foot print of the cell with its generated evanescence wave. The combination of the two methods offers the availability of monitoring vesicle releasing events and amperometry spikes simultaneously.

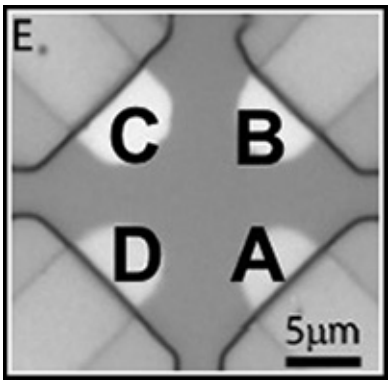

Figure 1: The micrograph showing the geometry of the 4-electrode ECD device.

To fully utilize the TIRF technology, the specific site of release must be known to locate the fluorescence signal. Therefore, we developed the electrochemical detection (ECD) array with four electrodes between which a cell can be placed, as shown in Figure 1 [1]. Individual fusion events can be detected amperometrically with ~ 200 nm precision, utilizing a map of random walk simulations while the cell surface can be imaged with TIRF microscopy [3].

A 4-inch, 175 μm thick glass wafer was used for the fabrication of the ECDs. Patterns were transferred onto the wafer through general lithography with NFOL 2020 negative photoresist. The photoresist was spin-coated on the wafer with 3000 rpm for 30s, resulting in a thickness of 2 μm. After the soft bake, alignment and exposure was performed with ABM contact aligner for 7s at 12.14 mJ/s. Following the post exposure bake, the photoresist was developed using 726 MIF for 70s. Then 10 nm Ti/150 nm Pt were deposited on the device using the AJA sputtering

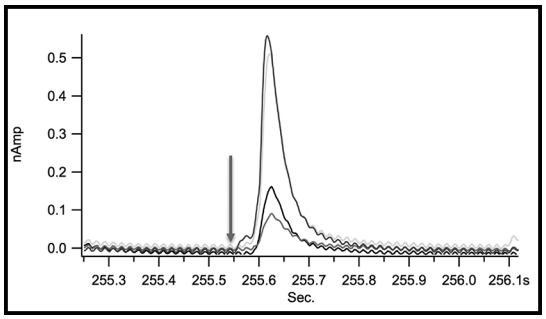

Figure 2: An amperometric spike related to the fluorescent signal in Figure 3. The arrow shows the event start point.

system followed by a lift of process using 1165. A 300 nm thick SiO_2 layer was deposited using Oxford PECVD. By using general lithography and Oxford 81 ether, a window was opened at the tips of the four electrodes to expose them to the environment.

To determine the role of Syntaxin clusters in fusion events in chromaffin cells, fluorescent labelled Syntaxin-CSYS construct was expressed in the cells by overnight infection of semliki forest virus harboring the gene for the expression of Syntaxin-CSYS. Syntaxin-CSYS was cloned into pSFV vector to make virus for the expression in bovine chromaffin cells. A fluorescent image of cell footprint on ECD arrays was collected by the TIRF microscopy. Transmitter release from the single fusion event was detected by the four ECD electrodes as correlated amperometric spikes with different amplitudes, depending on the diffusion distance between the release site and the respective electrode. Fluorescent movie by the TIRF microcopy and release events by the ECD array were recorded simultaneously, A combinatorial fluorescence change with the start of amperometric spike was observed.

A time superresolution analysis of fluorescence loss and amperometric spike start time by ECOM method shows the dispersal of syntaxin clusters coincide with the fusion pore formation.

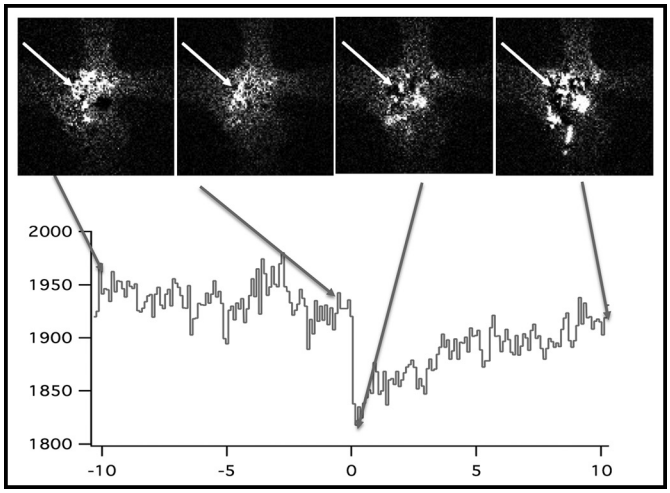

Figure 3: Fluorescent signal correlated with the amperometric spike in Figure 2. The arrows indicate the position of the event and corresponding signal strength.

References:

[1] Kisler, K., et al., J. Biomater. Nanobiotechnol., 2012. 3(2): p.243-253.

[2] Liu, X., et al. Analytical Chem., 2011, 83: p. 2445-2451.

[3] Zhao, Y., et al., PNAS., 2013. 110(35): p.14249-14254.

Microfluidic Device for Studying Harmful Algal Blooms

CNF Project Number: 2262-13
Principal Investigator: Mingming Wu
User: Young Joon Suh

Affiliation: Department of Biological and Environmental Engineering, Cornell University
Primary Source of Research Funding: United States Department of Agriculture
Contact: mw272@cornell.edu, ys668@cornell.edu
Website: http://biofluidics.bee.cornell.edu/
Primary CNF Tools Used: ABM contact aligner, YES polyimide bake oven, MVD100

Abstract:

Harmful algal blooms (HABs) are increasing worldwide causing degradation of lake ecosystems, and endangering recreational and drinking water resources. The exact mechanisms that lead to harmful algal blooms remain elusive, but they are often correlated with many chemical and physical environmental cues including nutrients, temperature, and fluid flows. Current assay formats such as in pond and test tubes are not appropriate for probing the role of many environmental factors. Here we developed a microfluidic platform, where cells are cultured in an array of microhabitats with controlled nutrient and chemical gradients. Using this platform, we explored the roles of cell-cell communication signals in the growth, motility and clustering of a common HAB forming cyanobacteria, *Microcystis aeruginosa*. Our ultimate goal is to find a set of environmental conditions under which rapid cyanobacteria growth is triggered and use this knowledge to discover effective control solutions for HABs.

Summary of Research:

Microfabrication of this microfluidic device is challenging since the height of the side channels and the microhabitats are different as shown in Figure 1. The double-layer SU-8 method was chosen to fabricate this device. The wafer was first dehydrated in an oven to remove water vapor. SU-8 2100 was spun on the silicon wafer at 3000 rpm for 30 seconds to form the first 100 μm thick layer. The edge bead was removed using acetone-wetted wipes. Then, a soft bake was performed on the wafer by ramping up the temperature slowly at 2°C/min from room temperature to 65°C in an hour. Then, the temperature was increased to 95°C at 2°C/min and was left on the hot plate overnight. Next day, the wafer was cooled down to room temperature slowly by turning off the hot plate.

The first layer of SU-8 was exposed to the microhabitat pattern using the 365 nm filter at 250 mJ/cm^2 on a contact aligner (ABM contact aligner, ABM, Inc., Silicon Valley, CA). Then, the second layer of SU-8 was poured and spun at 3000 rpm for 30 seconds. Edge bead removal was performed using the acetone-wetted wipes. Then, the soft bake was performed. Using 320 mJ/cm^2 on the same contact aligner using the align marks, both layers of SU-8 were exposed to the pattern of side channels. Then, a post-exposure bake was performed. For post exposure bake, the wafer was heated to 65°C from room temperature at 2°C/minutes and maintained for five minutes. Then, the wafer was ramped up to 95°C at 2°C/min and was maintained for 15 minutes. Then, the wafer was cooled down to room temperature by turning off the hotplate. Then, the wafer was developed using the SU-8 developer. Isopropanol was used to rinse the wafer. Hard bake was performed using the YES polyimide oven. Finally, FOTS treatment was done using the MVD100.

References:

[1] Beum Jun Kim, Lubna V. Richter, Nicholas Hatter, Chih-Kuan Tung, Beth A. Ahner, and Mingming Wu, An array microhabitat system for high throughput studies of microalgal growth under controlled nutrient gradients, Lab Chip, 15: 3687-3694 (2015).

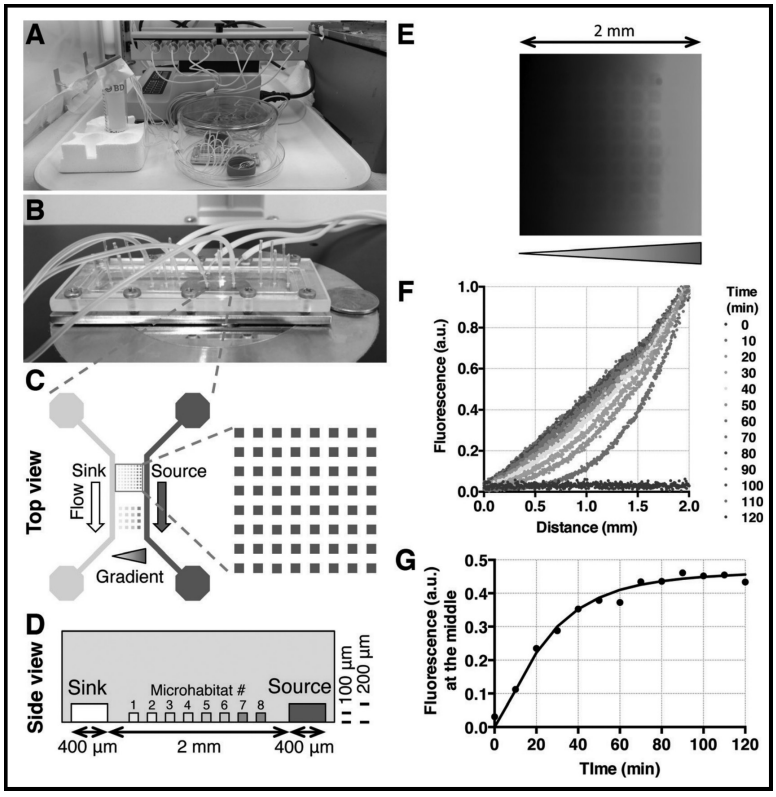

Figure 1: Microfluidic platform design and gradient characterization. A. An image of the microfluidic platform under fluorescent light for the growth of photosynthetic microalgae. The microfluidic platform is enclosed in an upside-down Pyrex® container with water reservoirs for humidity control. A syringe pump is used to perfuse media through the device. B. An image of the microfluidic platform on a microscope stage. Each platform contains four individual devices patterned in an agarose gel membrane. Tubing is used for connecting to the syringe pump for flow control. C. Top view of a device. Nutrients/buffers flow through the two side channels and form a nutrient gradient in the microhabitat array area through molecular diffusion. The top array contains 64 microhabitats, each has a dimension of 100 µm × 100 µm × 100 µm, with a gap of 100 µm between the two adjacent habitats. The bottom array contains 16 microhabitats, each has a dimension of 200 µm × 200 µm × 100 µm, with a gap of 200 µm. Cells are pre-seeded before sandwiching the agarose gel membrane between a plastic manifold and a glass slide. D. Side view of a device. The distance between the source and sink channels is 2 mm, and the cross-sectional area of each side channel is 400 µm × 200 µm. The nutrient concentration is the same for each column of the array, with the column number labeled. E. A fluorescence image of the array microhabitat taken at t = 1 h, where t = 0 is defined to be the time when fluorescein/buffer are introduced into the side channels. F. Time-evolution of fluorescence intensity profile in the array microhabitat area with a 10 min interval and total time duration of 120 min. Each colored line represents the fluorescence intensity profile at a time point. G. Experimental results (dotted line) are validated against that (solid line) from COMSOL computation. Time evolution of fluorescence intensity in the middle of the array (or 1 mm away from sink channel) is shown here.

Chip-Based Frequency Combs for High-Resolution OCT

CNF Project Number: 2364-15

Principal Investigator: Michal Lipson[1]

User: Xingchen Ji[2]

Affiliations: 1. Department of Electrical Engineering, Columbia University, New York, NY 10027;
2. School of Electrical and Computer Engineering, Cornell University, Ithaca, NY 14853

Primary Source of Research Funding: Defense Advanced Research Projects Agency

Contact: ML3745@columbia.edu, xj53@cornell.edu

Primary CNF Tools Used: LPCVD, e-beam lithography, Oxford 100 etcher, AJA sputter deposition

Abstract:

We demonstrate chip-based frequency combs as a novel source for optical coherence tomography (OCT). For the first time an OCT image of human tissue is acquired using a silicon nitride microresonator. The potential for ultrahigh-resolution optical coherence tomography (UHR-OCT) is shown.

Summary of Research:

Optical coherence tomography (OCT) is a well-established medical imaging modality that has been used in fields such as ophthalmology, cardiology and dermatology [1-3]. Near infrared light sources with a full width half maximum (FWHM) bandwidth over 150 nm may allow for an axial resolution down to one micrometer in tissue [4]. An OCT broadband light source that can simultaneously achieve both, large bandwidth and deep signal penetration, remains out of reach.

Superluminescent diodes (SLDs), widely used in commercial OCT systems, have typical spectral bandwidths of up to 100 nm. Multiplexing of SLDs represents a viable approach to increase the bandwidth, but the overall achievable bandwidth is still limited by the gain medium. On the other hand, supercontinuum (SC) sources could in principle be used to achieve high resolution OCT. However, SC generation relies on pulsed lasers with kW-range peak power [5] and it suffers from instabilities in the output intensity and irregularities in the spectral shape, as a result of the complex interplay of linear and highly nonlinear effects during its generation [6].

Here we present a novel source for OCT based on chip-scale lithographically-defined microresonators with potential for sub-micrometer axial resolution and deep penetration. When optically pumped with a low-power continuous-wave laser source, they can generate broadband frequency combs. Such frequency combs have been demonstrated in numerous chip-scale platforms in the past decade [7-13]. The parametric gain in these photonic structures enables ultra-broad optical bandwidths which can exceed an octave [11-13] in contrast to traditional gain materials and is not limited by the gain bandwidth tradeoff.

We use an ultra-low loss silicon nitride resonator with a large cavity length of 1.9 mm in order to ensure that the generated frequency

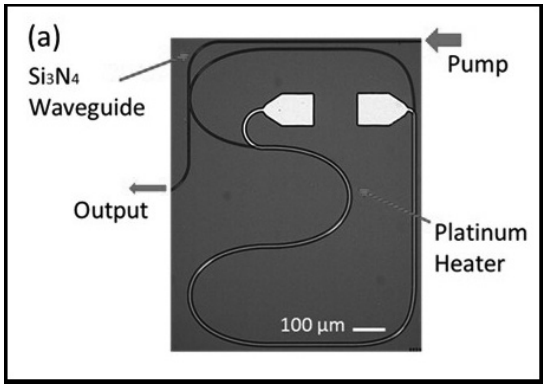

Figure 1: Microscopy image of the silicon nitride on-chip microresonator.

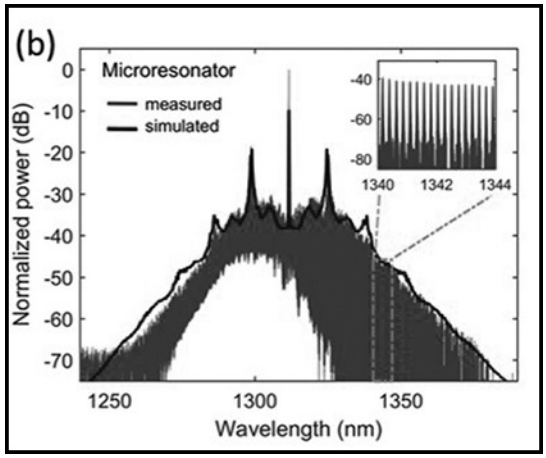

Figure 2: Purple: Measured frequency comb spectrum generated using the silicon nitride microresonators. Black: Simulated frequency comb. See full color version on pages xxviii-xxix

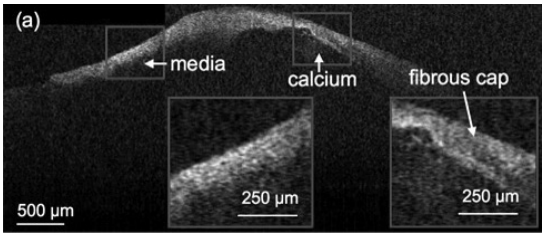

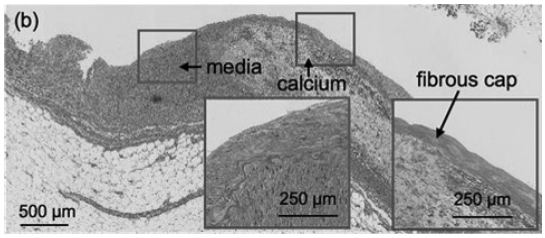

Figure 3, left: *A stitched frequency-comb-based OCT B-scan of human coronary artery with a fibrocalcific plaque. Critical features are observed, including fibrous cap thickness, calcium, and media are depicted in OCT images, indicating a great potential for clinic applications.* ***Figure 4, right:*** *H&E histology.*

comb has small line spacing critical for large imaging range. Our resonator design leads to a line spacing (38 GHz), which makes it compatible with current OCT spectrometers. Figure 1 shows the fabricated resonator. Using optical pump power as low as 117 mW, we generated frequency combs with a 38-GHz frequency spacing (shown in Figure 2).

The generated frequency comb spectrum has a FWHM of 47 nm corresponding to a theoretical axial resolution of 16.3 μm in good agreement with our measured FWHM of the axial point spread function of 18 μm. In order to perform OCT imaging a comb with low temporal coherence is required. We ensure that the comb lines are not locked in phase by tuning of the cavity resonance relative to the pump frequency using a mircoheater that is integrated on the chip. In order to generate these frequency combs, we use pump source of a low-cost distributed feedback (DFB) laser. The microresonator platform could enable inexpensive sources for OCT since it leverages mass fabrication on wafer-scale and allows miniaturization of OCT systems. Also, this platform has the potential to generate combs an octave span to enable UHR-OCT.

We acquire OCT images of human tissue with a standard commercial spectral domain (SD)-OCT system using the microresonator platform. Figures 3 shows *ex vivo* OCT of human coronary samples imaged with our microresonator frequency comb source using a commercial SD-OCT system. Sections of tissue were stained with hematoxylin and eosin (H&E). A pathologist who specializes in cardiovascular pathology annotated coronary tissue structure in histology image. Figure 3 shows a stitched frequency-comb-based OCT image of a human left anterior descending artery in comparison with the H&E histology in Figure 4. OCT B-scans were stitched using the method previously used in cervical image processing [14]. In the red inset, a gradually decreasing trend of backscattering can be visualized within the transition region from a fibrous region to the media. The right inset in Figure 3 reveals a typical pattern of a fibrocalcific plaque [15], where a layer of signal-rich fibrous cap is on the top of calcium, a signal-poor region with a sharply delineated border. Importantly, overlying the fibrocalcific plaque region, we observe a thickness change from dense fibrous cap for stable plaque structure to thinner fibrous cap for unstable plaque structure, the latter of which has been found in great frequency in patients with acute coronary syndrome and acute myocardial infarction.

In summary, we have demonstrated the first OCT imaging based on a chip-scale source. We expect that miroresonator frequency combs have great potential for UHR-OCT.

References:

[1] Carrasco-Zevallos OM, et al. Biomed. Opt. Express 8(3):1607-1637 (2017).

[2] Bouma BE, et al. Biomed. Opt. Express 8(5):2660-2686 (2017).

[3] Huang, D., et al. Sci. N. Y. NY 254, 1178 (1991).

[4] Povazay B, et al. Opt. Lett. 27(20):1800-1802 (2002).

[5] Genty, G., Coen, S. and Dudley, J. M. JOSA B 24, 1771-1785 (2007).

[6] Corwin, K. L., et al. Appl. Phys. B 77, 269-277 (2003).

[7] Kippenberg, T. J., Holzwarth, R. and Diddams, S. A. Science 332, 555-559 (2011).

[8] Suh, M.-G., Yang, Q.-F., Yang, K. Y., Yi, X. and Vahala, K. J. Science 354, 600-603 (2016).

[9] Kuyken, B., et al. Nat. Commun. 6, 6310 (2015).

[10] Wang, C. Y., et al. Nat. Commun. 4, 1345 (2013).

[11] Okawachi, Y., et al. Opt. Lett. 36, 3398-3400 (2011).

[12] Pfeiffer, M. H. P., et al. Optica 4, 684 (2017).

[13] Del'Haye, P., et al. Phys. Rev. Lett. 107, (2011).

[14] Gan, Y., et al. Biomed. Opt. Express 6, 1090-1108 (2015).

[15] Tearney, G. J., et al. J. Am. Coll. Cardiol. 59, 1058-1072 (2012).

Handheld Chem/Biosensor Combining Metasurfaces and Engineered Sensor Proteins to Enhance Surface Plasmon Resonance (SPR)

CNF Project Number: 2430-16

Principal Investigator and User: Lori Lepak

Affiliation: Phoebus Optoelectronics, LLC

Primary Source of Research Funding: Department of Defense

Contact: llepak@phoebusopto.com

Website: www.phoebusopto.com

Primary CNF Tools Used: DWL2000 photomask writer, JEOL 9500 electron beam lithography, ASML DUV stepper, SC4500 evaporator, Oxford 81 etcher, Zeiss SEM, DISCO dicing saw

Abstract:

Since 2003, Phoebus Optoelectronics has enabled custom R&D solutions in the fields of metamaterials, plasmonics, antennas, and sensors. We work closely with our customers throughout device development, from product realization to small volume manufacturing. Our R&D portfolio spans the spectral ranges of visible light, infrared, terahertz, and microwave radiation, for applications in high resolution infrared imaging systems, wavelength and polarization filtering, tunable optical components, beam forming and steering, solar cells and renewable energy devices, and chemical and biological toxin sensors. Our agile team makes extensive use of the resources at the CNF for our nano/micro fabrication and testing, to provide cost efficiency and rapid turnaround. In the present report, we discuss recent efforts to develop a chem/bio toxin detection system, which provides the state-of-the-art sensitivity of a typical benchtop system with the superior SWaP performance of a handheld system. Our surface plasmon resonance (SPR)-based sensor is expected to be capable of detecting ng/mL concentrations of selected toxins in under five minutes.

Summary of Research:

SPR is a highly sensitive, label-free optical detection technique, whose underlying physics is illustrated in reflection mode in Figure 1. A laser passes through a prism, at an incident angle θ, on a gold film which is in contact with an analyte solution on its opposite side. The illumination produces an evanescent wave (surface plasmon), which significantly reduces the reflectance at a resonant angle. The resonant angle is strongly dependent on the local refractive index, within a few tens of nanometers of the gold surface, and thus is extremely sensitive to enzyme-substrate or antibody-antigen binding events near the surface. The resonance is independent of the geometric configuration of the optical elements (see [8] for mathematical derivation.), such that these results also apply to devices which operate in transmission mode.

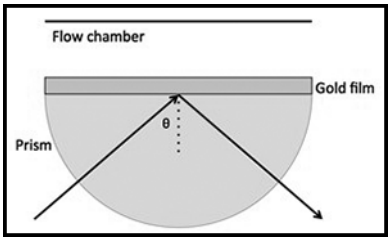

Figure 1: Surface plasmon resonance spectroscopy schematic. Reproduced from reference [8].

As illustrated in Figure 2, Phoebus has combined two recently developed technologies to enable an SPR sensor system, which provides enhanced sensitivity at lower SWaP, relative to technologies currently on the market. First, Phoebus detects toxins using computationally designed proteins (CDP's), engineered to undergo an exceptionally large conformational change upon binding their specific target. This conformation change increases the density of the protein layer, thereby locally increasing the effective refractive index, which in turn enhances the SPR signal by a factor of 100-1000x competing systems. Second, Phoebus uses the resources of the CNF to fabricate plasmonic chips patterned with a metamaterial surface to enable extraordinary optical transmission (EOT), a phenomenon unique to metastructures in which light is transmitted through apertures much smaller than the incident wavelength, at anomalously large intensities relative to the predictions of conventional aperture theory.

EOT was first observed by T.W. Ebbesen in 1998 [1]. Since its founding in 2003, Phoebus has successfully harnessed EOT by incorporating metasurfaces into devices used

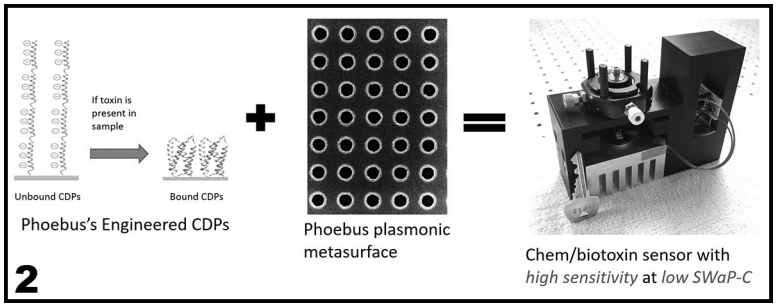

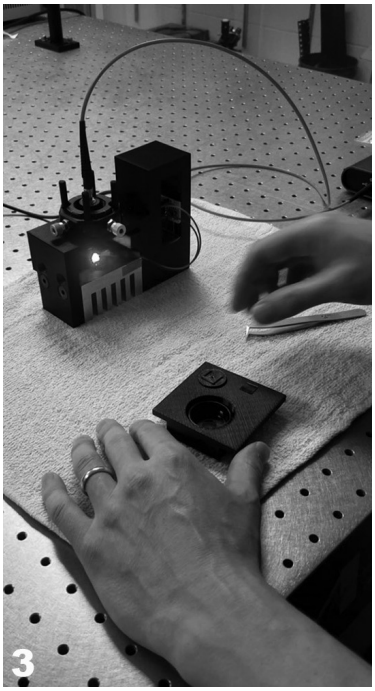

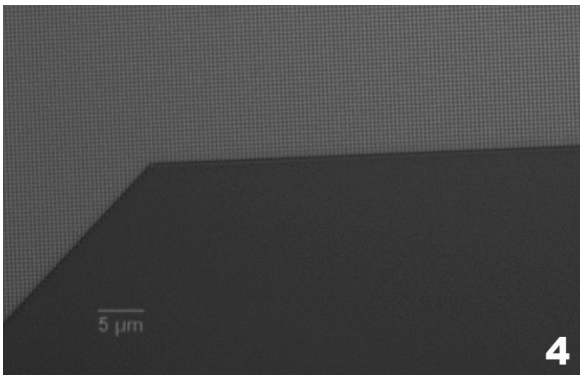

Figure 2, top left: *Phoebus-engineered sensor system combines; (a) Designed CDPs which undergo extreme conformational changes upon binding target (b) Gold metasurface, patterned to maximize transmission at SPR resonant wavelength into (c) a high sensitivity, low SWaP-C chem/biotoxin sensor system.* ***Figure 3, top right:*** *Complete Phoebus handheld biosensor system.* ***Figure 4, above:*** *Optical microscope image of a metasurface used in disposable biosensor chip.*

to perform light filtering [2-3], photon sorting [4-5], polarimetric detection [6], high speed optical detection [7], and most recently, in our SPR plasmonic sensor chips [8].

These two innovations are combined by attaching the engineered CDP's to the patterned gold metasurface using standard thiol-based attachment chemistry, to make a disposable sensor chip. As shown in Figure 3, this chip is inserted into the complete 3D printed module. All of the optical elements are already assembled in-line as indicated, for a transmission-based detection system. Except for Phoebus's disposable sensor chip, all of the optical components are inexpensively commercially available, which helps to make our overall system a highly cost-effective toxin sensing solution.

Our second-generation metasurface chips, shown in an optical microscope image in Figure 4, consist of an array of gold pillars, which serve both to bind the designed IDPs and to undergo SPR. To make the chip, we patterned the wires using the JEOL 9500 e-beam lithography system, evaporated Cr/Au, and performed a liftoff. This process is capable of consistently producing lines down to ~ 200 nm wide, with smooth enough sidewalls for an operable optical device.

References:

[1] Ebbesen, T.W., et al., "Extraordinary optical transmission through sub-wavelength hole arrays." Nature, (1998). 391(6668): p. 667-669.

[2] Crouse, D. "Numerical modeling and electromagnetic resonant modes in complex grating structures and optoelectronic device applications." Electron Devices, IEEE Transactions on 52.11 (2005): 2365-2373.

[3] Crouse, D., and Keshavareddy, P. "Polarization independent enhanced optical transmission in one-dimensional gratings and device applications." Optics Express 15.4 (2007): 1415-1427.

[4] Lansey, E., Crouse, D., et al. "Light localization, photon sorting, and enhanced absorption in subwavelength cavity arrays." Optics Express 20.22 (2012): 24226-24236.

[5] Jung, Y.U, et al. "Dual-band photon sorting plasmonic MIM metamaterial sensor." Proc. SPIE 9070, Infrared Technology and Applications XL, 90702X (June 24, 2014); doi:10.1117/12.2050620.

[6] Crouse, D., et al. "A method for designing electromagnetic resonance enhanced SOI metal–semiconductor–metal photo-detectors." J. of Optics A: Pure and App Optics 8.2 (2006): 175.

[7] Mandel, I., et al. Theory and Design of a Novel Integrated Polarimetric Sensor Utilizing a Light Sorting Metamaterial Grating. Sensors Journal, IEEE, (2012): Vol. PP, 99

[8] Lepak, L., et al. "Handheld chem/biosensor using extreme conformational changes in designed binding proteins to enhance SPR" Proc. SPIE 9862, Advanced Environmental, Chemical, and Biological Sensing Technologies XIII, 9862-7 (April 17, 2016); doi:10.1117/12.2222305.

Scalable Sensor Array Platform for Analysis of Quantal Transmitter Release Events

CNF Project Number: 2460-16

Principal Investigators: Xin Liu, Manfred Lindau

User: Meng Huang

Affiliation: School of Applied and Engineering Physics, Cornell University

Primary Source of Research Funding: National Institutes of Health

Contact: ML95@cornell.edu, mh2236@cornell.edu

Primary CNF Tools Used: ABM contact aligner, AJA sputtering system, Unaxis 770 deep silicon etcher, Aura 1000 resist stripper, YES Asher, YES image reversal oven

Abstract:

Neurontransmitters are released in a quantal event by fusion with membranes. We develop and fabricate a CMOS sensor array capable of parallel electrochemical detection of vesicle release events from chromaffin cells. To enable amperometry measurement, polarizable platinum electrodes are deposited on the Al/Cu metal contact on the CMOS chip by sputtering. SU-8 insulation layer is also applied to protect the surface structure of the chip and avoid incomplete coverage of the metal contact by shifting the position of the electrodes as well as form deep wells to trap cells. A silicon wafer with deep etched wells is used as holder for the CMOS chips for better handling and pattern transfer.

Summary of Research:

Neurontransmitters are released into the extracellular space in a process known as exocytosis [1]. The amperometry measurement provides precise details about the released transmitters in a single quantal event. However, amperometric spikes vary from cell to cell even under the same condition [2]. Therefore, a large number of measurements for vesicle release events must be performed to achieve a change in the mean value. Here, we present the CMOS IC sensor array capable of parallel amperometry measurement of vesicle release events and the post-fabrication to enable its functionality.

The CMOS sensor chip is fabricated at MOSIS by On Semiconductor C_5F/N. Polarizable electrode materials such as platinum are not offered in this process. Instead, Al/Cu metal contact are deposited to serve as interconnection of the chip. However, amperometry measurement requires polarizable electrodes for low noise current measurement as the oxidation current is usually on the order of pA. Hence, it is necessary to have a post-fabrication process in the CNF clean room to deposit platinum electrodes directly onto the Al/Cu metal contacts for amperometry measurement. AJA sputtering system is used to deposit Ti(60s)/Pt(500s) bilayer with 400w power on the electrode to have a uniform metal film as well as good side wall coverage.

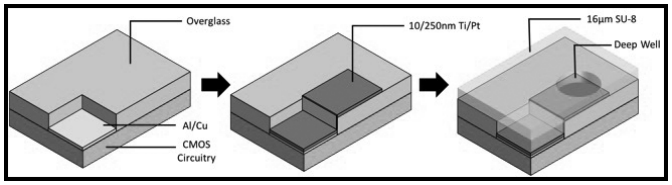

Figure 1: The geometry of shift electrode. The opening of the working area is redefined. In our case, one passivation SU-8 layer is applied with redefined shape (round) of the new opening for better cell trapping.

To avoid possible defect such as incomplete coverage of the Pt electrode, a shift electrode strategy is performed to redefine the position and shape of the working electrodes (Figure 1) [4]. The shifted electrodes also enable cell trapping by SU-8 deep wells. The patterned poly(L-lysine) in register with the electrodes will promote cell adhesion, while poly(ethylene glycol) is applied in between wells will resist cell adhesion [5]. Pt electrodes are deposited over the Al/Cu contact, but instead of just covering the contact window, they are extended to cover some part of the overglass. A 16 μm SU-8 2025 thick layer is fabricated on the surface of the CMOS chip. Deep wells with 20 μm in diameter are opened by general lithography at the redefined electrode position.

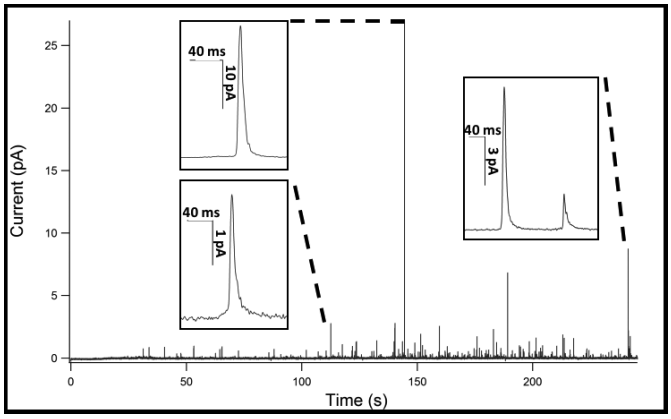

Figure 2: Amperometry recording at one pixel. Many amperometric spikes are observed, validating the function of the device.

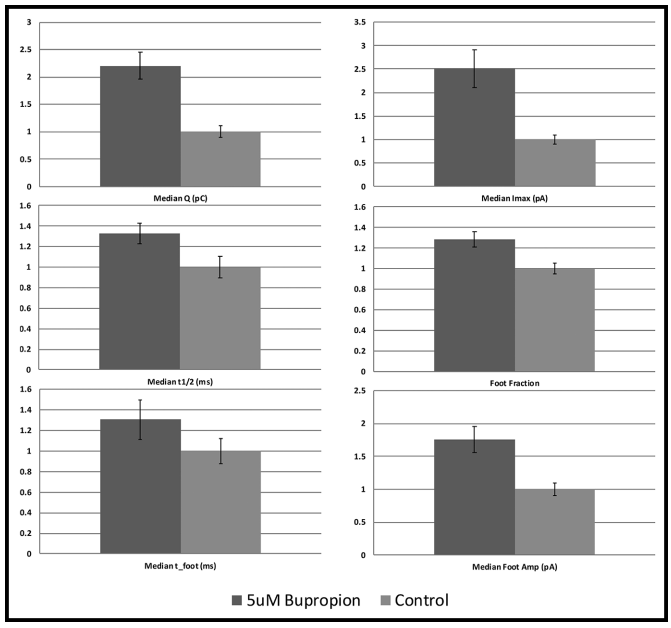

Figure 3: Comparison of various normalized amperometric parameters between the bupropion treated and the control group.

Microcontact printing of poly(L-lysine) and poly(ethylene glycol) will be performed for promotion and resistance of cell adhesion.

Previously we have demonstrated live cell recording on the device. Highly parallel amperometry measurement with low noise is shown in Figure 2 [6]. The device will significantly increase the efficiency of amperometry measurement.

To further utilize the advantages of the CMOS IC with deep wells, effects of several drugs and labels on the quantal release kinetics, such as bupropion, citalopram and FFN511, has been investigated. Figure 3 shows the results for the comparison of various amperometric parameters between the bupropion treated group and the control group. The results were collected from only four experiments from only four separate days, which would normally take weeks or months to get the statistical significance.

References:

[1] Kisler, K., et al., J. Biomater. Nanobiotechnol., 2012. 3(2): p.243-253.

[2] Colliver, TL., et al., J. Neurochem., 2000. 74(3): p. 1086-1097.

[3] Kim, B., et al., Biosens Bioelectron., 2013. 41: p. 736-744.

[4] Heer, F., et al. Biosens Bioelectron., 2004, 20(2): p. 358-366.

[5] Liu, X., et al. Analytical Chem., 2011, 83: p. 2445-2451.

[6] Huang, M., et al. Pflügers Archiv., 2018, 470(1): p. 113-123.

Droplet-Microfluidic Device for Stem Cell Culture

CNF Project Number: 2461-16
Principal Investigator: Benjamin D. Cosgrove
User: Andrea J. De Micheli

Affiliation: Meinig School of Biomedical Engineering, Cornell University
Primary Sources of Research Funding: Cornell Start-Up Funds, NIH Grant # R00AG042491 (Cosgrove)
Contact: bdc68@cornell.edu, ad689@cornell.edu
Website: http://blogs.cornell.edu/cosgrove/
Primary CNF Tools Used: Heidelberg DWL66FS/2000, SÜSS MJB4 contact aligner, SU-8 hotplates, SU-2 spinners

Abstract:

We are working on a droplet-microfluidic device to generate microscopic beads of poly(ethylene glycol), a biomaterial we use to study the interaction between muscle stem cells and their environment. The device is made from PDMS cast on a SU-8 patterned wafer generated by standard SU-8 photolithography techniques at Cornell NanoScale Facility.

Summary of Research:

Microfluidics have enabled a more high-throughput and comprehensive examination of biological systems. In particular, the interaction between stem cells and their local environment (the niche) can be studied using biomaterial constructs that attempt to recreate physical and biological aspects of the niche. We used a droplet-microfluidic device (designed and built at CNF) to generate hundreds of thousands of beads of the biomaterial poly(ethylene glycol) (PEG) with various physical and biochemical properties. We will be using these ~ 100 μm PEG beads as artificial microenvironments to screen for muscle stem-cell-niche interactions that are characteristic of muscle physiology.

So far, we have created PEG beads with different levels of incorporated laminin and observed myoblast binding in culture.

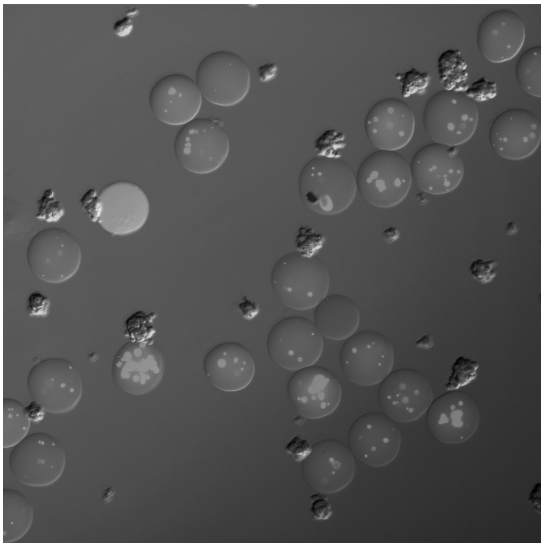

Figure 1: 100 μm PEG beads coated with the fluorescent (Alexa647) protein laminin (red). Clusters of myoblasts can be seen adhering to the beads. See full color version on pages xxviii-xxix

Figure 2: Left: SU-8 wafer with patterned structures. Right: A series of eight PDMS microfluidic devices.

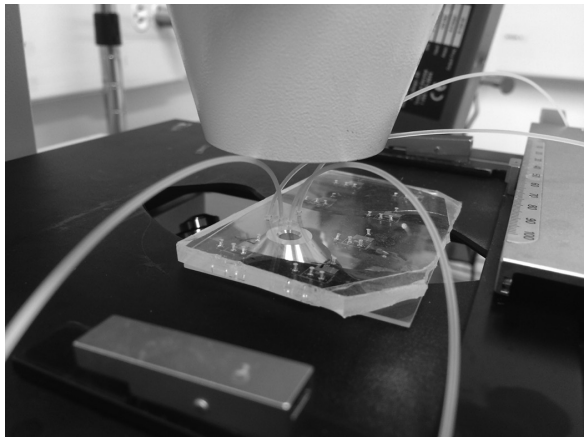

Figure 3: Droplet-microfluidic setup for generating PEG beads. Courtesy De Vlaminck lab.

Metasurfaces for Infrared Spectroscopy of Live Cells in a Microfluidic Chamber

CNF Project Number: 2472-16

Principal Investigator: Gennady Shvets

Users: Glen Kelp, Junlan Lu, Shourya Dutta Gupta

Affiliations: Applied and Engineering Physics, Cornell University; Department of Physics, University of Texas at Austin

Primary Source of Research Funding: Cornell University

Contact: gshvets@cornell.edu, gk389@cornell.edu, JL3286@cornell.edu, sd789@cornell.edu

Website: http://shvets.aep.cornell.edu

Primary CNF Tools Used: JEOL 9500, CVC SC4500 evaporator, ZEISS Supra SEM, PDMS casting station

Abstract:

Non-invasive and label-free identification of different cell types allows for early stage diagnosis and leads to more efficacious potential treatment of various human diseases. For example, early stage cancer detection enables many more treatment options and potential cure as compared to detection in the later stage of cancer. In this respect, circulating tumor cells (CTCs) in the blood stream have been shown to be a strong indicator of early stage of various cancers. However, separation, capturing and identification of CTCs still possess significant challenges with regarding to their extremely low concentration as well as the inability of traditional methods to characterize them accurately. Other diagnostic techniques, such all-optical diagnostics of aspiration biopsies, have similar requirements for rapid capture and identification of cancer cells. The following approach is pursued in our lab: simultaneous capture and spectral cytopathology using a combination of dielectrophoresis (DEP) and metasurface-enhanced infrared reflection spectroscopy (MEIRS).

Summary of Research:

Mid-IR spectroscopy is one of the prominent ways of identifying different materials via their fingerprint molecular vibrations. In the past, this has been used for spectroscopically distinguishing cancerous versus non-cancerous tissue. Typically, at least a complete monolayer of cells is required for performing such a characterization. This limitation on the number of cells is a large hindrance for adapting this technique for the detection of CTCs, due to their inherently low concentration in blood. It has been previously shown by our group that mid-IR spectroscopy performed using plasmon resonant metasurfaces (Figure 1) allows one to enhance the sensitivity of this technique significantly and we used this approach to accurately characterize a single protein layer [1]. The increase in sensitivity arises from the highly enhanced optical electric fields created near the structures. Furthermore, the metasurface only probes a small region close to the cell membrane due to the rapid decay of the enhanced fields away from the metasurface.

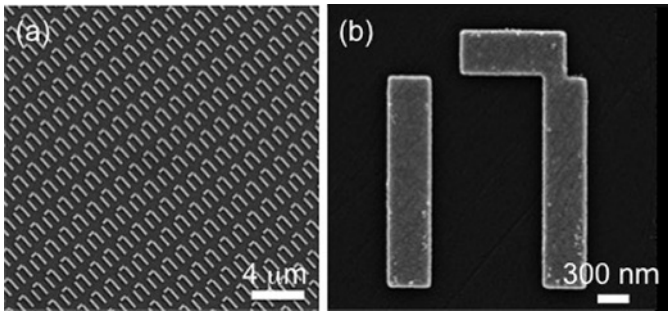

Figure 1: SEM micrographs of the plasmonic metasurface sensor used for MEIRS. (a) Low magnification image showing the periodic plasmonic microstructures. (b) SEM image of a single unit cell of the metasurface. The metasurface is designed to exhibit very high electric fields in the vicinity of the structure. Depicted unit cells are repeated on the substrate plane to form arrays 500 × 120 $(\mu m)^2$ in size. These metasurfaces are made of gold and fabricated on CaF_2 substrates using electron beam lithography.

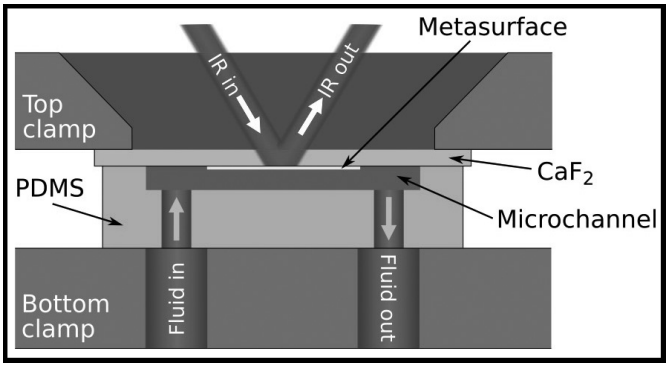

Figure 2: Schematic of a microfluidic device for capturing cells onto the metasurface sensor and measuring their mid-IR spectra. CaF_2 substrate is coupled to a PDMS microchannel allowing cell solution to flow over the sensor surface. PDMS and CaF_2 are fixed together with acrylic clamps compatible with standard microscope slide mounts. Cell solution is pumped through the channel with a syringe pump and voltage is applied on the wire electrodes within the metasurface using a function generator (not shown).

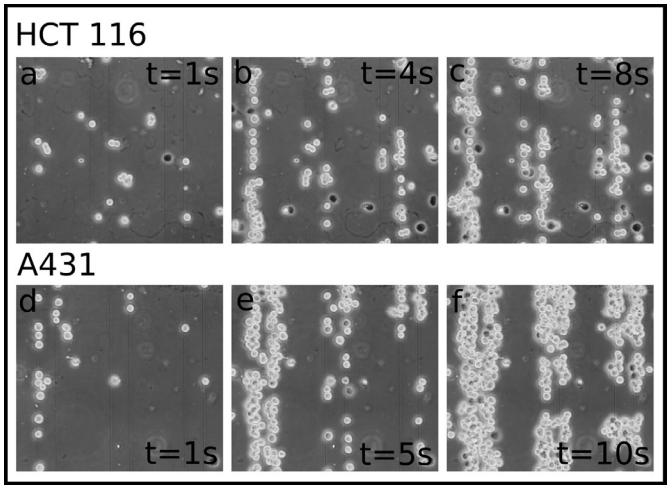

Figure 3: Cells captured on the sensor surface using DEP at different times. (a)-(c) Colon cancer cells (HCT 116). (d)-(f) Skin cancer cells (A431). Three metasurfaces are visible on each image, with two wire electrodes embedded in each metasurface. The DEP force is strongest on the wires, causing cells to form lines on them.

Deposition of cells directly onto the metasurface sensor is achieved with the use of dielectrophoresis. Since cells are essentially dielectric particles, a nonuniform AC electric field can be set up around the metasurface by applying voltage on electrodes embedded in the sensor design, causing cell movement due to DEP force (proportional to electric field gradient). IR spectra of the cells captured and immobilized on the metasurface can then be simultaneously collected under an IR microscope. A schematic of a device constructed to capture cells and collect their mid-IR spectra is shown on Figure 2.

Attachment of cells onto the sensor surface can be further improved by covering the sensor with antibodies. By tuning the frequency of AC signal applied to the electrodes, it is also possible to capture specific cells while repelling other kinds of cells in a multi-species cell solution. Separation of different cell types is especially important while working with blood samples that have very low concentration of CTCs. In the case of CTCs, the separation of tumor and blood cells with DEP is very effective, since those cell types have very different dielectric properties and therefore the frequency of the electric field can be chosen such that CTCs move to the sensor while pushing the blood cells away from it.

Examples of cells captured onto the wires on the sensor surface are depicted in Figure 3. The device can be mounted on a standard IR microscope, allowing instantaneous collection of cell mid-IR spectra for their identification. We have shown that different cell types (e.g., cancerous and non-cancerous) have different mid-IR fingerprints. The difference in the spectral features between various cell types can thus be used for identifying them. The spectra are acquired in an aqueous environment during flow, which is generally not the case in most of the studies in literature. As the whole experiment is performed within a flow chamber enclosing the metasurface sensor, and over the course of just a few minutes, it paves the way for automated and rapid identification and characterization of cells.

References:

[1] Fano-resonant asymmetric metamaterials for ultrasensitive spectroscopy and identification of molecular monolayers. Chihhui Wu, Alexander B. Khanikaev, Ronen Adato, Nihal Arju, Ahmet Ali Yanik, Hatice Altug, Gennady Shvets; Nature Materials 11, 69-75 (2012).

Listeria Sensor Chip via Surface Plasmon Resonance (SPR)

CNF Project Number: 2498-16

Principal Investigator and User: Lori Lepak

Affiliation: Phoebus Optoelectronics, LLC

Primary Source of Research Funding: National Institutes of Health

Contact: llepak@phoebusopto.com

Website: www.phoebusopto.com

Primary CNF Tools Used: DWL2000 photomask writer, ASML DUV stepper, AJA sputterer, Au electroplating, AJA ion mill, ZEISS SEM, DISCO dicing saw

Abstract:

Since 2003, Phoebus Optoelectronics has enabled custom R&D solutions in the fields of metamaterials, plasmonics, antennas, and sensors. We work closely with our customers throughout device development, from product realization to small volume manufacturing. Our R&D portfolio spans the spectral ranges of visible light, infrared, terahertz, and microwave radiation, for applications in high resolution infrared imaging systems, wavelength and polarization filtering, tunable optical components, beam forming and steering, solar cells and renewable energy devices, and chemical and biological toxin sensors. Our agile team makes extensive use of the resources at the CNF for our nano/micro fabrication and testing, to provide cost efficiency and rapid turnaround. In the present report, we discuss recent efforts to develop a biosensor system, which provides the state-of-the-art sensitivity of a typical benchtop system with the superior SWaP performance of a handheld system. Although our proof-of-concept prototype system is designed to detect *Listeria monocytogenes*, our system may be easily adapted to target any viral or gram-negative bacterial pathogen of interest, simply by designing new detection proteins specific to the new targets. We expect our system to find broad applications in public health and safety, medicine, and agriculture.

Summary of Research:

Metamaterial structures exhibit the unique phenomenon of extraordinary optical transmission (EOT), first observed by T.W. Ebbesen in 1998 [1]. In EOT, light is transmitted through apertures much smaller than the incident wavelength, at anomalously large intensities relative to the predictions of conventional aperture theory. Since its founding in 2003, Phoebus has successfully harnessed EOT by incorporating metasurfaces into devices used to perform light filtering [2-3], photon sorting [4-5], polarimetric detection [6], high speed optical detection [7], and most recently, including the present effort, in our SPR plasmonic sensor chips [8].

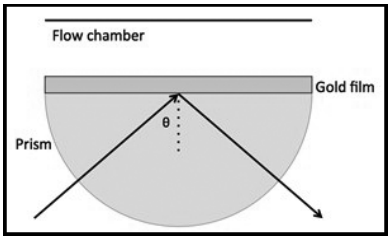

Figure 1: Surface plasmon resonance spectroscopy schematic. Reproduced from reference [8].

SPR is a highly sensitive, label-free optical detection technique, whose underlying physics is illustrated in reflection mode in Figure 1. A laser passes through a prism, at an incident angle θ, on a gold film which is in contact with an analyte solution on its opposite side. The illumination produces an evanescent wave (surface plasmon), which significantly reduces the reflectance at a resonant angle. The resonant angle is strongly dependent on the local refractive index, within a few tens of nanometers of the gold surface, and thus is extremely sensitive to enzyme-substrate or antibody-antigen binding events near the surface. The resonance is independent of the geometric configuration of the optical elements (see [8] for mathematical derivation.), such that these results also apply to devices which operate in transmission mode.

Phoebus's technology, for the first time, enables an inexpensive (<$1,000), hand-held system for the optical detection of *Listeria* via surface plasmon resonance (SPR), with a sensitivity currently only available in

expensive (>$100,000) benchtop SPR systems. We have achieved this by combining two key innovations: 1) Computationally designed proteins (CDPs), engineered to simultaneously bind their target pathogens with the specificity of wild-type enzymes, while undergoing an exceptionally large conformational change upon binding to maximize the SPR signal, and 2) Disposable plasmonic sensor chips, fabricated using the resources of the CNF, to pattern plasmonic chips with a metamaterial surface to enable as shown in Figure 2.

Our fabricated first-generation metasurface chips, shown in Figure 3, consist of an array of gold wires, which serve both to bind the designed CDPs and to undergo SPR. These two innovations are combined by attaching the engineered IDP's to the patterned gold metasurface using standard thiol-based attachment chemistry, to make a disposable sensor chip. This chip is inserted into a handheld 3D printed module, as shown in Figure 3. All of the optical elements are already assembled in-line as indicated, for a transmission-based detection system. Except for Phoebus's disposable sensor chip, all of the optical components are inexpensively commercially available, which helps to make our overall system a highly cost-effective toxin sensing solution.

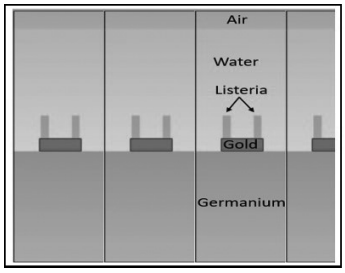

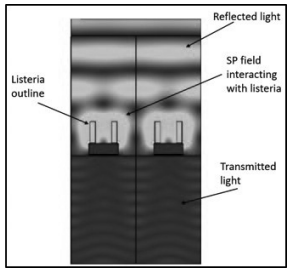

Figure 2: (Left) Unit cell of Listeria sensor. The full plasmonic chip consists of an array of these structures. (Right) Electric field profile at SP resonance, when bound to individual Listeria.

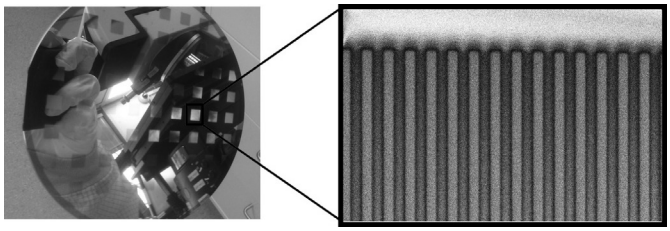

Figure 3: (Left) Wafer of plasmonic chips, fabricated on ASML DUV stepper. (Right) SEM image of a typical metasurface used in sensor chip.

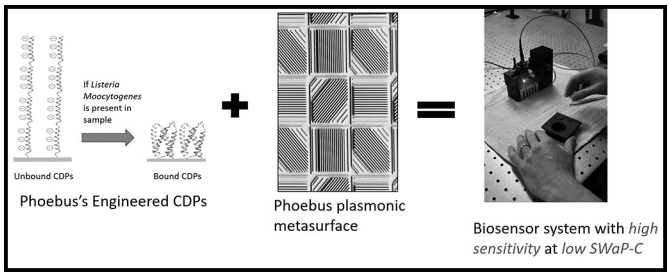

Figure 4: Phoebus-engineered sensor system combines (a) designed CDPs, which undergo extreme conformational changes upon binding target and (b) gold metasurface patterned to maximize transmission at SPR resonant wavelength into (c) a high sensitivity, low SWaP-C chem/biotoxin sensor system.

References:

[1] Ebbesen, T.W., et al., "Extraordinary optical transmission through sub-wavelength hole arrays." Nature, (1998). 391(6668): p. 667-669.

[2] Crouse, D. "Numerical modeling and electromagnetic resonant modes in complex grating structures and optoelectronic device applications." Electron Devices, IEEE Transactions on 52.11 (2005): 2365-2373.

[3] Crouse, D., and Keshavareddy, P. "Polarization independent enhanced optical transmission in one-dimensional gratings and device applications." Optics Express 15.4 (2007): 1415-1427.

[4] Lansey, E., Crouse, D., et al. "Light localization, photon sorting, and enhanced absorption in subwavelength cavity arrays." Optics Express 20.22 (2012): 24226-24236.

[5] Jung, Y.U; Bendoym, I.; Golovin, A.B.; and Crouse, D.T. "Dual-band photon sorting plasmonic MIM metamaterial sensor." Proc. SPIE 9070, Infrared Technology and Applications XL, 90702X (June 24, 2014); doi:10.1117/12.2050620.

[6] Crouse, D., and Keshavareddy, P. "A method for designing electromagnetic resonance enhanced silicon-on-insulator metal-semiconductor-metal photodetectors." Journal of Optics A: Pure and Applied Optics 8.2 (2006): 175.

[7] Mandel, I.; Gollub, J.; Bendoym, I; Crouse, D. Theory and Design of A Novel Integrated Polarimetric Sensor Utilizing a Light Sorting Metamaterial Grating. Sensors Journal, IEEE, (2012): Vol. PP, 99

[8] Lepak, L., et al. "Handheld chem/biosensor using extreme conformational changes in designed binding proteins to enhance surface plasmon resonance (SPR)" Proc. SPIE 9862, Advanced Environmental, Chemical, and Biological Sensing Technologies XIII, 9862-7 (April 17, 2016); doi:10.1117/12.2222305.

Gut-on-a-Chip using Microfluidic Devices

CNF Project Number: 2502-16
Principal Investigator: Alireza Abbaspourrad
User: Seyedramin Pajoumshariati

Affiliation: Food Science Department, Cornell University
Primary Source of Research Funding: Principal investigator's start up
Contact: alireza@cornell.edu, sp777@cornell.edu
Website: https://abbaspourradlab.cornell.edu/
Primary CNF Tools Used: Object 3D Printer, VersaLaser engraver/cutter, MVD 100, PDMS casting station

Abstract:

Current methods to test genotoxicity and cytotoxicity either use live animals *in vivo*—e.g., a food or drug is administered to a rodent, then monitored for physiological and behavioral changes, histology, and blood results—or we use *in vitro* tests, in which a few bacterial or mammalian cell lines are cultured inside a transwell insert, and then monitored for cell viability. Both have striking limitations. The first one assumes that we can model the pathophysiology of human diseases on animals, an assumption that has led to the costly failure of many clinical drug trials (approximately nine out of ten. It is also unpredictable and fraught with ethical concerns). The second one assumes that a single type of epithelial cancer cell line (i.e., Caco2) inside a transwell insert has the same uptake mechanism and behavior as the diverse microenvironment of the human gastrointestinal tract, which is in fact not composed of only one type of cell but a wide array of crypt stem cells, goblet cells, enterocytes, enteroendocrine cells, tuft cells, Paneth cells, immune cells, and microbiota—all of which influence each other through intricate cross-talking mechanisms such as paracrine and autocrine signaling in order to maintain cell viability.

Summary of Research:

Gut-on-a-Chip. Current *in vitro* models cannot adequately address the complexity of gut environment because of its rapidly changing nature. Herein, we present a "Gut-on-a-Chip" model system to explain intricate crosstalk in the gut microenvironment, using a microfluidic technique to encapsulate the gut constituent cells in the intestinal microenvironment including organoids, immune cells, and microbiome within microgels. Appling this technique, we decouple contact-independent cell-cell interactions from the contact-dependent effects of soluble mediators. This model can be used to evaluate the effect of biopharmaceutical products and food ingredients on the intestinal cells and microbiome and will be served as a unique approach for pathological threat detection in gut environment.

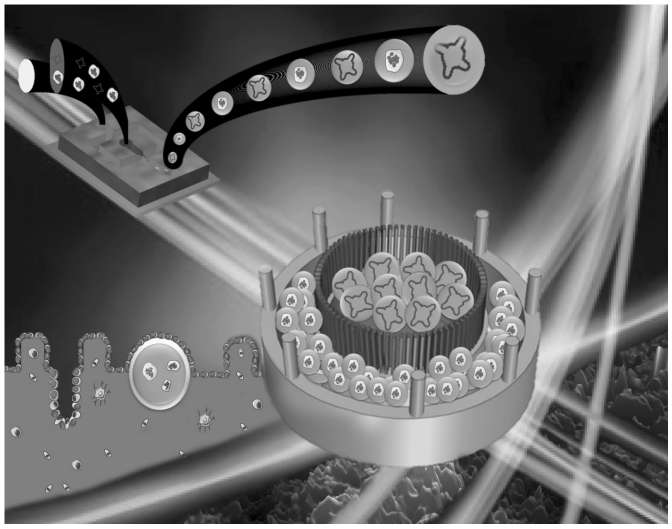

Figure 1: Schematic of the 3D printed insert for co-culture of organoid-embedded microgels along with Peyer's patch embedded microgels. See full color version on pages xxviii-xxix.

References:

[1] Pajoumshariati, S. R., M. Azizi, D. Wesner, P. G. Miller, M. L. Shuler, and A. Abbaspourrad. 2018. Microfluidic-Based Cell-Embedded Microgels Using Nonfluorinated Oil as a Model for the Gastrointestinal Niche. ACS applied materials and interfaces 10:9235-9246.

Retinal Implant Project

CNF Project Number: 2504-16

Principal Investigator: Douglas Shire, Ph.D.

Users: Marcus Gingerich, Ph.D.[1,4], Douglas Shire, Ph.D.[1,3,4], Patricia Wong[2,4]

Affiliations: 1. Department of Electrical Engineering, Cornell University; 2. Department of Neuro-Ophthalmology, Massachusetts Eye and Ear Infirmary; 3. VA Cleveland Healthcare System; 4. Bionic Eye Technologies, Inc.

Primary Sources of Research Funding: Louis Stokes Cleveland VA Medical Center; NIH/NIBIB U01EB018873; NIH/NIBIB R01EB022013, Massachusetts Lions Eye Research Fund

Contact: dbs6@cornell.edu, mdg37@cornell.edu, pwong@bionicvisiontechnologies.com

Website: http://www.bostonretinalimplant.org

Primary CNF Tools Used: PT-72, lithography toolset/MA6, DWL2000, evaporators, AJA sputter, Gamma spray coater, SEMs, gold electro-plating, Class 2 lithography toolset, Oxford PECVD, Oxford 100 etcher, Glenn 1000, YES polyimide oven, VersaLaser engraver/cutter

Abstract:

The purpose of the Retinal Implant Project is to restore useful vision to patients who are blind with degenerative retinal diseases. The primary illnesses we hope to treat are retinitis pigmentosa (a primary cause of inherited blindness) and age-related macular degeneration (the leading cause of blindness in the developed world). Both these diseases cause the eventual destruction of the photoreceptor cells — rods and cones — in the retina, leaving intact the ganglion cells which transmit electrical impulses (and hence visual information) to the brain. The ganglion cells may be stimulated, however, with biphasic current pulses from a microfabricated electrode array. Blind surgical volunteers have consistently described visual percepts that resulted from such stimuli, and this has led our team to develop a wireless, implantable retinal prosthesis.

Summary of Research:

The implanted portion of our device consists of power and data secondary receiving coils, and in a sealed titanium (Ti) can a small number of discrete components, and a custom designed application specific integrated circuit (ASIC) which consists of circuitry for clock and data recovery, current drivers for electrodes in a stimulating electrode array, and a programmable function generator capable of stimulating with a wide range of pulse widths and amplitudes. The current outputs drive high-charge capacity sputtered iridium oxide film (SIROF) stimulating electrodes, which in turn give rise to the visual percepts mentioned above.

CNF-fabricated components of this system have included various proof-of-concept test structures and tools used in the research effort and an integrated combination flexible circuit and stimulating electrode array. Si wafers serve as carriers for these freestanding films during processing. The electrode leads are fabricated inside of 'sandwiches' of polyimide and amorphous silicon carbide (SiC), while the SIROF electrodes are reactively sputter-deposited.

Assembly of the intraocular components of the prosthesis is accomplished by flip chip solder ball bonding of the IC and solder attachment of discrete components onto an internal flexible circuit board which is hermetically sealed into an ultraminiature Ti can. The RF coils are soldered and glued to the integrated external flex-array which is in turn thermosonically bonded to the hermetic feedthrough of the Ti can. Finally, the thermosonic bonds are protected and insulated with an over-mold. An external patient interface unit, will consist of a video camera for capturing images, a digital signal processor, and a radio frequency (RF) transmitter and coil to relay power and data to the implanted device.

Scientific challenges still remain in realizing a chronically implantable retinal prosthesis. While our first-generation device was primarily encapsulated in polymers for short term proof-of-concept implant studies, our second-generation system focused on a system which would last many years *in vivo*. Our more recent efforts have focused on developing a device with 256+ stimulation channels

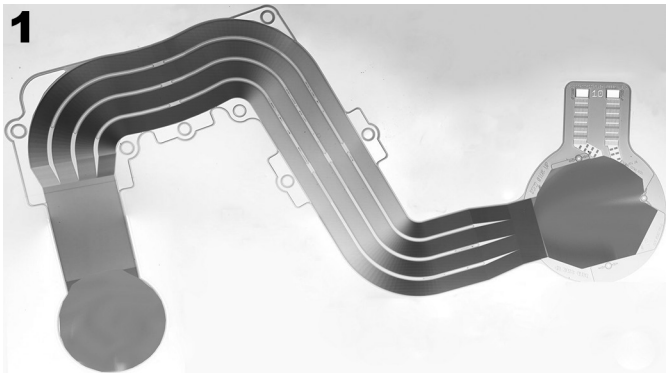

Figure 1, above: A picture of a single complete electrode array.

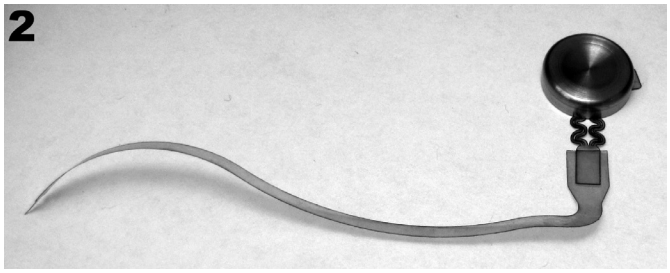

Figure 2, above right: A picture of a VersaLaser-cut mechanical mockup of an indwelling brain electrode system including a titanium hermetic enclosure.

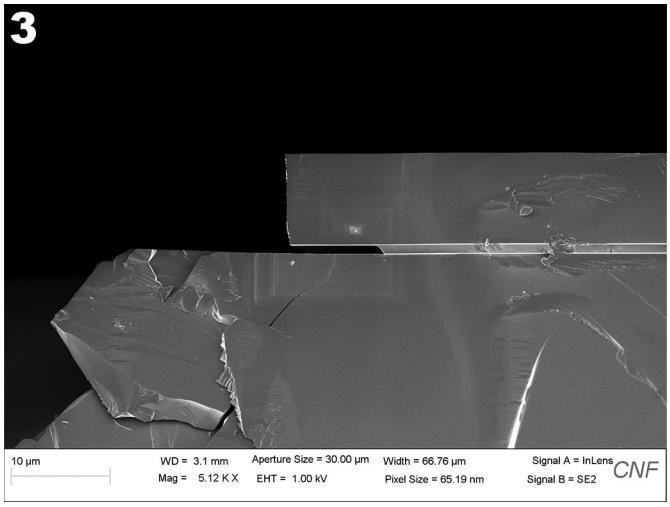

Figure 3, below right: An SEM picture of the partial release of the buried oxide layer of an SOI test sample using the Primaxx vapor HF etch system.

which is still small enough and of a configuration to be easily implanted in the ocular orbit and continue to function for many years *in vivo*. Thus, a major effort has been the development of a technological platform to build a robust, hermetically packaged, high-density subretinal visual prosthesis with a lifetime of > 10 years in biological saline that is scalable to hundreds of I/O channels.

Recent efforts in the CNF have included, among other things, optimizing a reliable microfabrication process for the flexible micro-electrode array (see Figure 1). This included microfabricating a mechanical support for the implantable radio frequency power and communication coil. We have also explored a process of fabricating indwelling electrodes for long-term implantation in brain tissue. A preliminary VersaLaser-cut mockup of such an electrode is shown attached to a titanium hermetic enclosure in Figure 2 in order to evaluate mechanical properties and the overall size and shape. Additionally, we explored a method of fabricating part of that electrode array in Si and releasing it from an SOI substrate using the Primaxx vapor HF etch tool to etch the buried oxide layer (Figure 3).

The project has continued the development and implementation of a microfabrication process to incorporate SU-8-based 3D electrodes into a hybrid electrode array to achieve a more optimal interface between the electrode and the target neural cells. Fabrication work at the CNF has included process development required for such high aspect structures including the challenges of lithography with the presence of such extreme topography. Many of these lithography processes have been successfully realized using the Gamma spray coating tool.

The latest microfabrication processes utilize numerous CNF tools including the Heidelberg 2000 mask writer, MA6 aligner, polyimide YES curing oven, PT72 RIE, SC4500 evaporator, Gamma spray coater, Au electroplating station, K and S Au ball bonder, Oxford PECVD, Oxford 100 etch tool, parylene coater, as well as numerous metrology tools.

References:

[1] J. F. Rizzo, J. Wyatt, J. Loewenstein, S. Kelly, and D. Shire, "Methods and Perceptual Thresholds for Short-Term Electrical Stimulation of Human Retina with Microelectrode Arrays," Investigative Ophthalmology and Visual Science, vol. 44, no. 12, Dec. 2003, pp. 5355-5361.

Disseminating Glycocalyx Biopolymer-Induced Microvesicle Shedding through Nanoparticle Tracking Analysis and Cryo-Electron Microscopy

CNF Project Number: 2574-17

Principal Investigator: Matthew Paszek[2]

Users: LaDeidra Monét Roberts[1], Rose Yin[2]

Affiliations: 1. Nancy E. and Peter C. Meinig School of Biomedical Engineering, 2. Robert Frederick Smith School of Chemical and Biomolecular Engineering; Cornell University

Primary Source of Research Funding: National Institutes of Health DP2 1DP2GM229133-01

Contact: mjp31@cornell.edu, lmr254@cornell.edu

Website: https://www.paszeklab.com/

Primary CNF Tools Used: Malvern NS300 NanoSight

Abstract:

Cancer-derived microvesicles (MVs) have been linked to cancer progression through their ability to propagate an oncogenic phenotype in normal cells. However, the mechanism of their biogenesis is not clearly established. The biogenesis of MVs is inherently a mechanical process where direct vesicle shedding from the plasma membrane requires physical bending. Through scanning electron microscopy, we have found that biopolymers within the sugar-rich coating on the plasma membrane known as the glycocalyx contribute induce membrane bending. Through nanoparticle tracking analysis (NTA), we also have found that molecular crowding within the glycocalyx drives membrane bending for microvesicle biogenesis. Lastly, we show that using nanoparticle tracking analysis in tandem with cryo-transmission electron microscopy (cryo-TEM) allows us to validate and visualize microvesicles and other extracellular vesicle sub-types to better understand mechanisms of biogenesis and shedding.

Summary of Research:

Theory has predicted membrane instabilities and formation of spherical structures in the presence of molecular membrane surface crowding. Remarkably, we have found that increased expression of cancer-associated biopolymers, including mucin-1 (Muc1), induce membrane instabilities as well as drive formation and shedding of spherical microvesicles through conventional scanning electron microscopy (SEM), nanoparticle tracking analysis (NTA) using the Malvern NS300 NanoSight, and cryo-transmission electron microscopy (cryo-TEM). These results suggest that increased glycocalyx biomass might be a general mechanism for MV upregulation. Together, our data suggests that large, cancer associated glycoproteins and glycopolymers, such as Muc1, may perturb cellular communication in cancer through regulation of microvesicle biogenesis. Understanding these physical processes could lead to new therapies that target the mechanical basis of MV biogenesis and cancer.

Together, these experiments and theories describe an entropic mechanism through which the glycocalyx can strongly influence the plasma membrane shapes. We also find that the plasma membrane in these cells become unstable following inhibition of actin polymerization. These results suggest that the cytoskeleton counterbalances the entropic pressure exerted by cell surface glycopolymers and dynamics play a role in formation and release of microvesicles. Given that glycosylation changes dramatically and in tandem with cell fate transitions, and that the pool of monomers for construction of glycocalyx polymers is tightly coupled to specific metabolic programs, our work raises the intriguing possibility that the glycocalyx may serve as a conduit linking physical morphology to specific physiological and diseased states.

References:

[1] Antonyak, M.A., PNAS, 2011, 108, 4852-4857.

[2] Paszek, M.J., Nature, 2014, 511, 319-25.

[3] Shurer, et al., ACS Biomater. Sci. Eng., 2017, 4, 2, 388-399.

[4] Shurer, et al., in resubmission, 2018.

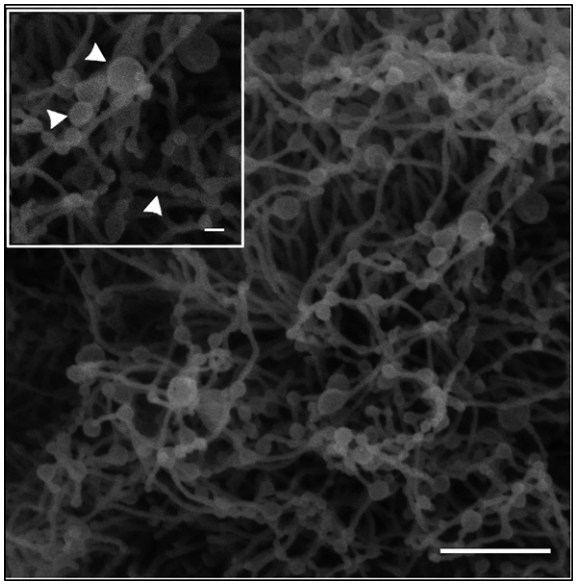

Figure 1: Nanoparticle tracking analysis shows that increased Mucin-1 (Muc1) expression induces membrane tubules and instabilities on the surface of MCF10A cells. (Inset; top left) Microvesicles (indicated by white arrows) present on the membrane tubes (scale bars: 200 nm).

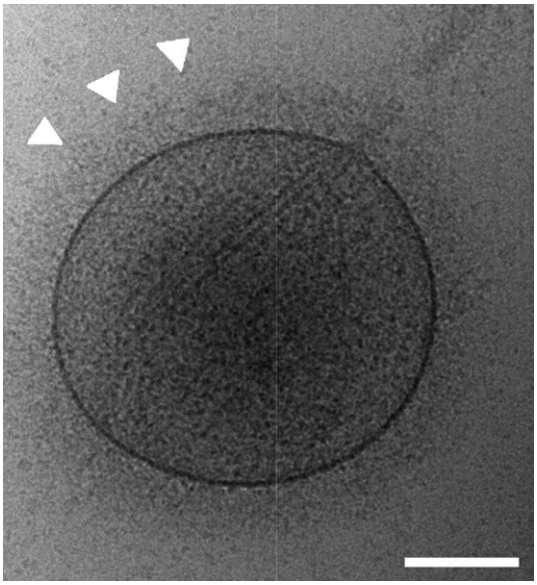

Figure 3: Cryo-TEM of a microvesicle shed from Muc1 MCF10A cells. The ultrastructure of the glycocalyx is indicated by white arrows (Scale bar: 100 nm).

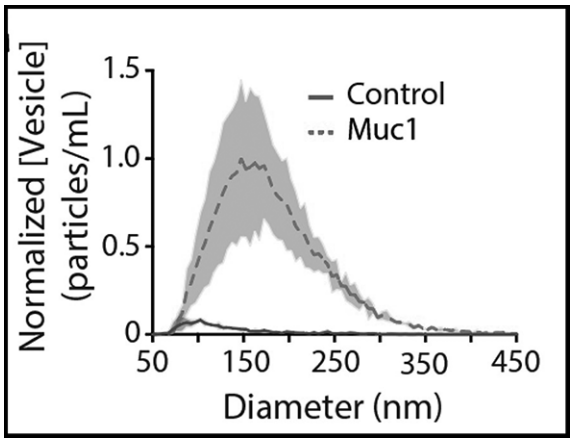

Figure 2: Increased expression of Muc1 induces microvesicle shedding in MCF10A cells compared to control MCF10A cells as shown in nanoparticle tracking analysis (n=3).

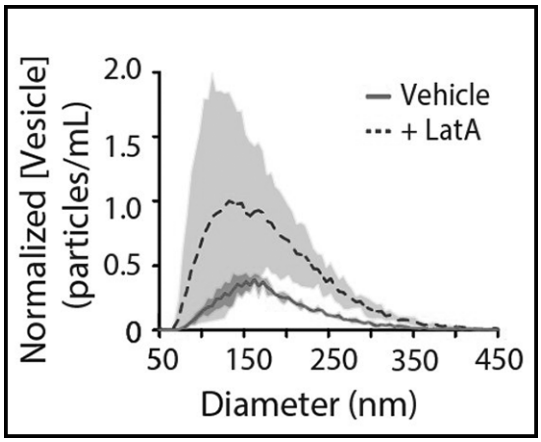

Figure 4: Destabilization of actin through 10 uM of Latrunculin A treatment in cells with increased Muc1 expression treatment shows enhanced microvesicle shedding compared to control Muc1 cells (n=3).

Investigation of the Mechanical Property of *Drosophila* Mature Oocytes using Microfluidic Devices

CNF Project Number: 2589-17

Principal Investigator: Mariana Wolfner

Users: Qinan Hu, Chih-kuan Tung, Mariana Wolfner

Affiliation: Department of Molecular Biology and Genetics, Cornell University

Primary Source of Research Funding: NIH/NICHD R21-HD088744-02 (Wolfner)

Contact: mfw5@cornell.edu

Primary CNF Tools Used: Lithography toolset, PDMS casting station

Abstract:

This project aims to study the mechanical properties of mature oocytes of the fruit fly *Drosophila melanogaster* using a microfluidic device, to better understand a conserved biological process required for embryonic development, egg activation.

Introduction:

At the end of oogenesis, the mature oocyte is developmentally arrested and needs to be "activated" to transition to embryonic development. Egg activation is conserved across species and is accompanied by a rise of intracellular calcium. In vertebrates, this calcium rise is triggered by fertilization. However, in *Drosophila*, despite conserved downstream events, egg activation is uncoupled from fertilization, and is triggered by mechanical pressure during ovulation. This process can be mimicked *in vitro* by letting the mature oocyte swell in a hypotonic solution containing calcium: the oocyte experiences pressure and takes up calcium-containing fluid from the environment, initiating a calcium rise and activating. The calcium rise initiates at the oocyte poles, and traverses the entire oocyte as a wave (analogous to the calcium waves seen in activating vertebrate and echinoderm oocytes). The *Drosophila* calcium wave can be visualized by our genetically-encoded calcium sensors GCaMP3 and GCaMP6.

Summary of Research:

To better understand the trigger for *Drosophila* egg activation we need to elucidate the mechanical requirement that initiates the calcium wave. Although all-round pressure on the membrane in a French Press can accelerate activation, and all-around pressure on the membrane as the oocyte swells in a hypotonic solution can to trigger calcium wave, our preliminary data have shown that point pressure by a microneedle can only induce a local rise of calcium level that does not propagate like a wave. This suggests to us that a larger regional or circumferential force must be needed to trigger the calcium wave.

To test this, we designed a set of microfluidic chambers with a tunnel-like shape and a narrow constriction in the middle. Mature oocytes can be squeezed through the constriction and we can observe whether a calcium wave starts when the oocyte experiences pressure from the narrow constriction. The wafers used as a mold for the chambers were fabricated at CNF. We then used them to cast our microfluidic devices using PDMS.

GCaMP-containing mature oocytes were loaded into a chamber, pushed through the constriction with syringe-driven fluid flow under a fluorescence microscope to check calcium level changes. To date, we have examined 27 oocytes, but only one of them showed a calcium rise when passing through the constriction in the chamber. Currently we are optimizing the design of the device to increase the chance of inducing a calcium rise and to obtain statistically meaningful results. One way would be to reduce the size of the constriction so that oocytes cannot pass through, allowing us to apply greater pressure using a syringe. The other possibility is to increase the length of constricted part of the tunnel so that oocytes are exposed to pressure for a longer period of time.

Rapid Point of Care Diagnostic for Sepsis Stratification

CNF Project Number: 2636-18

Principal Investigators: David Erickson, Ankur Singh

User: Taylor Oeschger

Affiliations: Biomedical Engineering, Mechanical Engineering; Cornell University

Primary Source of Research Funding: NSF, Atkinson Center Academic Venture Fund

Contact: de54@cornell.edu, as2833@cornell.edu, tmo55@cornell.edu

Primary CNF Tools Used: ABM contact aligner, Class II resist room, Heidelberg 2000 mask writer, profilometer, PDMS casting station, Hamatech wafer developer, UNAXIS 770 deep Si etcher, resist stripper, MVD 100

Abstract:

Sepsis is a rapidly progressing, life threatening immune response triggered by infection that affects many populations worldwide. Therefore, this research aims to create a microfluidic immune cell capture device that is capable of diagnosing sepsis at the point of care. To do this, we created a mold on a silicone wafer using deep silicone etching, which we then cast in polydimethylsiloxane (PDMS) and adhered to a glass slide to create a functional device. A drop of blood is lysed and quenched to remove red blood cells before leukocytes are captured on antibody coated pillars, where they can be quantified and correlated to a sepsis diagnosis. Development of an accurate point of care diagnostic device for sepsis would improve diagnostic speed, reduce hospital costs, and save many lives.

Summary of Research:

Sepsis is a life-threatening condition caused by the body's drastic response to microbial infection, which triggers a cascade of events that can lead to organ failure and death [1]. Neutrophil CD64 expression has been shown to increase under septic conditions making it a potential biomarker for sepsis [2,3]. In response to bacterial infection, neutrophil CD64 has been shown to be upregulated as early as one hour after infection [4]. This project aims to create a microfluidic device that can measure changes in quantities of immune cells and correlate them with a diagnosis of either onset, early stage, or late stage sepsis within hours from a whole blood sample. The long-term goal is to be able to quickly, inexpensively, and reliably determine the on-set and current stage of sepsis at the point of care so that treatment can be properly administered.

The microfluidic device will consist of two main sections: a lysing/quenching region and an antibody chamber for cell capture (Figure 1). Approximately 10 uL of whole blood will be exposed to lysing buffer followed by quenching buffer over a length of small pipes. This will remove red blood cells in order to obtain pure leukocyte populations. CD4+ T cells, CD4+CD25+ T reg cells, and CD64+ neutrophils will be captured on antibody coated pillars in the antibody capture chamber. These cells will be measured by counters or fluorescence and analyzed by a smart phone.

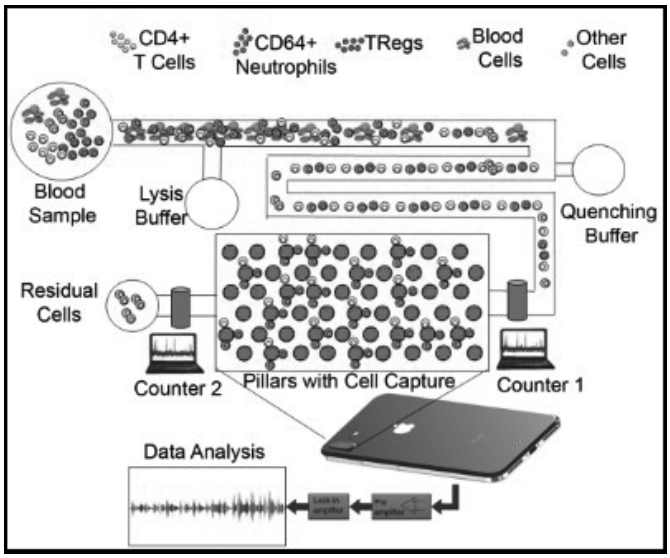

Figure 1: Schematic of microfluidic chip design.

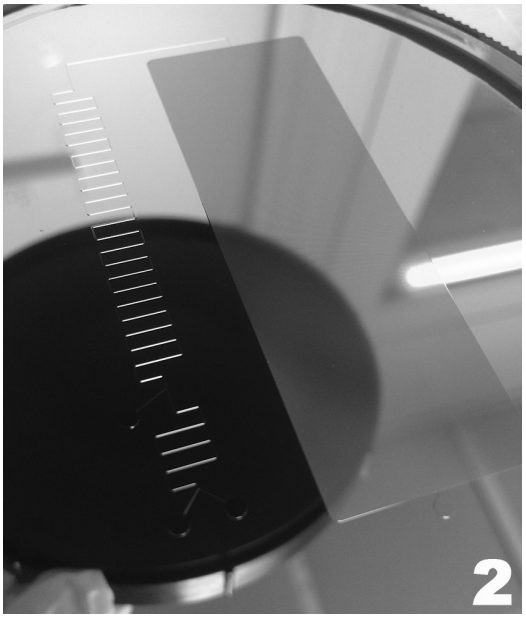

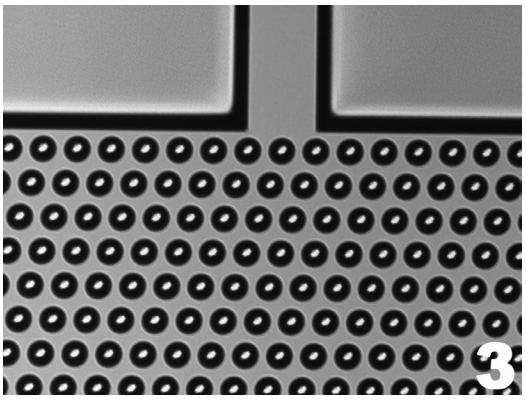

Figure 2, top: *Deep etched silicone wafer mold.* ***Figure 3, middle:*** *Ten times magnification of silicone mold inlet to antibody capture chamber.* ***Figure 4, bottom:*** *PDMS device cast from the silicon mold.*

The Cornell NanoScale Facility was used to create a silicon mold of the antibody chamber and the lysing/quenching region (Figure 2). The antibody capture chamber is approximately 20 mm by 60 mm with ~ 200,000 pillars that are 40 μm in diameter and 60 μm tall (Figure 3).

The mold was first attempted using SU-8 photolithography, but the large area of pillars had trouble staying adhered to the silicon wafer. As an alternative, the UNAXIS 770 deep silicon etcher was used. We were able to achieve uniform pillars much faster and more reliably using this method.

The final device is cast in polydimethylsiloxane (PDMS) and adhered to a glass slide using plasma cleaning (Figure 4). Prior to casting, we coated the silicon wafer mold in (1H,1H,2H,2H-perfluorooctyl)trichlorosilane (FOTS) using the MVD 100 tool to help prevent the PDMS from sticking to the mold.

The next steps are to test the device for functionality and ability to reliable capture and quantify cells.

References:

[1] Hotchkiss, R. S., and Karl, I. E.; 030109 The Pathophysiology and Treatment of Sepsis. n engl j med 3482, (2003).

[2] Cid, J., Aguinaco, R., Sánchez, R., García-Pardo, G., and Llorente, A. Neutrophil CD64 expression as marker of bacterial infection: A systematic review and meta-analysis. Journal of Infection (2010).

[3] Gros, A., et al. The sensitivity of neutrophil CD64 expression as a biomarker of bacterial infection is low in critically ill patients. Intensive Care Med. (2012).

[4] van der Meer, W., Pickkers Peter, P., Scott, C. S., van der Hoeven, J. G., and Gunnewiek, J. K. Hematological indices, inflammatory markers and neutrophil CD64 expression: Comparative trends during experimental human endotoxemia. J. Endotoxin Res. (2007).

Patterning of Native Proteins in Supported Lipid Bilayers

CNF Project Number: 2641-18

Principal Investigator: Susan Daniel

User: Zachary Manzer

Affiliation: Smith School of Chemical and Biomolecular Engineering, Cornell University

Primary Source of Research Funding: National Science Foundation

Contact: sd386@cornell.edu, zam42@cornell.edu

Primary CNF Tools Used: Heidelberg DWL66fs mask writer, ABM contact aligner, Unaxis 770 deep Si etcher, Anatech resist strip, MVD 100, P10 profilometer, FilMetrics F50-EXR

Abstract:

Many *in vitro* experimental studies fail to study membrane proteins in their native cellular environment and instead use solubilized systems in which all cellular components are mixed together and removed from their lipid scaffold. To more directly study these proteins, while still decoupling them from other cellular processes, we aim to create a microfluidic system in which protein embedded cell blebs can be patterned and studied. A supported lipid membrane will keep key membrane bound proteins in their native environment, thus enabling us to study them as if they were still inside the cell. Since the flow characteristics, channel dimensions, and the local environment are readily controlled, this platform gives us a way to easily mimic and manipulate the native cellular environment.

Summary of Research:

The use of a supported lipid scaffold from cellular membrane lipids has been shown by our group and others to preserve protein function in their native environment [1]. Previous work has been done in wells and straight channel devices on the millimeter scale, but the extension of this platform to allow for selective patterning will enable us to more extensively study protein and lipid interactions. These are important in virus binding mechanisms, drug delivery applications, as well as in fundamental studies of membrane dynamics.

A negative mask for a prototype microfluidic design was created using the Heidelberg DWL66fs mask writer and used with the ABM contact aligner to pattern photoresist that was spun onto a silicon wafer. After development, the profile of the patterns was analyzed on the P10 profilometer, a snapshot of which can be seen in Figure 1. Optimization of the process was conducted to produce consistent and even films, as measured by the profilometer and the FilMetrics F50-EXR. Once this was done, the exposed silicon was etched using the Unaxis 770 deep Si etcher, with the final form shown in Figure 2. As can be seen, there is still photoresist on the channels, which was removed by oxygen plasma cleaning in the Anatech resist strip. A final hydrophobic coating (FOTS) was applied using molecular vapor deposition to allow for PDMS molds to be easily removed once cast. The final wafer can be seen in Figure 3.

Once the mold was fabricated, Sylgard 184 was poured over the mold and cured. This can then be removed and bonded to a glass coverslip by using oxygen plasma cleaning on both surfaces. Synthetic liposomes containing a fluorescent marker was passed into the channels and allowed to incubate, where they will adsorb to the exposed surfaces and form a bilayer structure. Fluidity is confirmed by using a laser to photobleach the dye and then measuring the diffusion rate as the spot recovers. This process can be seen in Figure 4. Future work will involve more complicated device designs as well as leveraging the microfluidic for biotechnology applications, as mentioned.

References:

[1] Richards, M. J. et al. Membrane Protein Mobility and Orientation Preserved in Supported Bilayers Created Directly from Cell Plasma Membrane Blebs. Langmuir 32, 2963-2974 (2016).

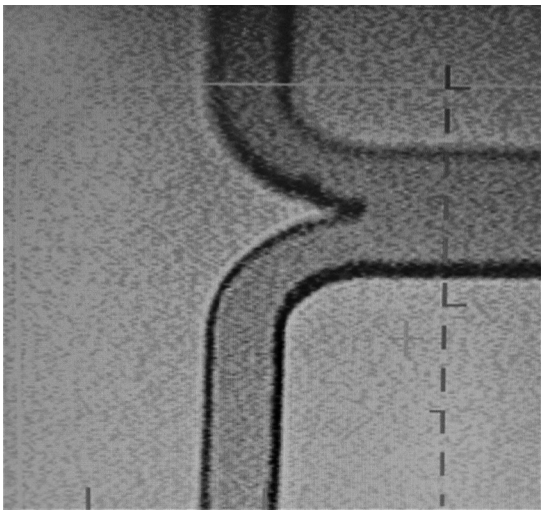

Figure 1: Image taken when measuring profile of exposed features. Depth of film was confirmed using FilMetrics F50-EXR.

Figure 2: Wafer after being removed from Unaxis 770 deep Si etcher.

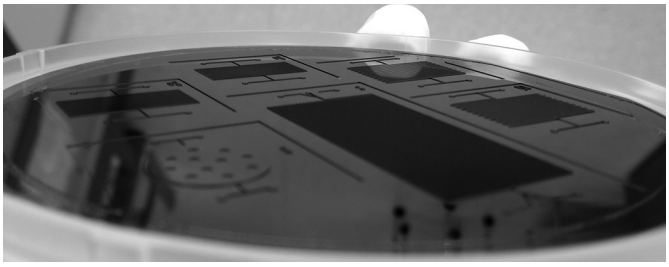

Figure 3: Wafer after being stripped in the Anatech resist strip and coated with FOTS in the MVD 100.

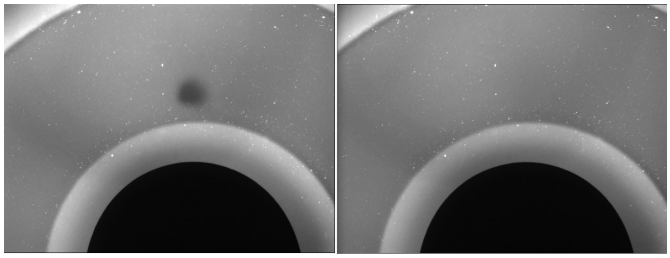

Figure 4: Fluorescence recovery after photobleaching (FRAP) confirms that a supported lipid membrane was formed in the device.